AD NUMBER

AD880496

NEW LIMITATION CHANGE

TO

Approved for public release, distribution unlimited

FROM

Distribution authorized to U.S. Gov't. agencies and their contractors; Critical Technology; Dec 1970. Other requests shall be referred to Air Force Flight Dynamics Lab [FYA], Wright-Patterson AFB, OH 45433.

AUTHORITY

AFFDL ltr dtd 27 Aug 1979

AFFDL-TR-70-104

FLOW-INDUCED PRESSURE OSCILLATIONS IN SHALLOW CAVITIES

H. H. HELLER
G. HOLMES
E. E. COVERT

BOLT BERANEK AND NEWMAN INC.

TECHNICAL REPORT AFFDL-TR-70-104

DECEMBER 1970

AIR FORCE FLIGHT DYNAMICS LABORATORY
AIR FORCE SYSTEMS COMMAND
WRIGHT-PATTERSON AIR FORCE BASE, OHIO

NOTICE

When Government drawings, specifications, or other data are used for any purpose other than in connection with a definitely related Government procurement operation, the United States Government thereby incurs no responsibility nor any obligation whatsoever; and the fact that the Government may have formulated, furnished, or in any way supplied the said drawings, specifications, or other data, is not to be regarded by implication or otherwise as in any manner licensing the holder or any other person or corporation, or conveying any rights or permission to manufacture, use, or sell any patented invention that may in any way be related thereto.

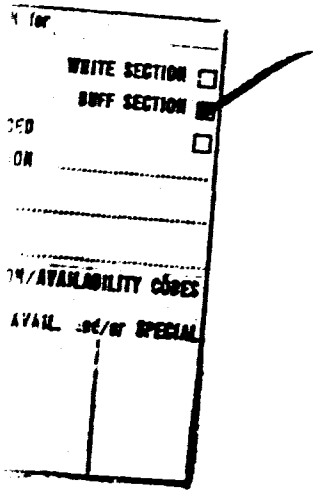

Copies of this report should not be returned unless return is required by security considerations, contractual obligations, or notice on a specific document.

200 - January 1971 - CO305 - 22-71-365

FLOW-INDUCED PRESSURE OSCILLATIONS IN SHALLOW CAVITIES

H. H. HELLER
G. HOLMES
E. E. COVERT

FOREWORD

This report was prepared by Bolt Beranek and Newman, Inc., Cambridge, Massachusetts, for the Aero-Acoustics Branch, Vehicle Dynamics Division, Air Force Flight Dynamics Laboratory, Wright-Patterson Air Force Base, Ohio, under Contract F33615-69-C-1428. The work described herein is a part of the Air Force Systems Command exploratory development program to predict the noise environment of flight vehicles. The work was directed under Project 1471, "Aero-Acoustic Problems in Air Force Flight Vehicles", Task 147102, "Prediction and Control of Noise Associated with USAF Flight Vehicles". Mr. S. L. McFarland of the Aero-Acoustics Branch was the task engineer.

The authors wish to thank their colleagues Mr. Alan Bilanan, Dr. Sheila E. Widnall and Dr. Eric E. Ungar for their valuable assistance during the course of the research project.

Manuscript was released by the authors on 1 July 1970 for publication as an AFFDL Technical Report.

This Technical Report has been reviewed and is approved.

Walter J. Mykytow

WALTER J. MYKYTOW
Asst. for Research & Technology
Vehicle Dynamics Division

ABSTRACT

This report presents the results of an experimental wind-tunnel study of flow-induced pressure oscillations in shallow cavities (length-to-depth ratio from 4 to 7). A variable-depth rectangular cavity was exposed to tangential flow over the open surface in the Mach-number range from 0.8 to 3, with flow stagnation pressures varying from 2 to 15 psia. The cavity was tested in an empty stage and with one or two stores. Third-octave band and narrowband fluctuating-pressure spectra were obtained at various locations within the cavity and under the approaching boundary layer; these spectra yielded information on broadband and resonant-response characteristics. Information on the longitudinal and lateral energy distribution, on recirculating-flow velocities, and on temperatures within the cavity was also obtained. This information was used to develop a scheme for predicting resonant frequencies and associated pressure-mode shapes, as well as discrete-frequency and broadband-pressure amplitudes.

TABLE OF CONTENTS

page

LIST OF FIGURES

LIST OF TABLES

LIST OF SYMBOLS

A	constant
a_c	cavity sound speed
a_0	free-stream stagnation sound speed
a_∞	free-stream sound speed
c	spring constant
D	cavity depth
f	frequency, Hz
g	acceleration of gravity
H	test section height
k	integer or wavenumber
k_v	vortex velocity/free-stream velocity
L	cavity length
M	Mach number, U/a_∞
M_s	shock propagation Mach number
m	integer or mass
n	integer
p_c	cavity static pressure
p_0, P_0	free-stream stagnation pressure
p_{rms}	rms fluctuating pressure
p_s	static pressure
p_∞	free-stream static pressure
q	dynamic pressure, $\frac{1}{2}\rho_\infty U^2$

Re	Reynolds number, $U\ell/\nu$
r	recovery factor, $(T_c - T_\infty)/(T_0 - T_\infty)$
S_1	Strouhal number, fL/U
S_2	Strouhal number, fL/a_0
s	acceleration
T_c	cavity static temperature
T_0	free-stream stagnation temperature
T_∞	free-stream static temperature
t	time
U	free-stream velocity
U_g	group velocity
U_p	streamwise velocity of shock pattern
U_s	normal shock propagation velocity
$\bar{u}_v$	average vortex velocity
W	cavity width or span
x,y,z	coordinates
ℓ	distance to cavity leading edge
α	phase delay parameter
γ	adiabatic exponent = 1.4
ζ	damping factor
Θ	angle
λ	(defined on p.6 and in Fig. 1)

λ	wavelength (in Appendix A)
μ	dynamic viscosity
ν	free-stream kinematic viscosity
ξ	acceptability factor
ρ_c	cavity air density
ρ_∞	free-stream density
ω	frequency, radians/second
$\frac{\partial h}{\partial x}$	slope of dividing streamline

SECTION I

BACKGROUND, SCOPE, AND OBJECTIVE

During the past fifteen years, a number of investigators have studied the aeroacoustic phenomena associated with pressure oscillations excited by flow over open cavities. Although these studies have shed considerable light on related aircraft structural and acoustic problems, additional information is needed for two important purposes: (1) to permit the designer to avoid unfavourable configurations and (2) to enable one to predict enough of the characteristics of the unsteady-pressure field so that one can assess its effect on crew and equipment. The present study is intended as a step toward supplying the lacking information and toward providing guidelines for accomplishing the aforementioned purposes.

The characteristics of unsteady flow over open cavities depend strongly on geometric, structural, and aerodynamic parameters. The occurrence and the magnitude of cavity pressure fluctuations are determined essentially by the balance between the energy available from the free-stream flow and the energy dissipated by cavity oscillations and the associated acoustic radiation. The predominant frequency regimes associated with cavity oscillations basically are functions of flow speed and cavity geometry; qualitatively small cavities – such as those that typically house air-probing instruments – produce high-frequency oscillations, and large cavities – such as bomb bays – produce low-frequency oscillations.

Aircraft structures are relatively insensitive to high-frequency excitation, but high-frequency acoustic energy, which is relatively well-transmitted by aircraft structures, may lead to adverse effects on crew performance or comfort. Low-frequency pressure oscillations, on the other hand, may lead to significant structural responses, which can produce structural damage, failure of store-restraint and release mechanisms, as well as damage of sensitive items within the stores; in addition, these oscillations also may affect the separation and the initial trajectory of a store.

Until the late fifties, research related to cavity pressure fluctuations concentrated on the subsonic speed range – e.g., see Refs. 1 and 2. Interest then turned towards transonic and (low) supersonic flow-speed research, giving rise to significant experimental[3] and theoretical work[3,4]. Of the many later research

projects dealing with cavity-related unsteady-flow phenomena, in both the subsonic and the supersonic speed ranges, the majority were wind-tunnel studies; a few flight programs were undertaken in the attempt to relate model results to full-scale measurements.

Almost all studies dealt with *empty* cavities of simple geometric shapes. A thorough wind-tunnel study — probably the best available — of a specific aircraft-bay configuration *including store* was performed by Rossiter and Kurn in 1963[5]. Some later flight tests performed at subsonic and transonic flight speeds, investigated a bay containing one asymmetrically located store[6]; however, this program was concerned primarily with vibratory response and yielded only limited pressure data on the store surface. These two studies appear to be the only ones — before now — dealing with cavity-flow/store interaction. One of the major objectives of the present study was to determine — in a systematic way — the effect of stores on pressure-fluctuation characteristics.

A cavity may be considered "deep" if its ratio of length (in the streamwise direction) to depth is smaller than unity; a cavity is considered "shallow" if its length/depth ratio is larger than unity. A *deep* cavity responds somewhat like an acoustic resonator, with the compressible fluid inside the cavity serving as the primary storage medium for oscillatory energy, which is provided by the shear layer above the cavity. The vorticity is primarily governed by the image vorticity in the forward and aft vertical walls of the cavity; therefore, the vortex motion tends to be in the direction of the depth, and the cavity is driven in a depth mode. A *shallow* cavity, on the other hand, converts input energy from the vortex sheet into fore-and-aft oscillations, because the vorticity is primarily governed by the images along the bottom wall; the cavity thus is driven in a length mode.

In the current study, emphasis was placed on shallow cavities, since these are of major interest for aircraft-bay configurations. Therefore, the theoretical considerations and the experimental study dealt only with cavities with length/depth ratios between 4 and 7. The present investigation also concerned itself only with cases where the cavity depth is much greater than the characteristic dimensions of the boundary layer upstream of the cavity; this restriction is justified by the practical cases of primary interest.

The broad purpose of the program — to achieve a better insight into the aeroacoustic phenomena that govern the response characteristics of bays (with and without store) to external flows at subsonic and supersonic speeds — required an evaluation of

existing theories and analytical approaches. The major portion of the total effort, however, consisted of an extensive parametric wind-tunnel study and the development of semiempirical prediction methods. Although complete understanding of all relevant phenomena is still lacking, the study did accomplish its primary objective – developing prediction schemes for the unsteady-pressure environment in open bays.

Although correlation of wind-tunnel test results with full-scale flight test results remains to be accomplished, one may have some confidence in the validity of the results pertaining to the dependence of oscillatory frequencies and broadband response on geometric and aerodynamic parameters. On the other hand, much more work needs to be done before the amplitude-limiting factors can be described with equal precision.

Section II of this Report discusses physical models of cavity oscillations and presents some theoretical aspects of the aeroacoustic behavior of shallow cavities. Section III describes the experimental study, Sec. IV deals with prediction methods, and Section V reviews the entire study. Some related problem areas and details are presented in the Appendices.

SECTION II

THEORETICAL BACKGROUND

A. Review of Physical Models

Of the relevant available literature – see Bibliography – this Section discusses only those studies that bear directly upon the subject of this investigation.

In his work on unsteady-pressure characteristics in cavities, Blokhintsev[7] simply equates an edge-tone frequency (determined by flow speed and distance of leading edge to trailing edge of a cavity) to an acoustic-resonance frequency of a cavity (calculated by Rayleigh) taking into account a mouth correction similar to that of a Helmholtz resonator. Experiments, however, revealed that some coupling mechanism between the edge-tone frequency and the cavity-response frequency had to be assumed in order to explain the deviation from the simple linear theory.

Gibson[3] solves the wave equation for rectangular cavities to determine possible resonance frequencies of a flow-cavity system. Using boundary conditions of "no pressure difference at the open surface" and " flow at the wall being parallel to the wall," he assumes the cavity to resonate at its natural frequencies in "room-mode resonances". Then, the resonant frequencies corresponding to different modes are given by

$$f_{res} = \frac{a}{2}\left[\left(\frac{k}{L}\right)^2 + \left(\frac{m}{W}\right)^2 + \left(\frac{2n+1}{2D}\right)^2\right]^{\frac{1}{2}} \qquad (1)$$

where a is the speed of sound in the cavity.

Equation 1 indicates all the resonant frequencies possible but cannot predict which of these frequencies will be excited by a particular configuration. Since resonant-mode frequencies – in particular those of higher order – are closely spaced on the frequency scale, almost any frequency of resonance can be justified by one room mode or another. To arrive at physical, meaningful, response characteristics, one must therefore select likely response frequencies – e.g., those corresponding to first- or low-order length and depth modes.

Gibson discusses various excitation mechanisms without arriving at a firm conclusion about the most likely one. He rejects the physical model of a jet-edge/cavity system that would cause the cavity to resonate at a nearby frequency. The argument is that this scheme could account only for one of the resonant frequencies of the cavity and not for all of the frequencies that in fact occur.

An alternate excitation mechanism – probably more valid in the high Reynolds-numbers regime at which he conducted the experiments – could be related to the broadband mixing noise in the shear layer over the cavity; the cavity would select those frequencies that correspond closest to its modal-response characteristics. Another source of mixing noise is the large captive vortex in the cavity driven by the outside flow. As an energy source, this vortex becomes proportionally weaker relative to the outside flow energy with increasing Mach number. This physical model could indeed account for the fewer response-frequencies that are excited at higher Mach numbers. (In light of the results of the present study, this model cannot be supported. See Sec. V.)

A final model considered by Gibson is the shedding of discrete vortices from the leading edge. Each time the vortex frequency – the fundamental or a higher harmonic thereof – approaches a resonant frequency of the cavity, oscillation is initiated. However, Gibson himself points out the inadequacy of this model at high Reynolds numbers, where discrete vortex frequencies are less likely and vorticity has a more random character. His experimental results were not sufficient to determine which of the various models is correct.

In analyzing those results, Covert[4] and Gibson[3] use a dimensionless Strouhal-number that, for a rectangular cavity, can be expressed as

$$S = \frac{f \cdot L}{U} = \frac{1}{2M} \left(\frac{T_C}{T_\infty}\right)^{\frac{1}{2}} \left[k^2 + \left(\frac{mL}{W}\right)^2 + \left(\frac{(2n+1)L}{2D}\right)^2\right]^{\frac{1}{2}} \qquad (2)$$

Since their rectangular cavities were neither very shallow nor very deep but rather cubical, length and depth modes (as well as apparently some spanwise modes) were observed. The experimental data, however, agreed reasonably well with the theoretical predictions of Eq. 2 only in the supersonic flow-speed range.

Dunham[1], whose primary work was in hydrodynamic cavities with flexible walls excited by water flow, also performed some relevant wind-tunnel tests at *low* speeds. His assumption of the formation of one or more large vortices in the flow above the cavity is physically appealing for the low-Reynolds-number regime. Through aerodynamic considerations, he shows that formation, convection, and trailing-edge impingement of the vortex results in a periodic entrainment and discharge of fluid into and from the cavity *mouth* whereby the mass of air in the cavity is periodically compressed but does not gain or lose any fluid. (Fig. 1) He thus effectively assumes — as do most other investigators — a hydrodynamic, rather than acoustic, feedback mechanism which is closely related to the geometry and aeroelastic properties of the cavity.

Using this model, Dunham also suggests the formulation of a Strouhal number S that employs (1) the ratio of length L of the cavity to the distance λ of the point of flow separation within the cavity from the rear wall and (2) the ratio of average vortex velocity $\bar{u}_v$ over a period T to the free-stream velocity U; thus,

$$S \equiv \frac{L}{\lambda} \frac{\bar{u}_v}{U} \tag{3}$$

However, because $\bar{u}_v$ and λ are difficult to determine, the above expression is probably of limited practical value.

Plumblee *et al.*[3] conclude from their extensive theoretical and experimental study that the response of cavities is dictated by the normal acoustic response of a cavity, indicating that the forcing mechanism would be the upstream boundary-layer turbulence. In the light of current knowledge, this idea cannot be supported.

The concept of treating the cavity oscillation as an acoustic response to pressure fluctuations in the turbulent boundary layer is valid only for a stable system. However, the combined system of cavity plus external flow is unstable; the amplitude of oscillations is very likely limited by nonlinear processes governing the shedding of vortices. As a demonstration that the excitation cannot be ascribed to boundary-layer turbulence, the introduction of a small flow spoiler upstream of the cavity, which increases the level of the input turbulence, is found to reduce oscillation amplitudes by an order of magnitude. Results of Krishnamurty's investigation[2] and of the current study show conclusively that an approaching laminar boundary layer is capable of initiating very

powerful oscillations that may exceed those resulting from a turbulent boundary layer for otherwise identical conditions.

Plumblee *et al.*[8] offer a prediction scheme for both the amplitudes and the frequencies excited; however, response calculations for shallow cavities require a substantial analytical effort. For the case of deep cavities, they offer a straightforward method to determine resonance frequencies; this method was later used by East[9] to predict resonance frequencies for deep cavities at low subsonic Mach numbers. East finds empirically that resonant conditions exist when the frequency of the acoustic resonance of the cavity equals the dominant frequency of the shear-layer feedback system, the argument being that only by virtue of this "doubly tuned amplification does the shear-layer unsteadiness (being the energy source) receive the least attenuation." East presents as an empirical relationship for resonant conditions

$$\frac{fD}{a}\left[1 + 0.65(L/D)^{0.75}\right] = 0.25 \qquad (4)$$

East essentially adopts the earlier model developed by Rossiter, who conducted several major studies[5, 10, 11, 12]. This model implies an acoustic feedback mechanism; periodic vortices are shed from the front lip of the cavity as a result of the arrival of an acoustic wave radiated from an acoustic source near or at the rear lip; this acoustic radiation, in turn, is a result of the vortices striking the rear lip. (Fig. 2) The mechanism produces frequencies of a sequence m-α, where m is the number of complete wavelengths of the vortex motion along the cavity; m must be postulated to equal the number of complete wavelengths of the acoustic radiation to satisfy the experimental evidence. α is a constant that takes into account the phase differences assumed to exist (1) between the upstream arrival of the acoustic wave and the subsequent shedding of a vortex and (2) between the downstream arrival of a vortex and the subsequent radiation of an acoustic signal. (This phase-difference constant seems to be somewhat dependent on the length/depth ratios.) On this basis, Rossiter derives, as a semiempirical formulation for resonance frequencies,

$$f = \frac{U}{L}\,\frac{(m - \alpha)}{\left(\frac{1}{k_v} + M\right)} = \frac{1}{L}\,\frac{(m - \alpha)}{\left(\frac{1}{k_v U} + \frac{1}{a_\infty}\right)} \qquad (5)$$

where $k_v U$ is the vortex convection speed, which is a fraction k_v of the free-stream flow speed U. The speed of sound, a, in the stream and in the cavity is assumed to be approximately equal.

East confirms Rossiter's model through additional experimental data and shows the effect of upstream boundary-layer thickness on the eddy convection speed and thus on the excitation frequency. He determines the unknown vortex convection speed through Eq. 5. This speed ranges from 35 to 60% of the free-stream flow speed, depending on the ratio of mean eddy-spacing to boundary-layer thickness.

Covert[4, 13] considers the cavity, the interface, and the external flow as problems of hydrodynamic stability and accounts successfully for the coupling between the internal energy-storage modes and the downstream transport of vorticity in the high-Reynolds-number regime for Mach numbers up to three or four. The response of a cavity depends on matching the perturbation potentials of the outer flow and the cavity flow (Fig. 3). Through theoretical reasoning it can be shown that a cavity is to respond only if the vortex sheet at the interface is perturbed so that it convects downstream at some other speed than that determined by the equilibrium – i.e., the steady-state condition at which no oscillations would exist. The perturbed vorticity then exerts a force onto the fluid, thus inducing a velocity in the fluid. The product of this force and this velocity determines the rate at which the vortex sheet (or vorticity) can do work on the cavity. Three cases are then possible: The rate of doing work is (1) less than, (2) equal to, or (3) larger than the ability of the cavity to dissipate energy through viscous losses or through acoustic radiation. In the first case, obviously any perturbations will be damped out and the cavity will not be excited. In the second case, at a certain definite, critical velocity, energy supply equals energy dissipation and the cavity energy-storage system is in a state of neutral stability. This critical velocity, which determines the lower bound at which the cavity can be excited, is termed "onset-velocity"[4, 13]. In the third case, where energy supply exceeds the ability of the cavity to absorb energy, the cavity will oscillate. The oscillation is controlled by the energy-storage system, which may be the fluid in the cavity (acoustic energy) or the elastic walls (as in Dunham's experiments). In treating the problem as a hydrodynamic stability problem, Covert calculates a curve of neutral stability that determines – for a given cavity configuration – the minimum velocity at which the cavity can respond. The cavity, however, can respond *only* at or near one of the natural frequencies of the energy-storage system; for onset conditions this is the *lowest* natural frequency.

Nothing is said about the upper velocity bound above which it has been found that the cavity ceases to respond; determining this upper bound would require a very complex analysis. Also, nothing can be said yet about the amplitude-limiting mechanisms that determine the levels in and around cavities, although the analysis suggests a high "Q" oscillator mechanism. Krishnamurty's results[2] as well as those obtained by East[9] and by the current study, suggest that shallow cavities are in fact analogous to a low "Q" oscillator. Theoretical considerations (Part B, below) advance alternate models that exhibit a low "Q" mechanism.

Most of the physical models discussed thus far assume the shedding of more or less discrete vortices from the cavity mouth as a "driving mechanism". Unfortunately, at high subsonic and supersonic free-stream flow speeds, such models are no longer acceptable. As pointed out by Baker[14], at these speeds the cavity mouth can effectively be regarded as being closed by a wake in which the vortex nature of the flow is diffused. In the supersonic-flow regime, the assumption of a random-character shear layer atop the cavity convected downstream at a speed probably halfway between the free-stream flow speed and the rotational flow speed in the cavity is presumably more valid. The shear layer itself then presumably follows the frequency of the natural energy-storage system, assuming a somewhat sinusoidal pattern, as suggested by Covert. To date, however, no valid physical model of the flow-field characteristics under a supersonic free stream seems to be available.

In conclusion, the few models offered to describe the phenomenon of pressure oscillations in shallow cavities in *subsonic* flow commonly assume a coincidence of a periodic shear-layer instability in terms of a rolling up of the shear layer into discrete vortices; this periodicity is closely tied to an acoustic response frequency — in this case a length mode of the cavity. Extension of this subsonic model into the supersonic regime failed, as did all simple frequency-prediction schemes. A model for the *supersonic* flow-speed regime can most likely be found in assuming a mutual reinforcement of a shear-layer instability and a cavity energy-storage system — a situation again closely tied to a free-stream flow speed and cavity geometry. In both subsonic and supersonic speed ranges, resonant frequencies can be expressed in terms of a Strouhal number. No valid, generally accepted model is available for amplitude prediction. Neither is there any theoretically derived scheme for predicting the aeroacoustic environment of *store-containing* cavities; prediction of frequencies and, in particular, of amplitudes is difficult enough for simple geometric shapes of *empty* cavities. There is, however, the qualitative observation of Leupold and Baker[15] that in some circumstances a resonance can be suppressed if the shear layer at the cavity is influenced by the store in the cavity.

B. Discussion of Response Characteristics of Shallow Cavities

Although the physical models discussed above are illuminating, they do not allow for quantitative predictions, other than the various simplified or semiempirical formulae for the resonant frequencies of a cavity.

A successful theoretical model should make possible prediction of both frequencies and amplitudes of the cavity response for a given set of conditions. Reference 4 tackled the problem of frequency prediction with considerable success, but the approximations necessary to permit computation of frequencies are applicable only to deep cavities. Approximation procedures appropriate to shallow cavities have not been found, and reliance has to be placed on semiempirical formulae such as those of Rossiter[12]. Covert's theory takes no account of either linear-dissipation effects due to viscosity or mass exchange or nonlinear effects. The discussion below is a preliminary attempt to relate the observed response of *shallow* cavities to these effects.

1. Dissipative mechanisms

Unlike deep cavities, which exhibit sharp narrowband behavior in their frequency/amplitude response characteristics, shallow cavities tend to exhibit a broader, less steep, response behavior and thus imply one of two possibilities: (1) if the cavity behaves as a linear system, the losses are quite high or (2) the cavity may behave as a nonlinear system. The former is plausible because the ratio of surface area to volume may be quite large in shallow cavities, and energy dissipation tends to increase with surface area.

If a cavity is considered as a classical single-degree-of-freedom system with an effective spring constant c and an effective mass m, then the (circular) natural frequency ω_n of that system obeys

$$\omega_n^2 = c/m \qquad (6)$$

One may note that ω^2 is equal to twice the strain energy stored per unit deformation and per unit mass. Similarly, the viscous damping coefficient c_1 is equal to twice the rate of energy loss at unit velocity amplitude; the damping factor, or ratio of c_1 to critical damping obeys

$$\zeta = \frac{c_1}{c_{crit}} = \frac{c_1}{2\sqrt{cm}} \tag{7}$$

For an acoustic cavity system, the "spring constant" c is approximately equal to γp, where p denotes the pressure, and γ the specific heat ratio; the mass is approximately equal to ρ/k^2 where ρ denotes the density and k the wavenumber of the oscillation for an acoustic cavity. Therefore

$$\omega_n^2 = \frac{\gamma p}{\rho} k^2 \tag{8}$$

The damping is usually attributed to radiation and viscous-energy dissipation; however, these two factors are small. If one afterwards neglects the quadratic terms, he finds

$$c_1 = \mu k^2 \tag{9}$$

where μ denotes the viscosity, so that

$$\zeta = \frac{1}{2} \frac{\mu k^2}{\sqrt{\gamma p \rho}} = \frac{1}{2} \frac{\mu}{\rho} \frac{k^3}{a} \tag{10}$$

This value turns out to be extremely small, of the order of $\sim 10^{-7}$, so that for a linear system, one need not include this source of damping in the model of the unsteady flow.

To evaluate the convective losses, one may consider the mass in the cavity as a function of time and apply the WBKJ approximation[16] to the simple mass-spring system to obtain an amplitude function x(t) in the following form:

$$x = e^{-c_1/2 \int_0^t dt/m(t)} \cdot \frac{e^{-i\int_0^t \sqrt{\frac{c}{m(t)}\left(1 - \frac{c_1^2}{4m(t)c} + \frac{c_1 m}{cm(t)}\right)}dt}}{\sqrt{\frac{c}{m(t)}\left(1 - \frac{c_1^2}{4m(t)c} + \frac{c_1 m}{cm(t)}\right)}} \tag{11}$$

This expression implies that the effects of variable mass can lead to large damping without a serious reduction in frequency.

For sinusoidal mass variation given by $m(t) = m_0 (1+\varepsilon \cos \omega t)$, where $\varepsilon < 1$, the real exponential factor in Eq. 11 becomes

$$\exp -\left[\frac{c_1}{m_0\omega\sqrt{1-\varepsilon^2}} \tan^{-1}\left(\frac{\sqrt{1-\varepsilon^2}\tan\frac{\omega t}{2}}{1+\varepsilon}\right)\right] \quad \text{for } -\pi \leq \omega t \leq \pi \tag{12}$$

whose argument varies from 0 to $c_1\pi/2m_0\omega\sqrt{1-\varepsilon^2}$ The damping can be quite large* if $\varepsilon \approx 1$. Also, the damping is large over part of the cycle and changes sign over part of the cycle, thus tending to make the wave one-sided.

If c is moderately large, then the natural frequency ω_n of the damped system may be obtained from

$$\omega_n t \approx \sqrt{\frac{c}{m_0}} \int_0^t \frac{dt}{\sqrt{1-\varepsilon\cos\omega t}} = \sqrt{\frac{c}{m_0}} \frac{2\sqrt{2}}{\omega\sqrt{2+\varepsilon}} F\left(k_0, \frac{\omega t}{2}\right) \tag{13}$$

where

$$k_0^2 = \frac{4\varepsilon}{2+\varepsilon} < 1 \quad (\text{for} \quad \varepsilon < 0.67) \tag{14}$$

and where

$$F\left(k_0, \frac{\omega t}{2}\right) = \int_0^{\omega t/2} \frac{d\theta}{\sqrt{1-k_0^2\sin^2\theta}} \tag{15}$$

represents an elliptic integral of the first kind.

*For example, for $\varepsilon = 0.5$,

$$\frac{c_1\pi}{2m_0\omega(1-\varepsilon^2)} \approx \frac{4.2\ c_1}{2m_0\omega} \approx 4.2\ \zeta$$

Recalling that

$$F\left(k_0, \frac{\omega t}{2}\right) \approx \frac{2}{\pi} k \cdot \frac{1}{2} \omega t - \frac{1}{2} \left[\sin \omega t\right] \left[\left(\frac{1}{2} \underline{k}\right)^2 + \frac{1 \cdot 3}{2 \cdot 4} \left(\frac{1}{4} \sin^2 \frac{1}{2} \omega t + \frac{3}{2 \cdot 4}\right) \underline{k} + \ldots \right] \tag{16}$$

and that

$$K \approx \frac{\pi}{2} \left[1 + \left(\frac{k}{2}\right)^2 + \left(\frac{1 \cdot 3}{2 \cdot 4} \underline{k}^2\right)^2 + \left(\frac{1 \cdot 3 \cdot 5}{2 \cdot 4 \cdot 6} \underline{k}^3\right)^2 + \ldots\right] \tag{17}$$

one finds that

$$\omega_n t = \omega_0 t \sqrt{\frac{2}{2+\varepsilon}} \left[1 + \frac{k^2}{4} + \left(\frac{1 \cdot 3}{2 \cdot 4} k^2\right)^2 - \frac{\sin \omega t}{\omega_0 t} \left(\frac{k^2}{4} + \ldots\right)\right] \tag{18}$$

for $\frac{k_0^2}{4} = \frac{\varepsilon}{2+\varepsilon} < \frac{1}{4}$.

Some values of the ratio ω_n/ω_0, as calculated from this result are tabulated below

ε	.1	.2	.5	.67
$\frac{\omega_n}{\omega_0}$	.999	.99	.96	1.07

Thus one finds that even for relatively large values of ε, the frequency is not altered very much. If $\varepsilon > 0.67$, drastic changes take place. The solution becomes exponentially unstable over part of the cycle.

As a speculation, then, one feels that any theoretical analysis must include the possibility of forced convection giving rise to a variable mass in the system. Note that even if $\omega_n/\omega_0 \approx 1$ there is a modulation due to the time-variable damping and the denominator of the WBKJ solution. Inclusion of variable mass does not make the equations *per se* nonlinear; however, the mass addition will probably be a nonlinear function of the external pressure.

2. Cavities with internal store

Consider now the effect of store in the cavity. If the store volume is small compared to the cavity volume, the cavity acoustic properties remain relatively unchanged. However, there is a marked effect if the store is located in the shear layer at the cavity mouth, because such a store then greatly influences the energy transfer to the cavity. Considering that the basic problem has yet to be solved for empty cavities, it is not surprising that no solutions exist for cavities with stores.

The presence of one or more stores in a cavity affects the acoustic behavior primarily for two reasons: (1) stores change the volume and shape of the cavity and may increase the boundary area of the acoustic volume and (2) waves may be refracted about the store. The first effect is relatively unimportant for wavelengths that are not short in comparison to the store diameter; the second effect is significant only for stores interfering with the boundary layer at the mouth of the cavity. Covert's results[4], which are based upon the behavior of the vortex sheet at the mouth, suggest that stability is sensitive to this interference. Ffowcs-Williams[17] shows that the nature of the moving streamline diminishes the generation of acoustic energy at supersonic Mach numbers. A store interacting with the streamline surface should reduce the streamline motion. Data[18] shows that interference with the vortex sheet at the mouth of the cavity greatly alters the frequencies and amplitudes of the sound.

C. Discussion of Pressure-Amplitude Predictions

All attempts to predict pressure amplitudes on a theoretical basis thus far have failed for lack of a detailed understanding of the physical process. The importance and effectiveness of relevant energy-dissipation mechanisms cannot be determined, since at present it is not even clear which of the various conceptually possible mechanisms (namely, viscous losses, acoustic radiation, shedding of strong periodic disturbances in the downstream boundary layer, and convective mass exchange) plays the dominant role. The linear amplitude-limiting model, which has been suggested, has had no practical success. The nonlinear effects, which are likely to affect the energy-input and/or energy-loss mechanisms, are largely unexplored and therefore not accessible to theoretical treatment.

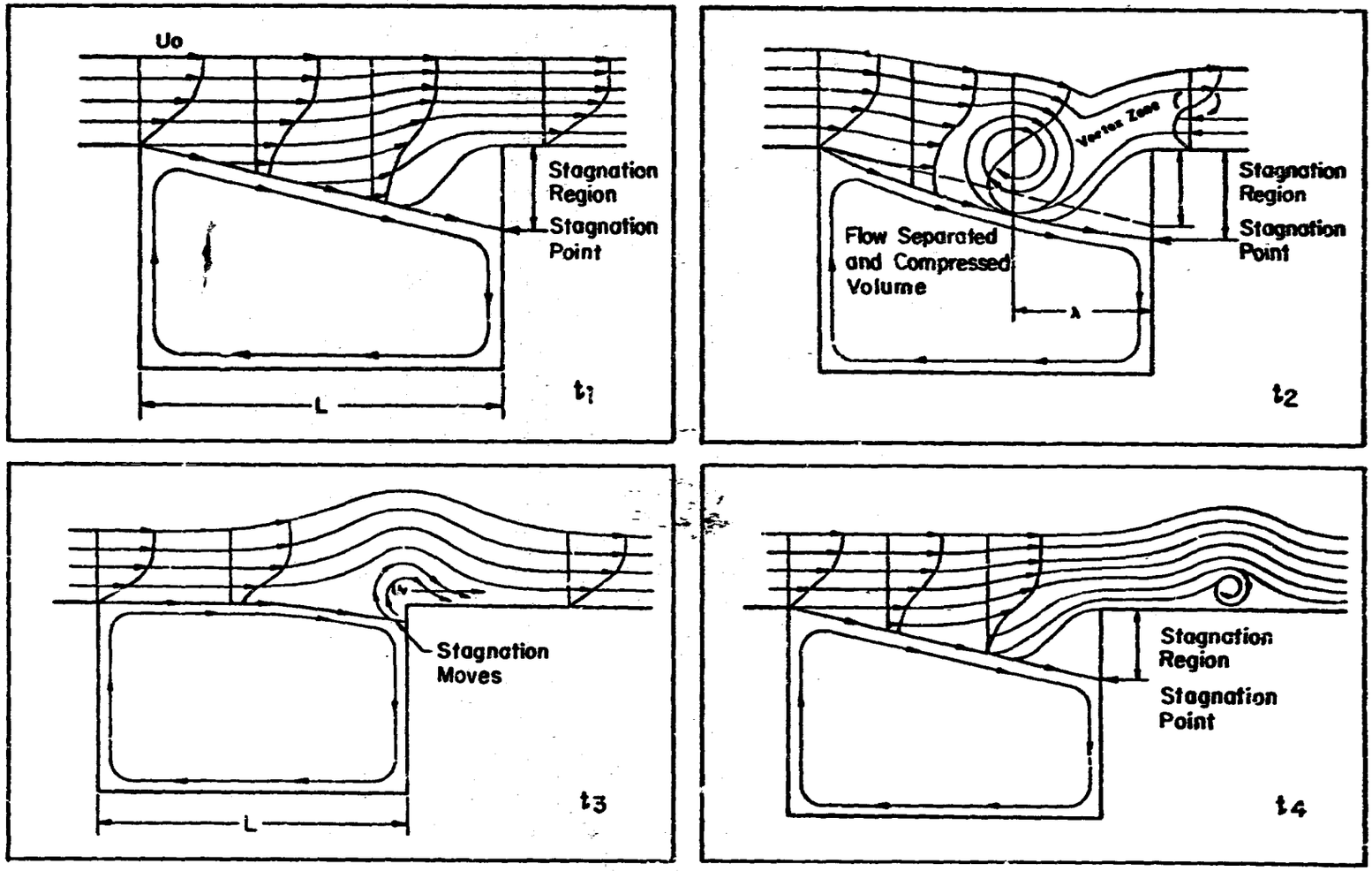

FIGURE 1. DUNHAM's HYDRODYNAMIC MODEL. (FROM REF. 1.)

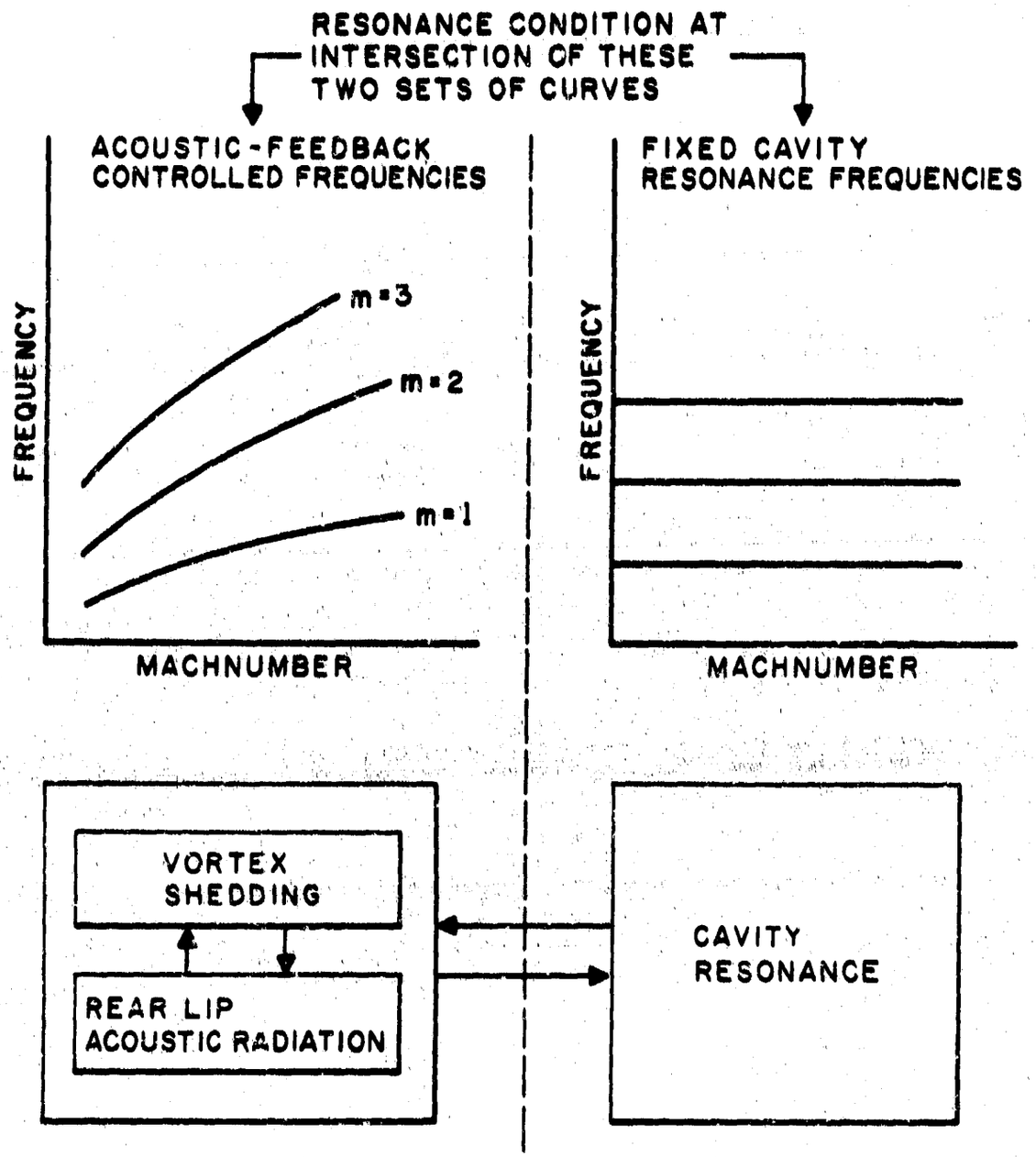

FIGURE 2. CONCEPT OF ROSSITER's MODEL.

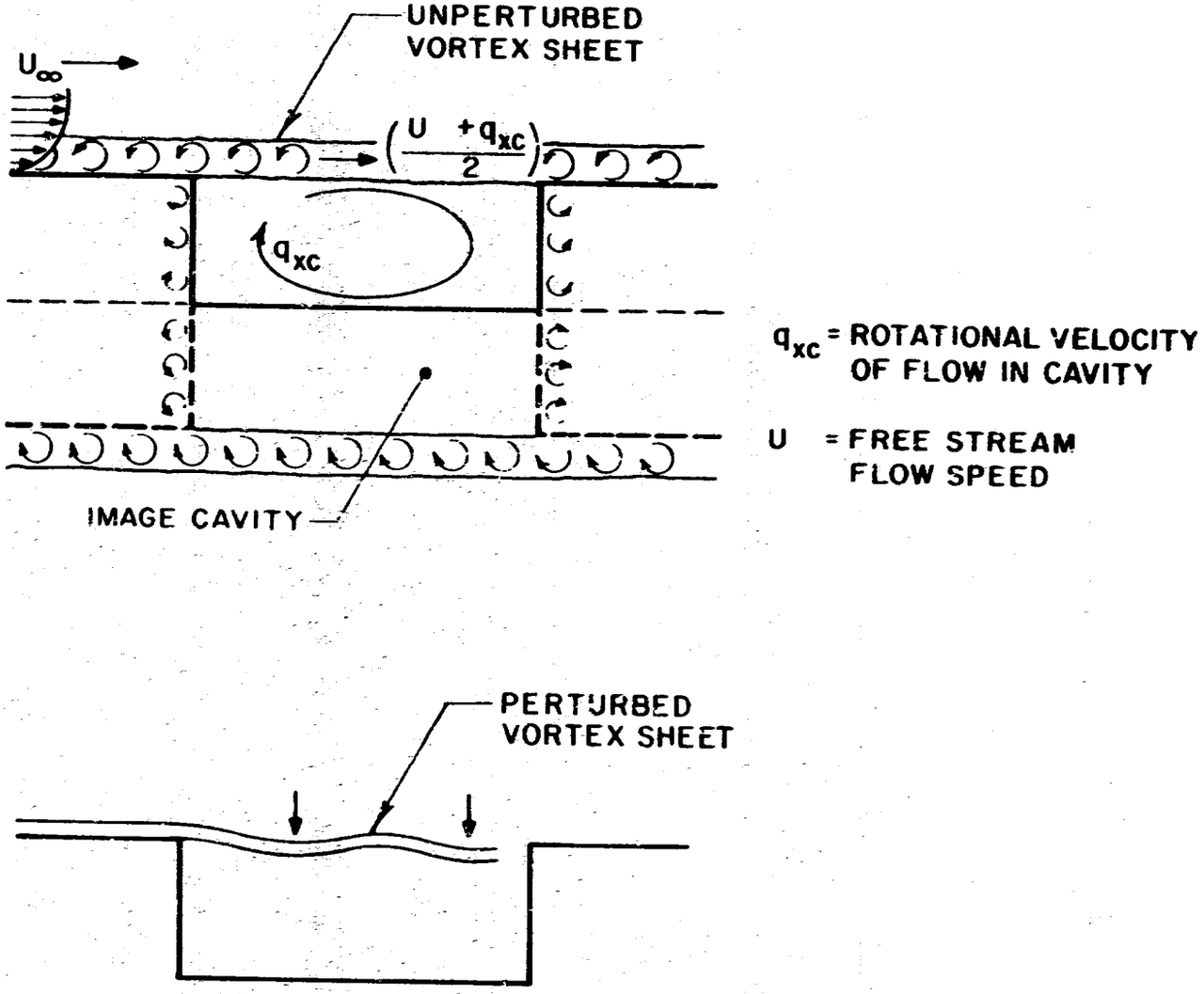

FIGURE 3. COVERT's MODEL-- EXISTENCE OF OSCILLATION DEPENDS ON THE ABILITY OF THE VORTEX SHEET TO DO WORK AND THE ABILITY OF THE CAVITY TO ABSORB WORK.

SECTION III

EXPERIMENTS

A. Scope of Experimental Studies

Few of the research projects concerning cavity oscillations pertain *directly* to aircraft structures, and even fewer present unsteady-pressure data in terms of spectra and levels. Primary criteria for the results being applicable to, say, an open weapon-bay configuration are that (a) the cavity be shallow, (b) the boundary-layer thickness upstream of the cavity mouth be much smaller than the cavity depth, and (c) the relevant Reynolds number based on the cavity depth be large – generally in excess of one million.

In this restrictive sense, the most useful studies are those by Krishnamurty[2], Plumblee *et al*[8], Morozov[18,19], White and McGregor[20], and, in particular, Rossiter[10,11,12] and Rossiter and Kurn[5]. With the exception of Refs. 10 and 11, all of these were wind-tunnel studies, of simple rectangular cavities or of scale models of bomb bays[5]. The only studies of store-containing cavities are reported in Ref. 5, which deals with scaled bomb-bay configuration and in Ref. 6, which contains data on a missile in an actual aircraft bay but offers only limited fluctuating-pressure information.

The experimental part of the current study, therefore, was directed at obtaining data both for empty and store-containing cavities for a variety of aerodynamic and geometric parameters so that existing results could be substantiated and then extended to yet unexplored regimes. Of particular importance was the acquisition of *fluctuating-pressure* data within and near the test cavity; however, data on *steady-state* pressure distribution, cavity temperature, and recirculating velocities of the captive vortex in the cavity were also obtained. Thus, a rather complete picture of the relevant aeroacoustic phenomena was developed.

The wind-tunnel test program was designed as a compromise between the desire to test realistic configurations and the need to explore a variety of configurations that might lead to a complete understanding of the mechanics of cavity oscillations.

Testing was restricted to shallow cavities with length/depth ratios of four or greater, as this is the range of greatest practical interest. The test Mach numbers ranged from 0.8 to 3. (No

testing was attempted at transonic Mach numbers, but even at Mach number 0.8 some tunnel-interference effects were apparent – see Appendix I.)

Tunnel stagnation pressures of 2, 5, 10, and 15 psia were used to determine how the unsteady pressures in the cavity compare with the free-stream dynamic pressure. Equivalent altitudes range from 11,000 ft (15 psia at Mach number 0.8) to 120,000 ft (2 psia at Mach number 3). (Variations in stagnation pressure at a given Mach number and stagnation temperature are accompanied by variations in Reynolds number and various tunnel boundary-layer parameters.)

The instrumentation was selected to provide both a general view of the mean flow and a detailed picture of the unsteady-flow components. Mean-flow instrumentation was designed to provide data on the mean pressure distribution, mean air temperature, and mean recirculation velocity in the cavity. Unsteady-flow instrumentation consisted of a number of microphones distributed within the cavity at locations selected to permit identification of all possible cavity-response modes. One microphone, located in a rod that extended over the length of the cavity could be moved back and forth to provide detailed pressure surveys.

Means were provided for processing the microphone output in one of three ways: (1) a tape recording for later analysis, (2) a narrowband variable filtering, and (3) a one-third-octave band real-time spectrum analysis.

E. Wind-Tunnel Test Set-Up

1. Facilities and apparatus

The wind-tunnel portion of the test program was conducted in the MIT Naval Supersonic Wind Tunnel, a continuous-flow tunnel with a test section 18 in. wide by 24 in. high for Mach numbers up to 2.5 and a test section 18 in. by 18 in. for higher Mach numbers. Nozzle blocks used in this test series produced nominal Mach numbers of 1.5, 2, and 3; however, a subsonic nozzle block was used for testing at the nominal Mach number of 0.8. Stagnation pressures available at these Mach numbers range from below 2 psia to about 20 psia. The approximate range of Reynolds number/ft is then 0.5×10^6 to 5×10^6. Exact figures are given in Table I.

TABLE I. FREE-STREAM PARAMETERS AS FUNCTION OF MACH NUMBER

Mach No.	Stagnation* Pressure (psia)	Dynamic Pressure (psia)	Static Pressure		Reynolds† Number/ ft × 10^{-6}
			(psia)	(dB)	
0.8	2	0.587	1.31	173.1	0.54
	10	2.94	6.56	187.1	2.7
1.5	2	0.856	0.544	165.5	0.59
	10	4.28	2.72	179.5	2.9
2	2	0.716	0.256	158.9	0.49
	10	3.58	1.28	172.9	2.5
3	2	3.43	0.0544	145.5	0.30
	10	1.71	0.272	159.5	1.5

*Assumed T_0 of 100°F.

†From NACA Report No. 1135.

During all tests the lower nozzle block was removed and replaced by a wooden insert occupying the lower 50% of the channel (Fig. 4). This insert was joined smoothly to a 1/2-in. thick aluminum plate which spanned the test section and in which the test cavity was installed. The plate was joined downstream to a simple plywood diffuser block.

2. Cavity model

An overall schematic of the cavity model is shown in Fig. 5. The aperture for the model is cut into the aluminum plate spanning the test section. The cavity itself, 20 in. long and 7 in. wide,

lies on the center line of the tunnel, approximately centered on the tunnel windows. The cavity structure includes a heavy aluminum base plate that attaches to the tunnel floor. The upstream and downstream walls of the cavity are 1-in.-thick aluminum plates, bolted to the base plate and the upper plate. The side walls are 1/2-in.-thick glass plates that are flat enough to give good Schlieren quality and are held in place by aluminum rods and compressed rubber gaskets.

The cavity depth is continuously (and remotely) variable between 2.8 in. and 6 in. The position of the cavity floor may be measured by reference to a transparent scale attached to one of the glass sidewalls. The floor is sealed against the cavity walls by Teflon strips, which rub against the upstream and downstream walls and must support end loads; these seals are backed by heavily compressed O-ring gasket material and brass packing strips. The seals against the side walls, which must provide an air seal only, are backed by foam-rubber packing.

On the cavity center line – 2 in. below the surface plane and spanning the length of the cavity – is a 3/4-in.-diameter steel rod, which carries a microphone.

The rigid metal and glass cavity structure cannot be expected to have high inherent vibration damping. Simple calculations of natural frequencies of the floor, walls, traversing-microphone support rod, etc. showed that it was not possible to design the structure so as to separate the frequency ranges of structural and expected acoustic resonances. It was hoped, however, that the massiveness of the structure would ensure a sufficient mismatch between the structural vibrations and the acoustic resonances to prevent significant coupling of the two.

3. Instrumentation

Measured experimental quantities fall into two categories – mean-flow quantities and unsteady-flow quantities.

Mean-Flow Quantities

Pressures: Stagnation pressure and static pressure of the airflow in the test section are read from gauges on the tunnel-control console. There are six static pressure taps within the cavity: three on the floor, one on the front bulkhead, and two on the aft bulkhead (Fig. 6). The pressures are read on silicone-fluid or mercury multitube manometers referenced to vacuum. The choice of manometer fluid is governed by the expected pressure range.

Cavity Recirculation Velocity: A pitot-static tube is located near the center of the cavity floor, 0.5 in. above the floor and facing aft. Pressures are read on the same manometer bank as are the static pressures. (The pitot tube faces aft in the cavity in anticipation of a recirculation driven by the mean flow.) The height above the floor is such that the tube clears the internal boundary layer on the cavity floors.

Cavity Temperatures: The hot junction of an iron-constantan thermocouple is set flush with the surface in a small epoxy plug near the center of the cavity floor. The cold junction is maintained at 32°F. This thermocouple provides an estimate of the static temperature of the recirculating flow in the cavity – and thus of the sound speed in the cavity. (Imperfect thermal insulation of the thermocouple from the aluminum plate and significant recirculation velocities may introduce some errors in this temperature measurement.)

Unsteady-Flow Quantities

Fluctuating Pressures: Unsteady-flow data were sensed by means of ten microphones. These microphones (BBN Type 376) are small piezoelectric units with the impedance matching circuit (FET) incorporated as an integral part of the unit. These microphones are located as shown in Fig. 7 – one upstream of the cavity in the approaching boundary layer, five in the cavity floor, one in the rear bulkhead of the cavity, one in each side wall, and one in the traversing rod.

Vibration: Vibration levels were measured at one center location on the cavity floor to permit estimation of whether or not these vibrations would interfere with the microphone measurements. One BBN Model 501 accelerometer was used.

Data Acquisition: Figure 8 is a block diagram of the data-acquisition system; the components are

10 BBN Model 376 transducers
1 BBN Model 501 accelerometer
1 common power supply (switched to each microphone individually and to the one accelerometer)
1 General Radio, Type 1551 sound level meter
1 General Radio, Type 1921 real-time analyzer
1 Tectronix, Type 305a oscilloscope
1 Polaroid camera (Tectronix attachment)
1 tape recorder (for occasional use only)
1 Bruël and Kjaer, Type 2107, narrowband frequency analyzer.

For each test condition, 1/3-octave band spectra were displayed in real-time on the scope screen and photographically recorded for later analysis.

4. Flow visualization

One black-and-white Schlieren photograph was taken during each test run. The exposure time of the Schlieren optical system - of the order of a few microseconds - gives effectively an instantaneous picture of the unsteady flow.

High speed motion pictures were taken during several of the runs. The Fastax camera was operated at a nominal speed of 2,500 frames per second, recording approximately 2.5 seconds real-time on one roll of film.

Wool tufts placed at several points in the cavity provided a qualitative view of the mean flow in the cavity.

5. Stores

The store configuration and mounting arrangement are shown in Fig. 9. The stores were of cylindrical shape (2-in. diameter) with a 3:1 ogive-nose cone. Total length of each store was 16 in. Being rigidly fixed to the cavity floor, the stores vary in position relative to the cavity mouth as the depth changes.

6. Test conditions

Tests were performed at all conditions shown in Table II.

7. Additional tests

Flat-Plate Tests: A reference fluctuating-pressure level in the upstream boundary layer was determined by a series of tests in which a covering plate was flush with the cavity mouth.

Half-Scale Cavity Tests: Appendix I discusses a series of tests with a cavity 11.4 in. long. These tests were necessary to check on a tunnel interference effect that was observed at subsonic Mach numbers.

TABLE II. TEST PROGRAM

Run Number	Mach Number	Store Configuration	Stagnation Pressure psia	L/D
1	0.8	0	2	4
2	↓	↓	↓	5.7
3	↓	↓	2	7
4 – 6	↓	↓	5	As Above
7 – 9	↓	↓	10	As Above
10 – 12	↓	0	15	As Above
13 – 24	↓	1	As Above	
25 – 36	0.8	2	As Above	
37 – 72	1.5	As Above		
73 – 108	2	As Above		
109 – 144	3	As Above		

C. Experimental Results – Empty Cavity

1. Schlierenoptical flow visualization

Figures 10 through 12 are Schlieren photographs taken during runs at L/D = 4, at Mach numbers 0.8, 1.5, and 2, and at one stagnation pressure of 10 psia. (Flow direction is from left to right.)

Tests at Mach number 0.8 produced an unexpected unsteady shock pattern that was visible in all Schlieren photographs – e.g., see Fig. 10. The variation in shock pattern from photograph to photograph for otherwise identical conditions implies

that the shock-wave pattern is not stationary – as one would expect for supersonic flow conditions. It was ascertained that the appearance of the shock pattern is not caused by some shortcoming of the facility; when the cavity mouth was covered with a flat plate (resulting in an undisturbed boundary layer), moving shock fronts were not observed. An explanation of this strong interference effect is presented in Appendix I.

Flow visualization in Figs. 10, 11, and 12 reveal the turbulent boundary layer atop the cavity mouth being heavily disturbed by the cavity response. One might attempt to draw the dividing streamline by following the upper contour of the boundary layer. This procedure would qualitatively indicate the instantaneous location of the dividing streamline; however, one should bear in mind that since the Schlieren system shows an integrated picture across the cavity width, identification of flow patterns is difficult. Figure 13 shows schematically a dividing – streamline oscillatory motion for conditions of cavity resonance. The shock-wave front travels away from the initial disturbance (i.e., the oscillating vortex sheet) much the same way an acoustic wave would propagate in this environment; the environment itself is characterized by the presence of high-speed flow – and, unfortunately, of the tunnel roof. The basic inclination of the shock front is, of course, determined by the Mach angle. Shock-front curvature is determined by the wavy shape of the initial disturbance. This qualitative behavior might be depicted in the Figures. As Fig. 13 shows, a short-time-exposure Schlieren photograph gives only an instantaneous picture of a boundary-layer situation.

One can see from these photographs that the oscillatory motion of the boundary layer near the cavity trailing edge could result in the periodic mass entrainment and mass ejection postulated in Sec. II B as a possible dissipative mechanism. Two more qualitative findings that could be associated with the behavior of the boundary-layer flow as visible in the photographs are:

1. The disturbance is greatest for the subsonic ($M = 0.8$) and the low supersonic ($M = 1.5$) Mach numbers and seems to decrease for higher Mach numbers ($M = 2$). [At a Mach number of 3, in particular, the flow is, in fact, quite undisturbed (Fig. 14). This visual observation of the disturbance magnitude correlates precisely with the magnitude of the fluctuating pressures for the various Mach numbers as measured by the microphones.]

2. The disturbance grows towards the trailing edge. (This observation correlates with the finding that the broadband

fluctuating-pressure levels also increase along the longitudinal axis towards the cavity rear wall.)

Figure 15 presents the flow picture for the empty cavity at L/D = 4, at M = 3, and at a stagnation pressure of only 2 psia. The boundary layer is evidently laminar and exhibits a wavy pattern – in contrast to Fig. 14 where, at P_0 = 10 psia, the boundary layer was turbulent and exhibited no evidence of a wavy pattern. Figures 16 and 17, in which the cavity mouth was closed with a coverplate, show the undisturbed boundary layer along the tunnel wall. For M = 3, a stagnation pressure of 2 psia produces a laminar boundary layer and a stagnation pressure of 10 psia produces a turbulent boundary layer. Reference fluctuating-pressure spectra were obtained for these conditions.

2. Mean-pressure data

Mean pressures were measured at 8 different locations during each run. Two of these locations provide information on the recirculation velocity through a pitot-static tube; the other six yield static-pressure information on the cavity floor and walls.

Typical results appear in Fig. 18, where data are presented as the difference between the static pressure in the cavity P_c and the free-stream static pressure P_∞ normalized with the free-stream static pressure. The distribution of static pressure on the cavity floor is shown for all Mach numbers for the empty cavity, for L/D = 4, and for 10 psia stagnation pressure. Data points were obtained from the pressure taps located at 0.1, 0.5, and 0.9 of the cavity length; additional data points for Mach number 3 and for 2 psia stagnation pressure – where the upstream boundary layer is laminar – are presented in the same plot. Figure 19 shows an arithmetic mean of the measured pressures at the three points, with the mean plotted as a function of Mach number. Also shown are points obtained by interpolation from Rossiter's results[12] for the same L/D ratio. The agreement is gratifying.

At low Mach numbers, pressures increase towards the rear of the cavity. At higher Mach numbers, the pressures at the front of the cavity increase, leading to a more uniform pressure distribution and a higher mean. Static pressures in the cavity are considerably higher for a laminar boundary layer than they are for a turbulent boundary layer.

3. Recirculation velocities

Visual observation of the tufts confirms the accepted picture of a mean flow comprising a single trapped eddy, driven by the mean flow.

The pitot-static tube was used to obtain estimates of the recirculation Mach numbers. If P_s is the local static pressure and P_0 the isentropic stagnation pressure, then the local Mach number is given by the expression

$$M_c = \left(\frac{2\varepsilon}{\gamma}\right)^{\frac{1}{2}} \left[1 + \frac{\gamma - 2}{4\gamma}\,\varepsilon + O(\varepsilon^2)\right] , \qquad (19)$$

where $\varepsilon = (P_0 - P_s)/P_s$ and $O(\varepsilon^2)$ represents terms of order ε^2.

Recirculation Mach numbers are calculated by assuming that the pitot-static tube measures P_0 and P_s and by retaining only the first term in the above expansion. The results are presented in Fig. 20. No attempt is made to distinguish between different store configurations, as the effect of stores on the velocity measured at the pitot-static tube is unclear from these results. It is apparent that the recirculation velocity increases with depth.

At Mach 3, when a laminar boundary layer upstream of the cavity exists at the low stagnation pressure, recirculation velocities frequently cannot be measured because the measured stagnation pressure is not larger than the measured static pressure. Only two points (solid) can be presented in Fig. 20. It seems that the turbulent boundary layer tends to drive a much greater recirculation than a laminar boundary layer.

4. Cavity temperatures

The temperatures measured at the thermocouple inside the cavity are presented as a recovery factor r equal to $(T_c - T_\infty)/(T_0 - T_\infty)$. T_c is the cavity temperature, T_0 is the stagnation temperature of the free stream, and T_∞ is the free-stream static temperature as computed from T_0 and the free stream Mach number. Calculated values of r are subject to error because of the difficulty in synchronizing measurement of T_c with a varying value of T_0.

Results are presented in Fig. 21, with only the range of recovery factor at each Mach number being shown. The scatter of the results makes it impossible to observe any dependence of recovery factor on cavity depth, store configuration, or stagnation pressure. Only a slight increase with Mach number is evident.

Recovery-factor data is of practical use in estimating the speed of sound in the cavity. Assuming that the measured T_c represents the temperature of the air in the cavity, then the sound speed in the cavity is represented as

$$a_c = a_\infty \left[1 + r \left(\frac{\gamma - 1}{2}\right) M^2\right]^{\frac{1}{2}}, \qquad (20)$$

a_c is the cavity sound speed; a_∞ is the free-stream sound speed. When $r = 1$, $a_c = a_0$, the stagnation sound speed. At $M = 0.8$, decreasing r from 1.0 to 0.8 decreases a_c by about 0.3%. At $M = 3$, decreasing r from 1.0 to 0.9 decreases a_c by about 3%. Thus, at the lower Mach numbers, the error involved in assuming that the cavity temperature is the free-stream stagnation temperature is negligible; at higher Mach numbers, the error is only a few percent.

It is not possible, at Mach number 3, to distinguish between recovery factors measured at 2 psia stagnation pressure (laminar upstream boundary layer) and at 10 psia stagnation pressure (turbulent upstream boundary layer). It is not appropriate, therefore, to assume that cavity recovery factors bear any relation to recovery factors in the upstream boundary layer.

5. Unsteady-pressure data — presentation of spectra

Of 144 wind-tunnel runs originally scheduled, 75 were performed. Each of these produced at least 10, usually 15, and sometimes 20 pressure-spectrum photographs. Only a limited number of spectra are presented in this Report. Spectra were selected either as evidence to support conclusions offered in the body of the Report or as background information in areas where definite conclusions cannot be drawn.

All spectra in this Report show fluctuating-pressure levels scaled with respect to the free-stream dynamic pressure, which is computed from nominal Mach numbers and nominal stagnation pressures. As in acoustics, the wide range of unsteady pressures requires the logarithmic presentation 20 log p/q, where p is the fluctuating

pressure and q is the dynamic pressure. The additive corrections in the following Table permit rapid translation to sound-pressure levels referenced to .0002 μbar or to free-stream static pressure. The latter translation makes possible a comparison of mean- and unsteady-pressure levels in the cavity.

TABLE III. PRESSURE-REFERENCE CONVERSION.*

Mach Number	Stagnation Pressure (psia)	Dynamic Pressure dB re 0.0002 μbar	Dynamic Pressure dB re Static Pressure
0.8	2	166.0	- 7.1
	10	180.0	- 7.1
1.5	2	169.4	3.9
	10	183.4	3.9
2	2	167.8	8.9
	10	181.8	8.9
3	2	161.5	16.0
	10	175.5	16.0

*To convert to 0.0002 μbar reference level, add the quantity in column (3); to convert to free-stream static reference, add the quantity in column (4).

All spectra were traced directly from an oscilloscope picture. Each step in the curve gives the level in each 1/3-octave band. Center frequencies of only every third 1/3-octave band are shown. Where more than one spectrum is shown on a figure, the curves are identified as often as is necessary to disentangle them.

6. Unsteady-pressure data – scaling with dynamic pressure

Figures 23 through 26 present 1/3-octave-band spectra of fluctuating-pressure levels measured at microphone #6, which lies close to one of the rear corners of the cavity floor (see Fig. 7). This location was chosen for analysis since levels are high at the rear of the cavity, and a microphone in a corner of the cavity should detect pressure oscillations in any normal mode.

The fluctuating pressures scale with free-stream dynamic pressure* at M = 0.8 (Fig. 23), at M = 1.5 (Fig. 24), and at M = 2 (Fig. 25). In each case the nondimensional amplitudes in a given band typically do not differ by more than 2 dB; this difference is not significantly greater than the inherent error of the data-recording-and-analysis procedure – e.g., the two stagnation pressures differ by a factor of 5, which is equivalent to 14 dB. The divergence is somewhat greater at higher frequencies.

At M = 3 (Fig. 26), however, the scaling fails. The pressure fluctuations (relative to free-stream static and dynamic pressures) differ at the two stagnation pressures both in amplitude and in frequency content. The significant difference in the test conditions between the two stagnation pressures is that at 2 psia, the boundary layer ahead of the cavity was laminar; at 10 psia it was turbulent (Figs. 14 and 15). At lower Mach numbers, the upstream boundary layer was always turbulent within the test range of stagnation pressures. As the stagnation pressure was increased during runs at M = 3, the flow transition was readily observed to occur at 3.4 to 3.6 psia. For comparison, see the Schlieren photographs (Figs. 16 and 17) obtained during flat-plate tests at M = 3, at 2 psia, and at 10 psia (stagnation pressure). The occurrence of transition could also be observed at microphone #1, located in the plate surface upstream of the cavity (Fig. 27).

From these results, it is evident that *some boundary-layer parameters must be included in a theory of the amplitude of the response of a cavity*. Available data are insufficient to define what these parameters must be; it has been found, so far, only that (1) for a turbulent upstream boundary layer, the pressure-fluctuation characteristics in the cavity are insensitive to a Reynolds number change of 5 to 1 (for the particular experimental conditions), and (2) the transition from a laminar to a turbulent boundary layer greatly alters the cavity response. For work related to the second conclusion see Ref. 8, which in addition to extensive data, presents a theory that the pressure oscillations in the cavity are generated by a linear response to pressure fluctuations in the turbulent boundary layer. Figure 26 disproves this

*Contrary to the original test plan (stagnation pressures of 2, 5, 10 and 15 psia), testing could be restricted to P_0 = 2 and 10 psia, since no failure of scaling with dynamic pressure was evident (Fig. 23).

theory; in fact, the laminar boundary layer produces the more intense fluctuations in the cavity, despite its own lower noise levels. Krishnamurty's results[2] support this latter conclusion.

However, it is still not known how (and whether) the upstream boundary-layer characteristics relate to the cavity response (other than in the gross sense of laminar vs turbulent). As a further illustration of this point, pressure-spectra obtained upstream of the cavity mouth and in the cavity for various test conditions are presented in Figs. 28 and 29. The lower curve shows the upstream boundary-layer pressure fluctuations; the upper curve shows the cavity response. The lack of scaling with boundary-layer pressure fluctuations is evident.

7. Unsteady-pressure data — longitudinal energy distribution

Microphones #2, #4, and #5 lie on the center line of the cavity floor. Microphone #2 is near the upstream wall, microphone #4 is in the center of the floor, and microphone #5 near the rear wall (Fig. 7). Figures 30 through 34 present pressure spectra measured at these microphones at all Mach numbers, at L/D-ratios 4 and 7, and $P_0 = 10$ psia. Spectra are also shown for $M = 3$, and $P_0 = 2$ psia. The energy distribution — summarized in Fig. 35 — is presented as the peak fluctuating pressure along the cavity axis, relative to the peak fluctuating pressure close to the forward wall ($x/L = 0.0375$).

The results show the following features:

1. Sound-pressure levels at the response frequencies of the cavity increase from front to rear of the cavity. The variation can be as high as 10 dB, corresponding to a factor of 3 on rms-pressure levels or a factor of 10 on acoustic-energy levels.

2. The variations in level are less pronounced for the deeper ($L/D = 4$) than they are for the shallower ($L/D = 7$) cavities.

3. The two observations support the idea advanced in Sec. II B that a shallow cavity is not acting as a classical acoustic resonator responding in its normal modes. It is easily shown that for a rectangular box resonating in any of its normal modes, the fluctuating pressures at positions such as those of microphones #2 and #5 should be equal. If we suppose the acoustic energy stored in a cavity to be proportional to (amplitude of the oscillations)^2 times (cavity

volume) and the energy exchanged per cycle with the free stream to be proportional to (amplitude)^2 times (surface area), then the energy stored divided by energy exchanged per cycle is proportional to depth. Thus deep cavities have a high Q-factor and resonate in their normal modes; shallow cavities have a low Q-factor and resonate poorly, if at all - though they may be driven by the free stream at relatively definite frequencies.

4. The energy distribution suggests that the cavities are driven by an energy input near their trailing edge; the cavity attenuates towards the leading edge. This concept is of interest with regard to the various cavity-oscillation models that are based on analogies with the edge-tone phenomenon. This finding could support Rossiter's model in which an acoustic feedback from the trailing edge of the cavity plays a dominant role in the cavity-response system.

8. Unsteady-pressure data – lateral energy distribution

Previous investigators have not excluded the possibility that cavity resonance in transverse modes may involve oscillations in a direction normal to the free stream and to the depth direction. Therefore, microphones were placed in two corners of the cavity floor and in each glass side wall for the specific purpose of detecting such modes. Thus, there are three pairs (Fig. 7) of microphones, #2 and #3, #5 and #6, and #8 and #9, the comparison of the spectra of which makes it possible to test for transverse pressure oscillations in the cavity.

Figure 36 illustrates the typical results, showing spectra from one such pair (#2 and #3) for one L/D ratio of 5.7, and at $M = 1.5$ for $P_0 = 10$ psia and at $M = 3$ for $P_0 = 2$ psia. No sign of transverse oscillations was present under any conditions – as could be expected from the observations described immediately above in the Section on longitudinal energy distribution. If a shallow cavity is to be regarded as a very ineffective resonator, then the only oscillations that will be evident will be those that are very strongly excited. It is apparent that strong excitation in the transverse direction is not available.

9. Unsteady-pressure data – resonant frequencies

During each run a B&K narrowband frequency analyzer was used to identify discrete frequencies in the output signal of one microphone. The following Table summarizes the results, showing two

different nondimensional frequencies: $S_1 = (fL)/(U)$, and $S_2 = (fL)/(a_0)$; where f is the measured frequency, L is the cavity length, U is the free-stream velocity, and a_0 is the stagnation sound speed of the free stream. Only when the discrete-resonant frequencies could readily be determined were they used to compute the nondimensional frequencies. Irregular modulation of either frequency or amplitude of the signals often made selection of a discrete-resonant frequency impossible.

TABLE IV. NONDIMENSIONAL RESONANT FREQUENCIES.

M	L/D	S_1	S_2	M	L/D	S_1	S_2
0.8	4	0.72	0.54	2	4	0.55	0.81
↓	5.7	0.72	0.54	↓	↓	0.87	1.29
↓	7	0.72	0.54	↓	↓	1.12	1.67
↓	↓	↓	↓	↓	5.7	0.55	0.81
1.5	4	0.59	0.74	↓	↓	1.28	1.91
↓	↓	0.98	1.22	↓	↓	1.60	2.33
↓	↓	1.28	1.59	↓	7	0.24	0.36
↓	5.7	0.59	0.74	↓	↓	0.54	0.80
↓	↓	1.28	1.59	↓	↓	1.14	1.70
↓	7	0.59	0.74	↓	↓	1.63	2.42
↓	↓	1.34	1.67	↓	↓		
				3	4	0.77	1.38
					↓	1.56	2.79
					↓	2.02	3.52
					5.7	1.11	1.98
					7	1.38	2.48
					1	1.59	2.85

NOTE: For given L/D, frequencies from different runs often coincide closely; in such cases only one typical frequency is given.

S_1 is plotted as a function of Mach number in Fig. 37a. No attempt is made to distinguish between different configurations at each Mach number, as values of resonant frequencies are relatively insensitive to variations in L/D, stagnation pressure, and store configuration. Though these variables determine in an unknown way the *occurrence* of such discrete frequencies, the values are closely independent of the particular configuration. Also shown in Fig. 37b are data points from this and other investigations of shallow cavities. All of the data points in the Mach-number range above 1.2 are from the current study – except for one data point each from investigation by Krishnamurty and Morozov and others from the water-table data of White and MacGregor. In the Mach-number range for which information is available, the present data is seen to be consistent with previous results.

At least four curves can be drawn through current and previous data points. Each shows the Strouhal number to decrease as the Mach number increases. Such curves are consistent with the semiempirical model of cavity excitation presented by Rossiter[12]. His formula as discussed in Sec. II relates Strouhal number to Mach number in the following:

$$S_1 = \frac{m - \alpha}{M + 1/k_v} \quad , \qquad m = 1,2,3...$$

He correlates his data using values of $\alpha = 0.25$, $k_v = 0.57$. Figure 37c shows the same set of data points together with curves representing S_1 for values of m from 1 to 5. The agreement is seen to be good at the lower Mach numbers (less than 1.5), but worse near Mach numbers 2 and 3.

In deriving his formula for S_1, Rossiter assumes that the sound speed in the cavity is the sound speed of the free stream; this is equivalent to assuming a cavity recovery factor of zero. At low Mach numbers this assumption introduces only a small error, but at high Mach numbers the error is much greater. Since recovery factors were measured in the current program and found to be close to unity rather than to zero, Rossiter's formula can be improved for the higher Mach-number range by assuming the cavity-sound speed to equal the stagnation sound speed. The formula for the Strouhal-number then becomes

$$S_1^* = \frac{m - \alpha}{\dfrac{M}{\left[1 + \dfrac{\gamma - 1}{2} M^2\right]^{\frac{1}{2}}} + \dfrac{1}{k_v}} \quad , \qquad m = 1,2,3... \qquad (21)$$

Figure 37d shows the data points, together with curves representing S_1' for the above values of α, k, and m. The correlation achieved for data from the present study at Mach numbers 2 and 3 is much improved. Note especially that the point representing Strouhal number 0.77 at Mach number 3 is shifted from the m = 4 to the m = 3 curve. Additional reasons for this point lying on the m = 3 curve are advanced below.

The Rossiter formula, so modified, appears to be the best available approach to correlating the discrete-frequency response of the cavity. It gives no indication of whether a particular response frequency will be observed, or what the magnitude will be. Rossiter does suggest a criterion for deep cavities for the appearance of resonant frequencies, but it is not applicable for these shallow cavities

10. Unsteady-pressure data -- mode shapes

In expectation of observing *acoustic* resonances in the cavity, a movable rod -- spanning the length of the cavity -- was installed. In this way, a microphone could be positioned by remote control over almost the whole length of the cavity. In early runs some effort was made to use the traversing microphone to locate maxima and minima of the rms pressure in bands containing resonant frequencies. This procedure proved to be too time-consuming and was replaced by a policy of measuring sound pressure at five or more points, often restricted to the upstream half of the cavity.

For each run for which the traversing microphone was used, the rms pressure in the most intense frequency band was plotted against position measured as a fraction of the cavity length -- 0 at the leading edge and 1.0 at the trailing edge. The reference for the fluctuating pressure was the free-stream static pressure. Note that effective plotting of mode shapes requires changing from a logarithmic (decibel) to a linear presentation of the rms pressures. Small errors in the logarithmic pressures (±1 dB, for example) become relatively large errors on a linear scale. For this reason, drawing of mode shapes through a small number of data points can be speculative. Figure 38 shows an attempt to draw such shapes. Higher-order modes in particular cannot be identified. There is striking external evidence confirming these mode identifications.

Figure 39 shows the resonant frequencies plotted as the second of the Strouhal numbers, S_2, comprising the speed of sound

rather than the free-stream flow speed as a function of Mach number. If it is assumed that the sound speed in the cavity is the stagnation sound speed a_0 – roughly a correct assumption – then the resonant frequencies of the cavity considered as a purely one-dimensional oscillator resonating in a lengthwide direction are $f = (na_0)/(2L)$ – i.e., $S_2 = n/2$ – where $n = 1,2,3...$ is the number of pressure nodes. Lines representing these ideal resonant frequencies are drawn on Fig. 39. Whenever the number of nodes associated with one of the resonant frequencies can be identified from one of the mode-shape plots, it is shown alongside the data point. Data points shown as crosses are identified from the real-time frequency analysis, and are given as band-center frequencies.

The association between frequencies with corresponding numbers of nodes and the idealized frequencies is obvious. It is not known, however, whether, given more complete data, this process can be continued to higher-order modes. Note also that the points on the Rossiter curves in Figs. 37c and d associate according to the number of nodes. Again, the reason for this is a subject for study.

There is a trend for the observed frequencies to correspond to the idealized resonant frequencies of the cavity at high Mach numbers. At lower Mach numbers the ideal resonant frequencies of the cavity are a poor guide to the observed frequencies, being in error by as much as 50%. As mentioned earlier, the cavity is a poor acoustic resonator, and the impedance at the surface exposed to the free stream differs greatly from that of a hard surface. Note that an assumption of an ideal open surface (zero pressure fluctuations) would lead to estimates of

$$S_2 = \frac{1}{2}\left[n^2 + \frac{L^2}{4D^2}\right]^{\frac{1}{2}} . \qquad (22)$$

These frequencies would differ from the observed frequencies by factors of two or more. Though a complete estimation procedure for the resonant frequencies of cavities awaits further study, the assumption of a "closed" cavity is better than that of an "open" cavity, especially at higher Mach numbers.

Note that the trend towards the ideal closed-box frequencies at high Mach numbers can be justified theoretically. Reference 21 indicates that, as Mach number tends to infinity, the pressure exerted by the outer flow on the air in the cavity can be approximated by

$$p' = \rho_c^2 a_c^2 M \frac{\partial h}{\partial x} , \qquad (23)$$

where p' is the pressure fluctuation at the interface between outer and inner flows, ρ_c and a_c are cavity air density and sound speed, respectively, M is the free-stream Mach number, and $\partial h/\partial x$ is the slope of the dividing streamline. At lower Mach numbers, this expression becomes much more elaborate; thus it is difficult to make theoretical models of unsteady cavity flows[4]. Here, we simply note that as M becomes large, pressure fluctuations become large relative to the interface displacement. The impedance presented by the interface becomes large proportionally as M increases; the closed-box frequencies are then approached.

The formula for S_1^* could be modified to demonstrate this limit, but it would then become even more empirical in nature. Also, the present data is not available at high enough Mach numbers to make this process worthwhile.

11. Unsteady-pressure data – oscillation waveforms

Tape recordings of the output of microphone #6 were made for all test configurations at Mach number 3. The intention was to determine the waveform of the pressure-time histories for some experimental conditions. Although this part of the test program was not very comprehensive, the results are interesting enough to justify their presentation. A sample time history is shown in Fig. 40a. These oscilloscope traces represent the unfiltered output signal.

The high-frequency oscillation seen in the photographs occurs at a frequency above 20 kHz and is identified as the lowest resonance frequency of the microphone diaphragm. The signal, after being filtered through a low-pass filter to exclude this resonance is shown in Fig. 40b. Experimental conditions for this oscillation waveform were L/D = 5.7 and P_0 = 2 psia. Figure 40c shows the filtered signal at the same conditions, but at P_0 = 10 psia. Real-time spectra of the output of microphone #6 under these conditions were previously shown in Fig. 26, which exhibits a peaked spectrum when P_0 = 2 psia and a broadband "haystack" spectrum when P_0 = 10 psia.

When the spectrum of the fluctuations is strongly peaked near 1250 Hz, the signal waveform is visibly periodic, and the peak frequency can be estimated readily by counting periods. When the spectrum of the fluctuations is broad, exhibiting no

clear resonances, the waveform is not strongly periodic. The waveform does, however, superficially appear to be composed, not of a sum of independent, randomly phased sine waves, but of a series of events similar in nature. The periodicity of aperiodicity lies in the spacing of these events. In one instance, the signal is composed of events occurring at regular time intervals and is strongly periodic; in the other instance, the spacing between events appears random, though with a definite mean, and the signal thus shows no clear frequency peaks.

It is not possible on this evidence to relate the difference in these waveforms to the salient difference between the experimental conditions of the two runs compared – i.e., a condition of either a laminar upstream boundary layer or a turbulent upstream boundary layer. These results do, however, suggest an approach for a distinction between "discrete-frequency" and "broadband" noise in the study of cavity oscillations.

In addition to showing this difference between periodic and aperiodic fluctuations in the cavity, all other tape recordings show very distinct nonlinear waveforms. A study of this nonlinearity may provide some insight into the mechanisms governing the amplitudes of oscillations in the cavity.

b. Experimental Results – Store-Containing Cavity

1. Unsteady-pressure data – effect of store insertion

Figures 41 through 45 present pressure spectra at microphone #6 for L/D = 4, 5.7, and 7, for a Mach-number range from 0.8 to 3, and P_0 = 2 and 10 psia. (Recall that for M = 3, P_0 = 2 psia resulted in laminar flow and P_0 = 10 psia caused turbulent flow.) For each condition, spectra are presented for the empty cavity (E), for the cavity containing one store (1), and for the cavity containing two stores (2).

In the absence of a theoretical model for the effect of stores on the cavity response and in view of the limitations on the extent of the present data, no attempt is made here to make other than these purely qualitative observations:

1. The present study confirms very strongly the observations of Leupold and Baker[15] that stores near the mouth of the cavity have a great effect in diminishing the rms-pressure amplitudes in the cavity. In planning a test of a store-containing

cavity of variable depth, one must decide whether to maintain the stores at a fixed distance from the cavity floor or at a fixed distance from the surface plane of the cavity. In this study, the stores were attached to the floor. In the high-floor position (L/D = 7), the upper surfaces of the stores lay just flush with the cavity-surface plane and interfered with the shear layer atop the cavity. In the low position (L/D = 4), the stores lay almost entirely in the deeper half of the cavity. The pressure spectra show that at L/D = 7, intensities in peak 1/3-octave bands are down by factors of the order of 10 dB and frequently are no longer identifiable above the broadband content of the spectrum.

The effect of insertion of store is summarized in Fig. 46. Pressure fluctuations in the most intense 1/3-octave band (frequently the main resonant mode of cavity response) are presented for empty, one- and two-store configurations, at each L/D ratio for M = 3 and P_0 = 2 and 10 psia; the latter conditions did not show any resonant frequencies. Note that the shallow-cavity results show especially strong suppression of resonance by the presence of stores.

The effect of store interference (two stores) with the shear-layer flow above the cavity is also observed in the Schlieren photographs (Figs. 47 through 50) obtained at M = 3. The oscillating laminar boundary layer atop the empty cavity is readily visible (Fig. 47). This stage corresponds to large narrowband amplitudes in the cavity response. (The relevant pressure spectrum was shown in Fig. 26.) Presence of store effectively kills the oscillatory motion of the laminar boundary layer (Fig. 48), causing the narrowband peak in the response spectrum to disappear. (Compare Fig. 44 spectrum denoted "2".)

The case of the turbulent boundary layer (Figs. 49 and 50) exhibits no qualitative difference in the appearance of the shear-layer characteristics. However, the turbulent shear layer for the empty cavity already showed no oscillatory motion, and the presence of store did not change this stage. Hence, the spectra for the two cases were almost identical (Fig. 45).

The observations lend qualitative support to the idea that the cavity response is dominated by energy-exchange mechanisms at the shear layer which are disrupted by the proximity of the stores.

2. An instance of a converse effect is seen in Fig. 44. Here, for the deeper cavity (L/D = 4) containing two stores, a new high response frequency appears in a band with center frequency 3150 Hz. This high frequency is thought to be an acoustic-response frequency of the enclosure formed by the stores, the cavity floor, and the walls. An acoustic resonance is conceivable, in view of the relative isolation of the enclosure from energy exchange with the free stream and the consequently higher Q-factor. Because of the complicated geometry of the enclosure, theoretical estimates of the normal-mode frequencies of the enclosure are not readily available.

3. The presence of one asymmetrically located store in the high-floor position results, in most cases, in only a moderate reduction of the peak level of the main narrowband response of the cavity. This observation indicates that the undisturbed half of the cavity shear layer is still capable of driving the cavity in a length mode. The addition of a second store, which effectively fills the cavity mouth area, prevents longitudinal modes of response.

   Moving one or two stores away from the shear layer towards the cavity interior (in our experiments by lowering the floor) so they will not interfere with the shear layer usually results in the stores having almost no effect on the cavity-response behavior.

2. Unsteady-pressure data – lateral energy distribution

Test results revealed that no transverse-oscillation modes could be detected within the empty cavity. This situation was explained by the unavailability of strong transverse excitation in a shallow cavity. For the first time, experiments were performed with an asymmetrically located store configuration. The possibility could not be excluded that the asymmetric case would result in some lateral oscillations. However, Fig. 51 shows that this was not the case. It was then to be expected that there would also be no transverse oscillations for the two-store configuration.

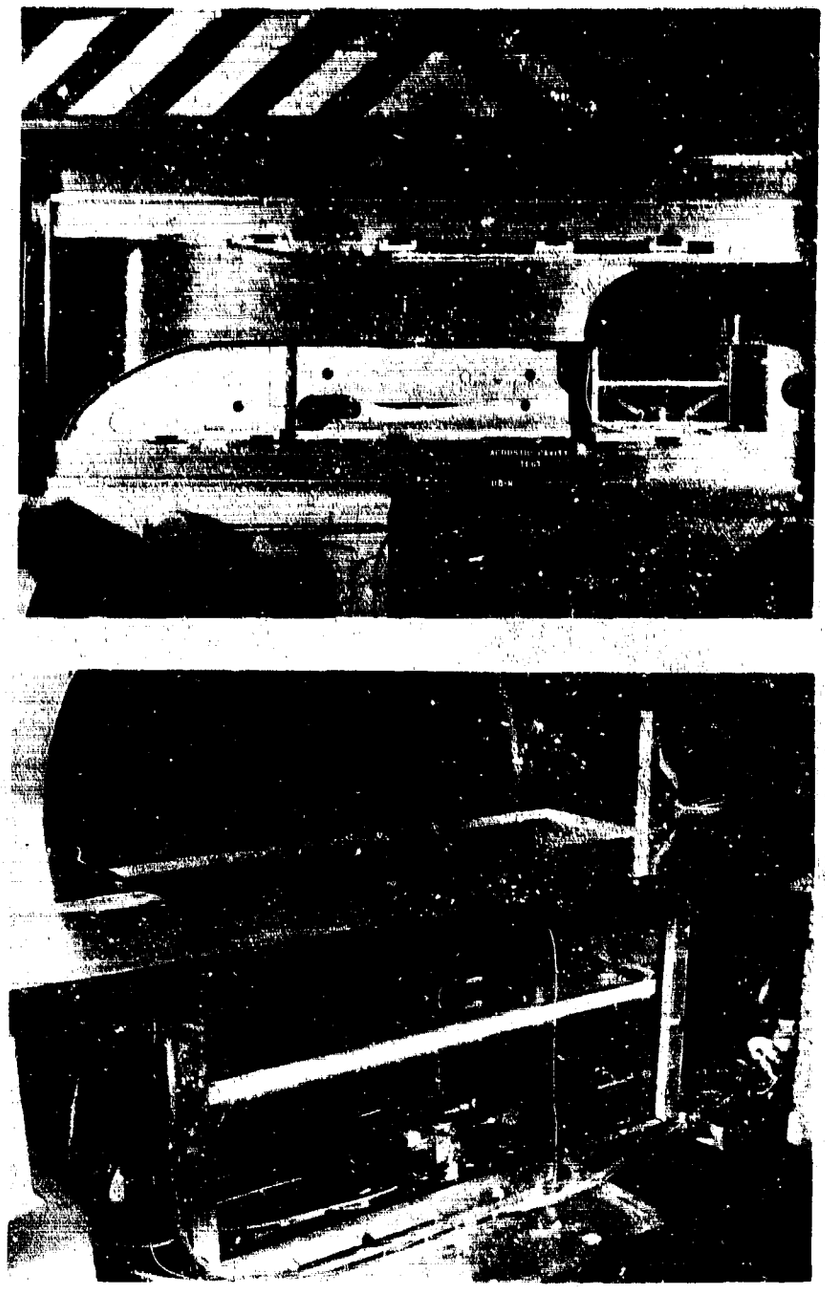

FIGURE 4. INSTALLATION OF EXPERIMENTAL CAVITY IN MIT NAVAL SUPERSONIC WIND TUNNEL (HALF NOZZLE BLOCK FOR SUBSONIC SPEEDS).

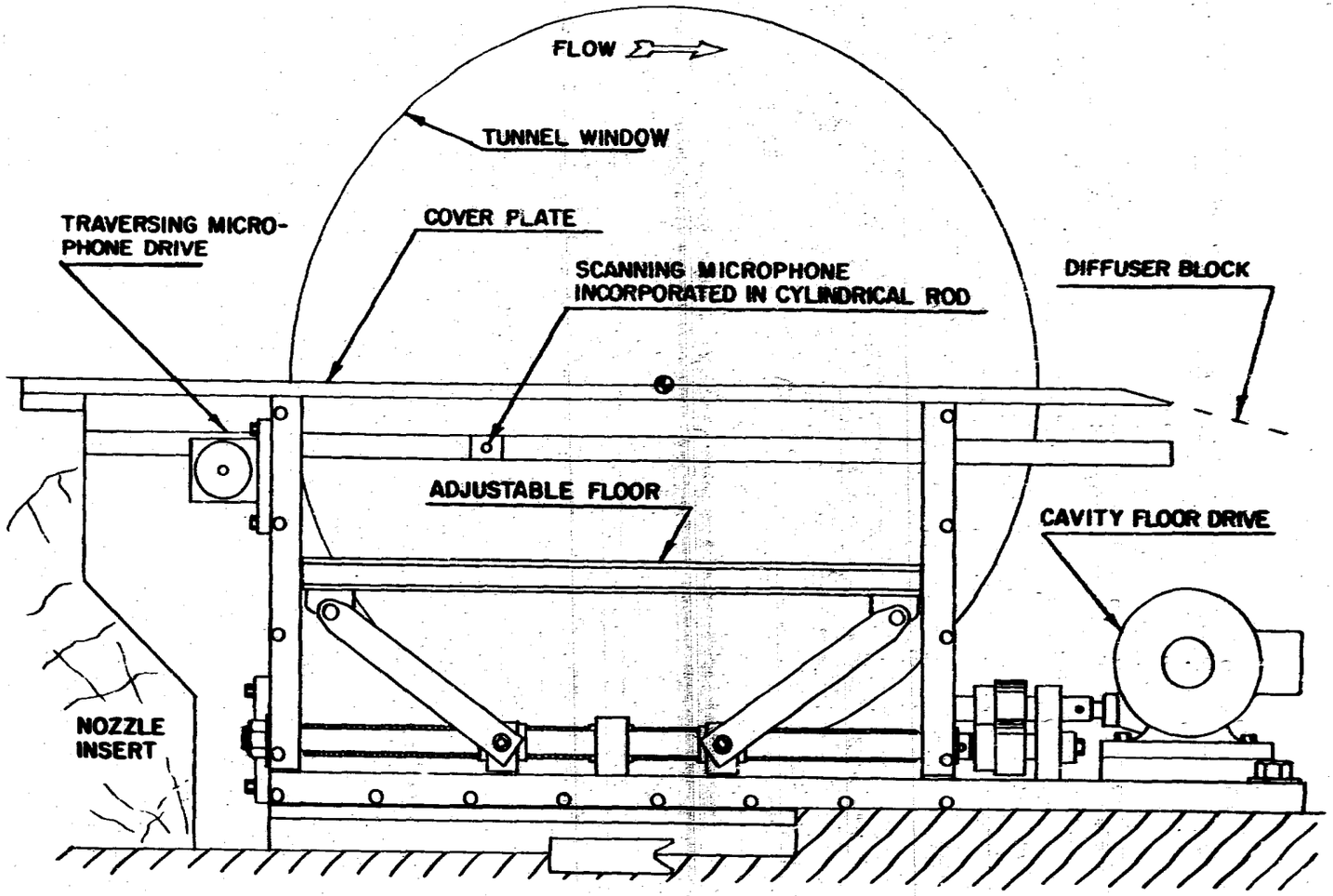

FIGURE 5. EXPERIMENTAL CAVITY (SIDE ELEVATION).

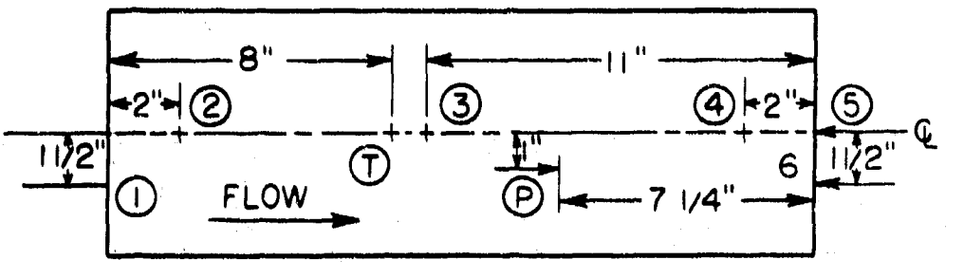

PLAN VIEW OF CAVITY

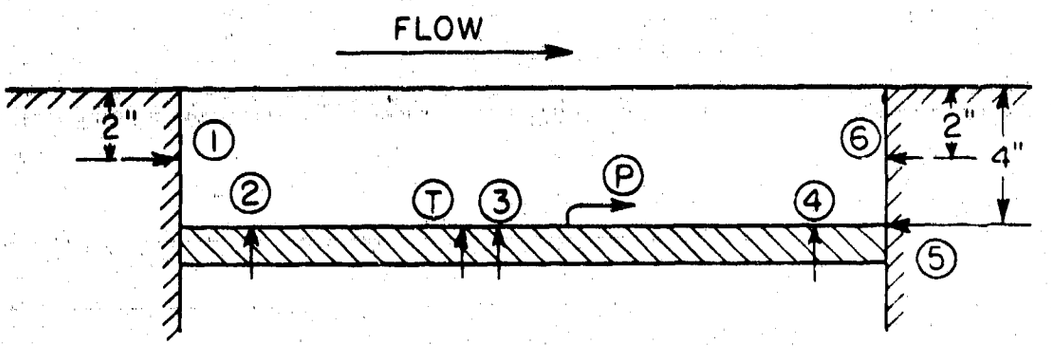

SIDE ELEVATION OF CAVITY. PRESSURE TAPS NUMBERED 1 TO 8; P IS THE PITOT-STATIC TUBE; T IS THE THERMOCOUPLE.

FIGURE 6. LOCATION OF STATIC-PRESSURE TAPS, PITOT-STATIC TUBE AND THERMOCOUPLE.

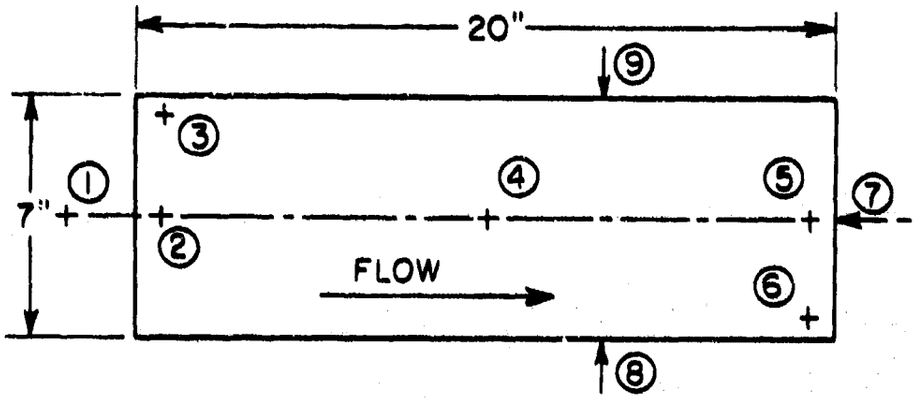

PLAN VIEW OF CAVITY. MICROPHONES 2,3,5 & 6 ARE CENTERED 3/4 INCH FROM EDGES OF FLOOR.

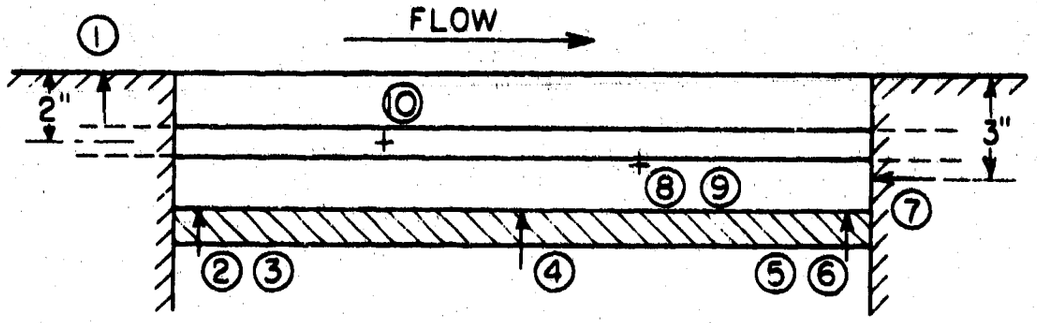

SIDE ELEVATION OF CAVITY. MICROPHONE 10 IS IN THE PROBE ROD; MICROPHONES 8 & 9 ARE IN THE GLASS WALLS, 2 1/2" BELOW SURFACE PLANE AND 6 2/3" AHEAD OF REAR WALL.

FIGURE 7. LOCATION OF MICROPHONES

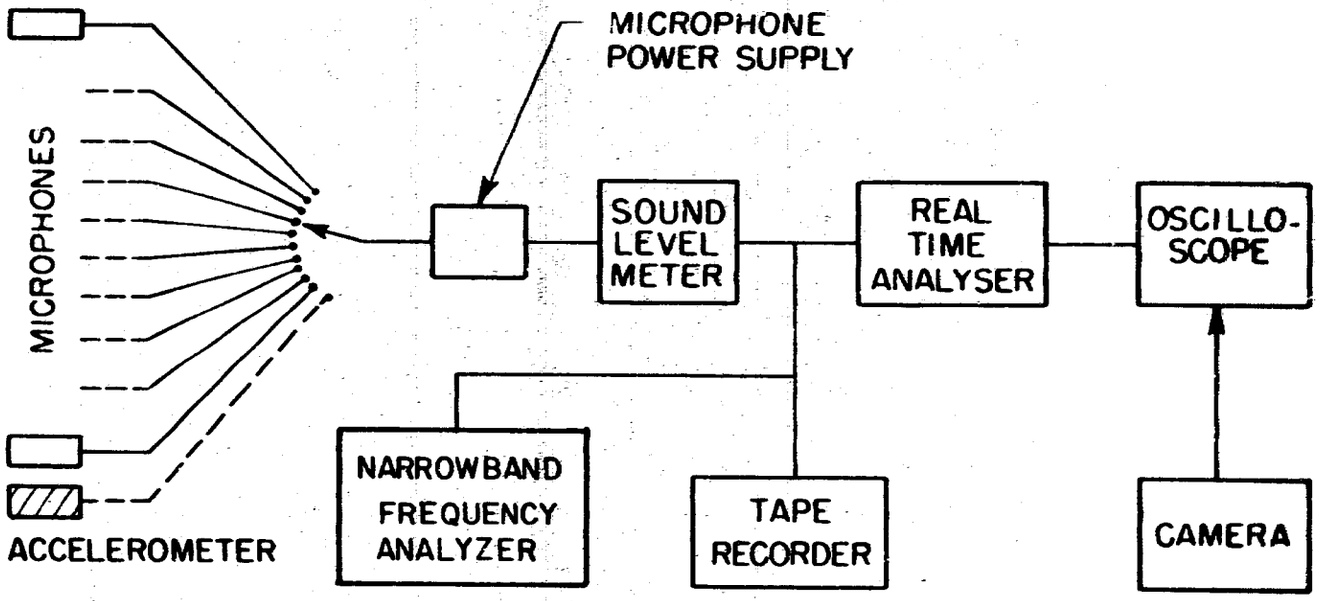

FIGURE 8. BLOCK DIAGRAM OF DATA-ACQUISITION INSTRUMENTATION.

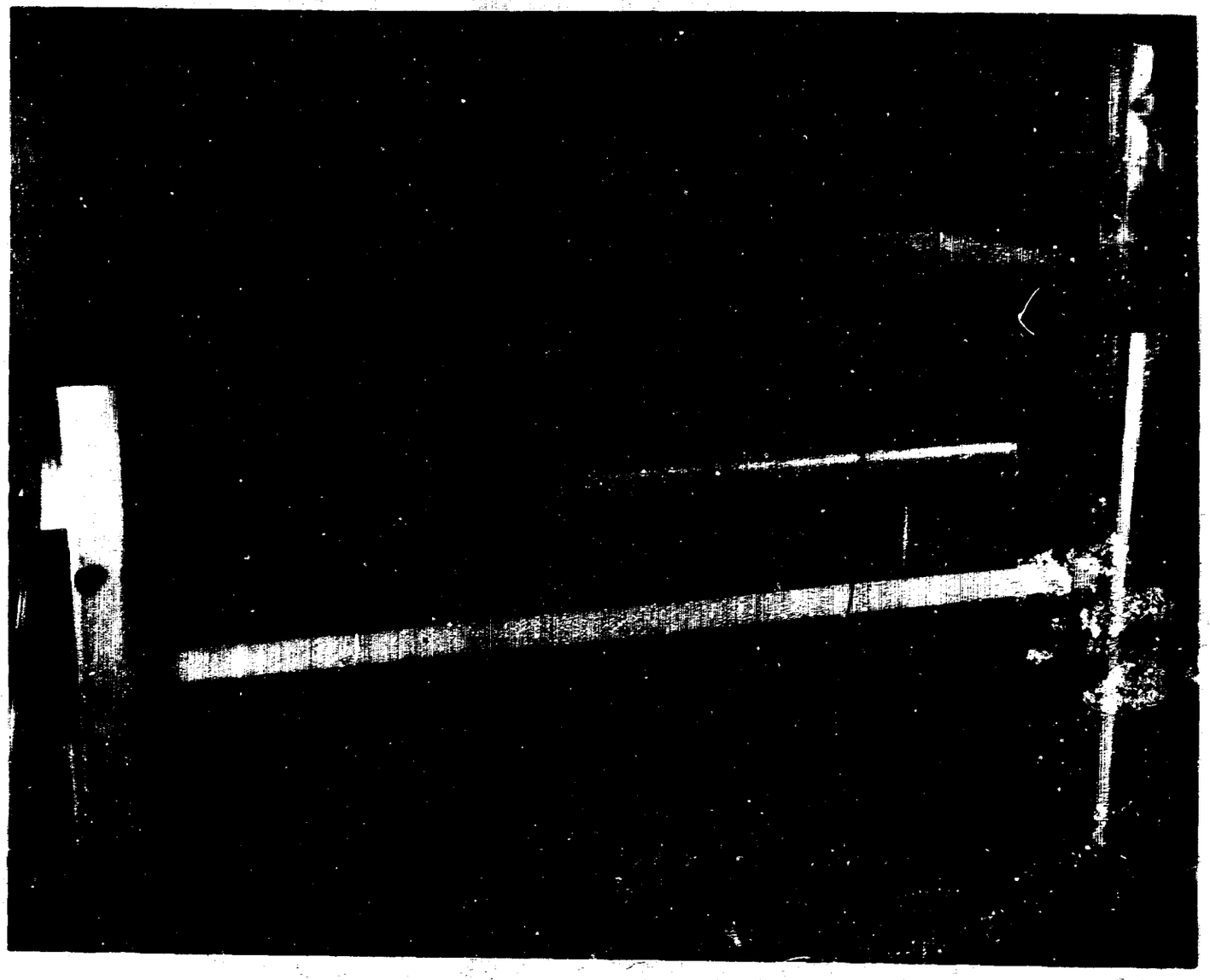

FIGURE 9. EXPERIMENTAL CAVITY WITH TWO STORES.

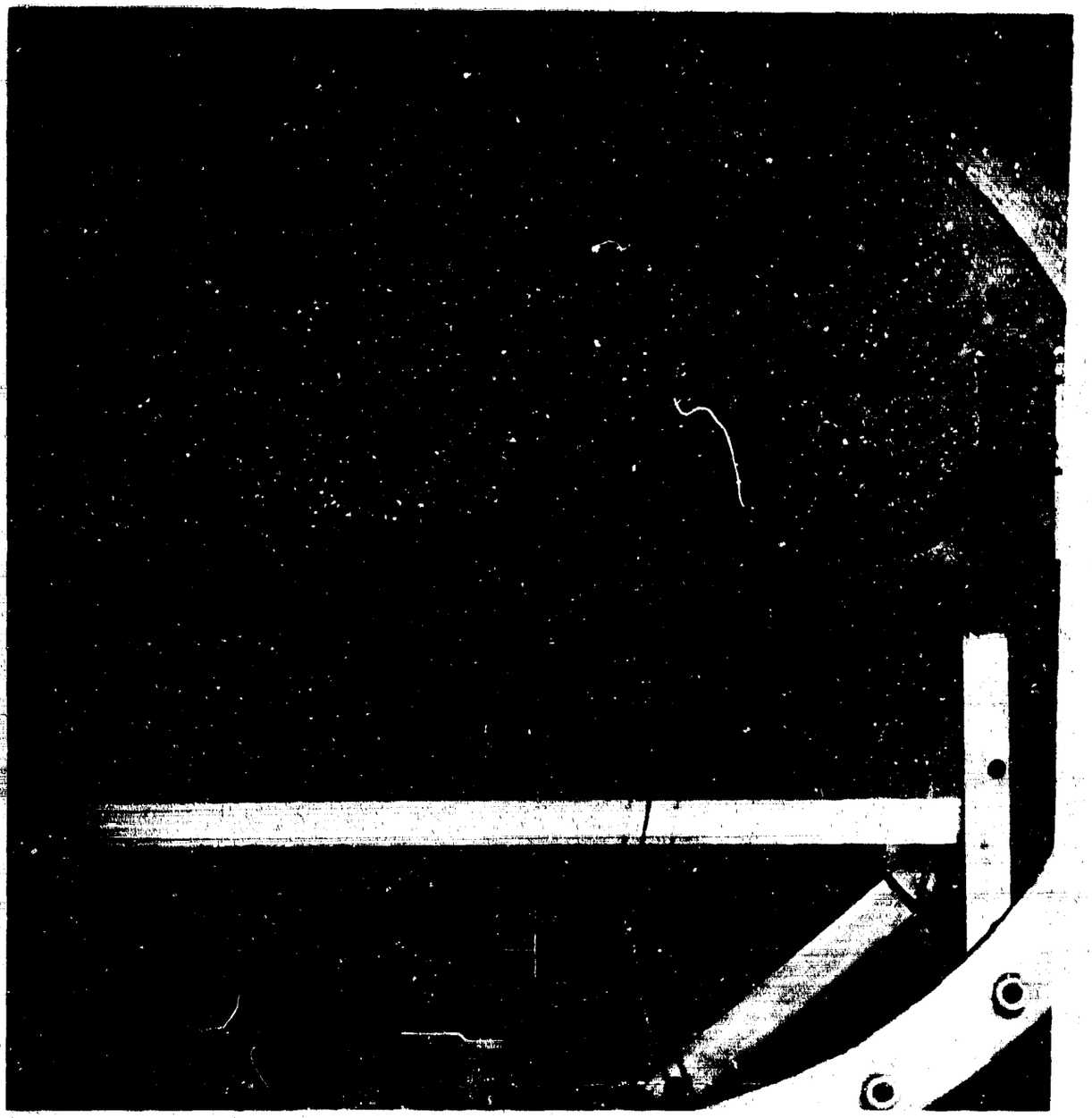

FIGURE 10. SCHLIERENOPTICAL FLOW VISUALIZATION – EMPTY CAVITY; TURBULENT BOUNDARY LAYER; M = 0.8; L/D = 4; P_0 = 10 psia.

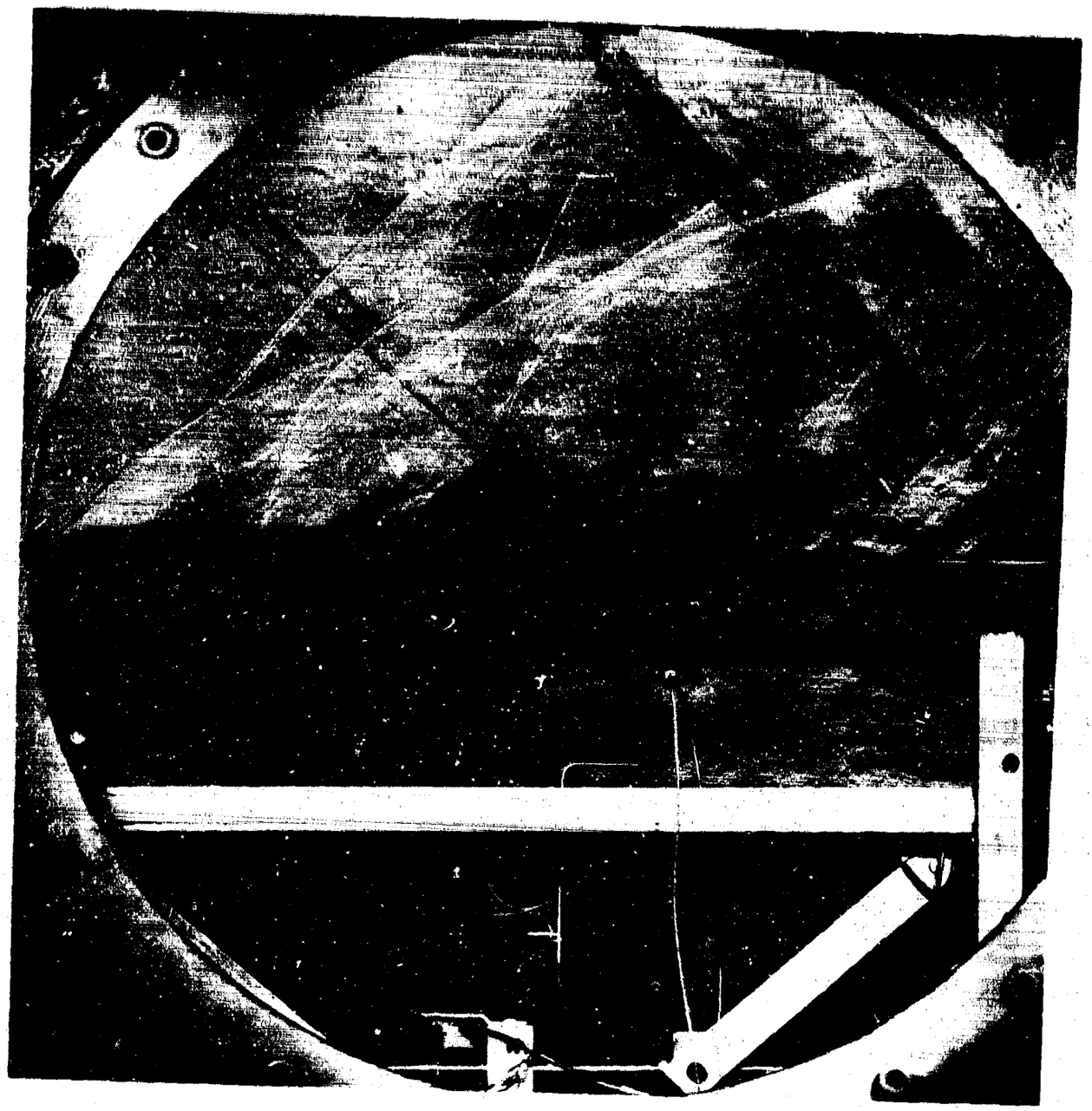

FIGURE 11. SCHLIERENOPTICAL FLOW VISUALIZATION — EMPTY CAVITY; TURBULENT BOUNDARY LAYER; M = 1.5; L/D = 4; P_o = 10 psia.

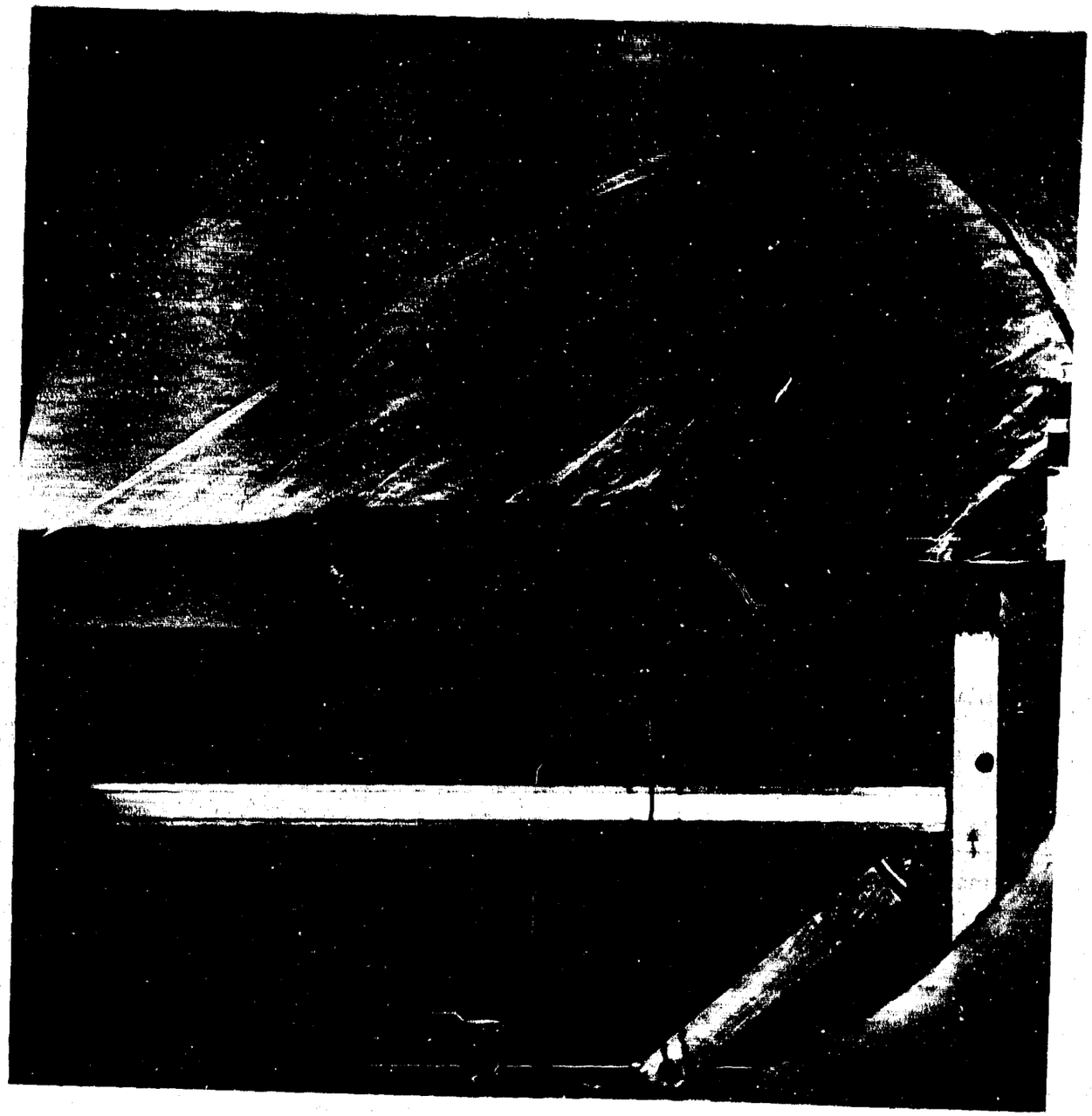

FIGURE 12. SCHLIERENOPTICAL FLOW VISUALIZATION – EMPTY CAVITY; TURBULENT BOUNDARY LAYER; M = 2; L/D = 4; P_o = 10 psia.

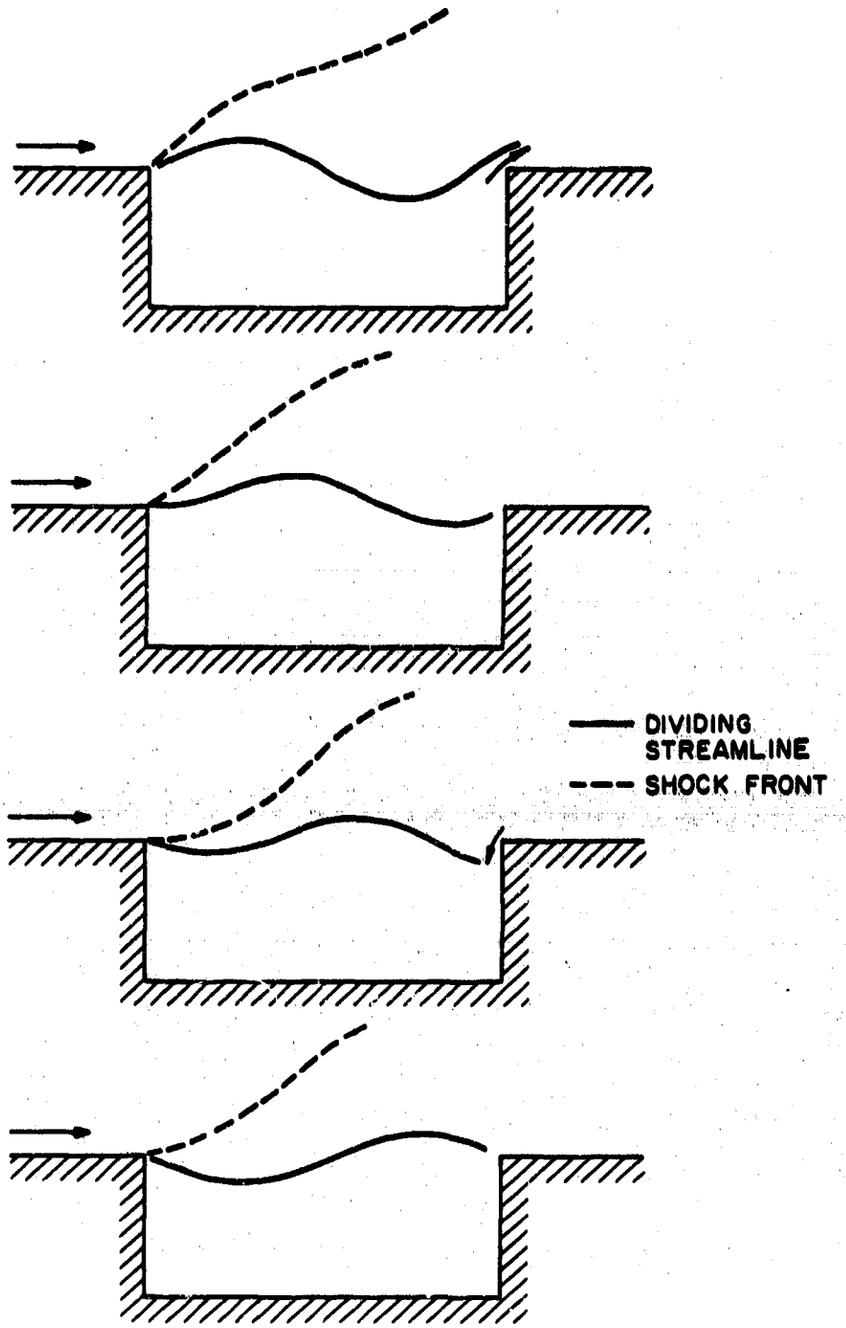

FIGURE 13. SCHEMATIC OF DIVIDING STREAMLINE OSCILLATION.

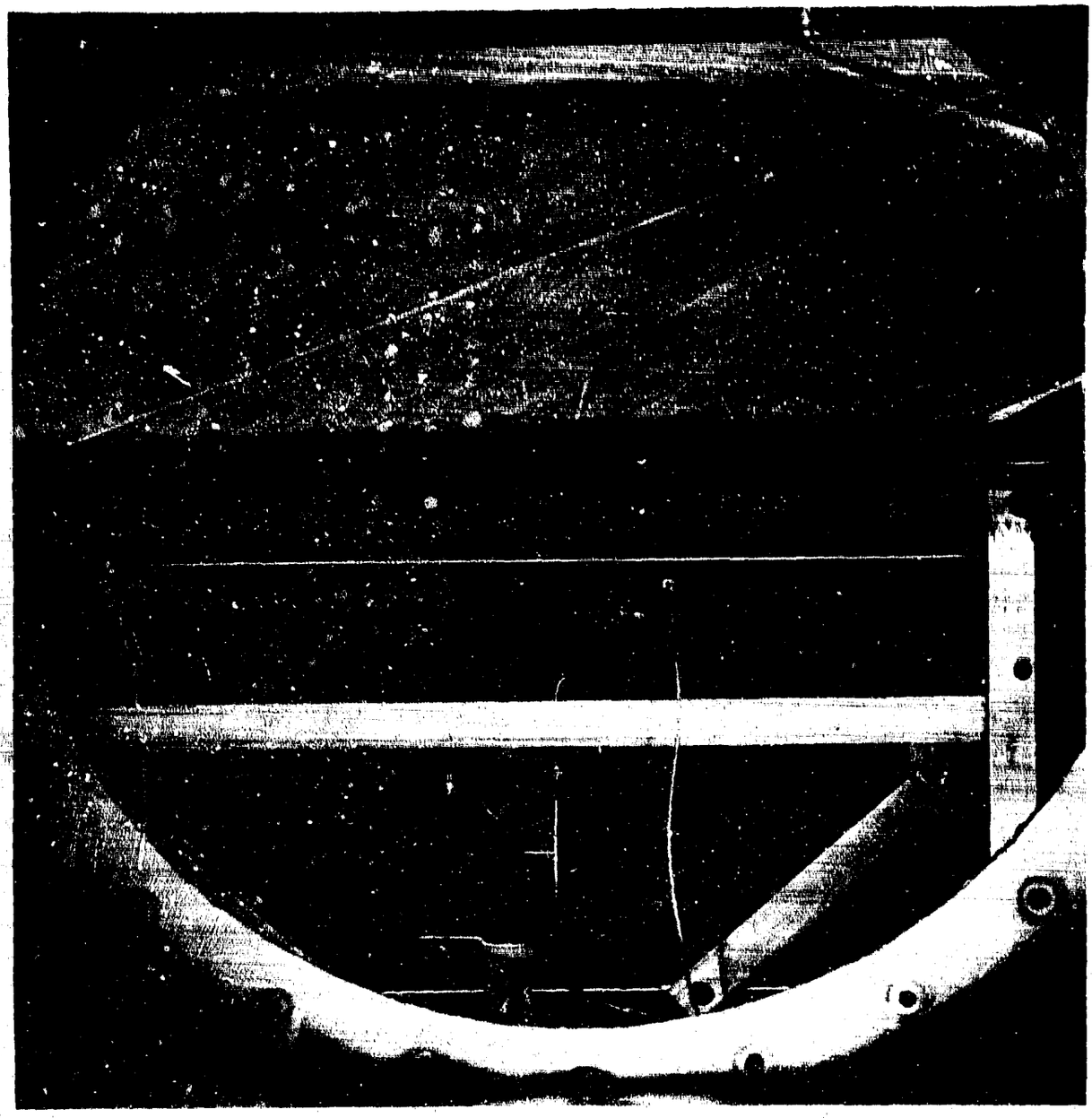

FIGURE 14. SCHLIERENOPTICAL FLOW VISUALIZATION – EMPTY CAVITY; TURBULENT BOUNDARY LAYER; M = 3; L/D = 4; P_o = 10 psia.

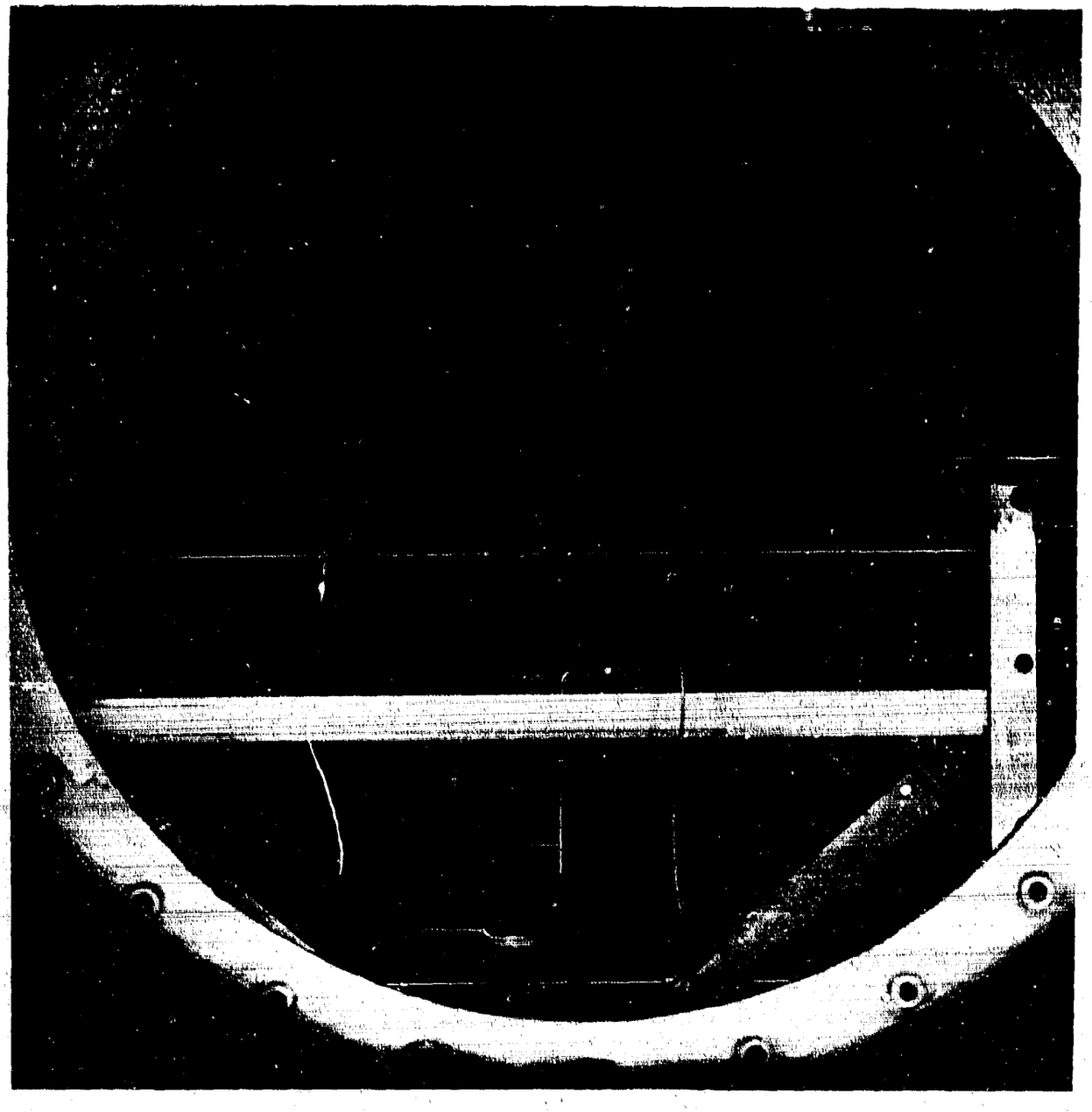

FIGURE 15. SCHLIERENOPTICAL FLOW VISUALIZATION — EMPTY CAVITY; LAMINAR BOUNDARY LAYER; M = 3; L/D = 4; P_o = 2 psia.

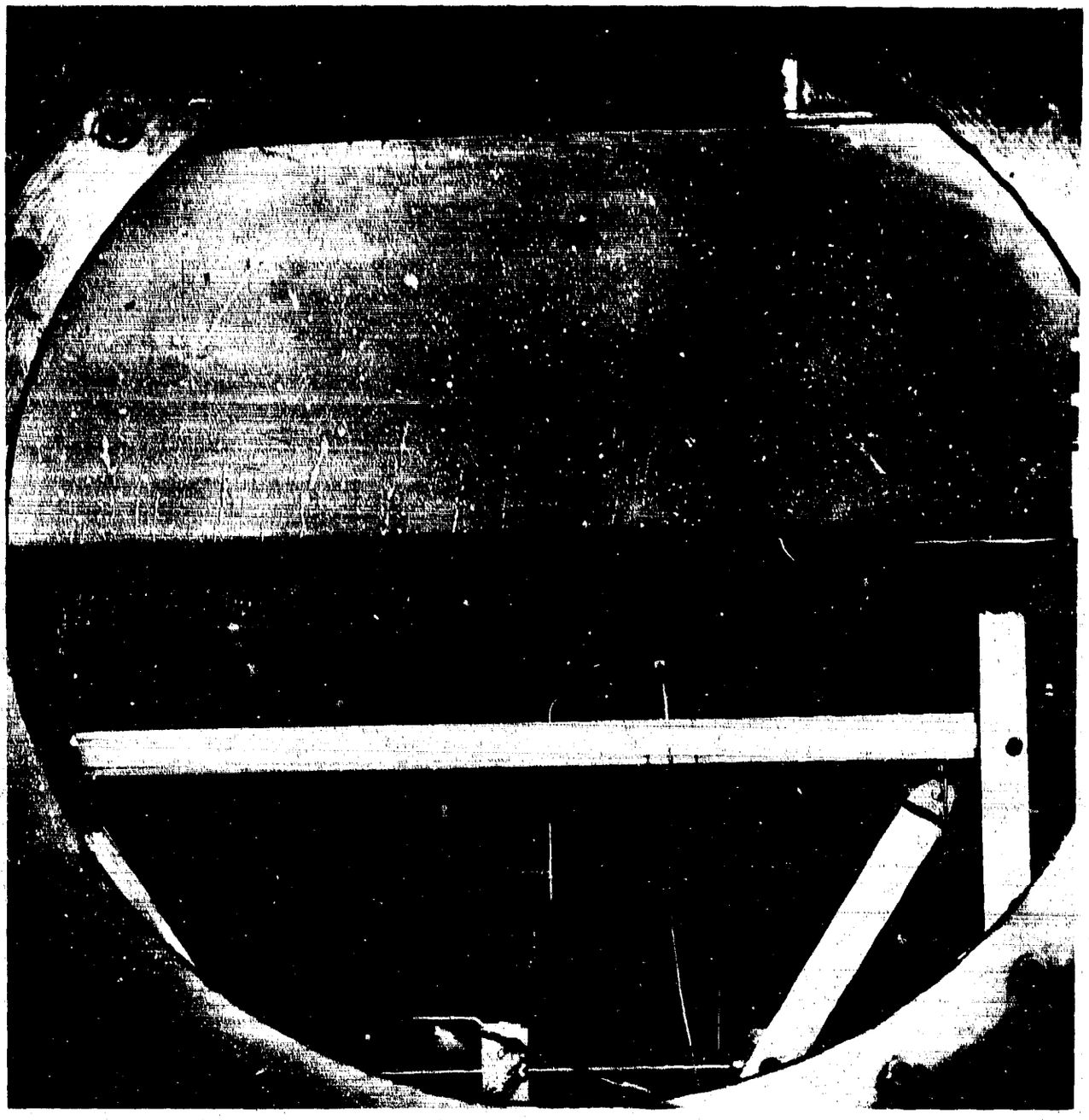

FIGURE 16. SCHLIERENOPTICAL FLOW VISUALIZATION — CLOSED CAVITY; LAMINAR FLOW; M = 3; P_0 = 2 psia.

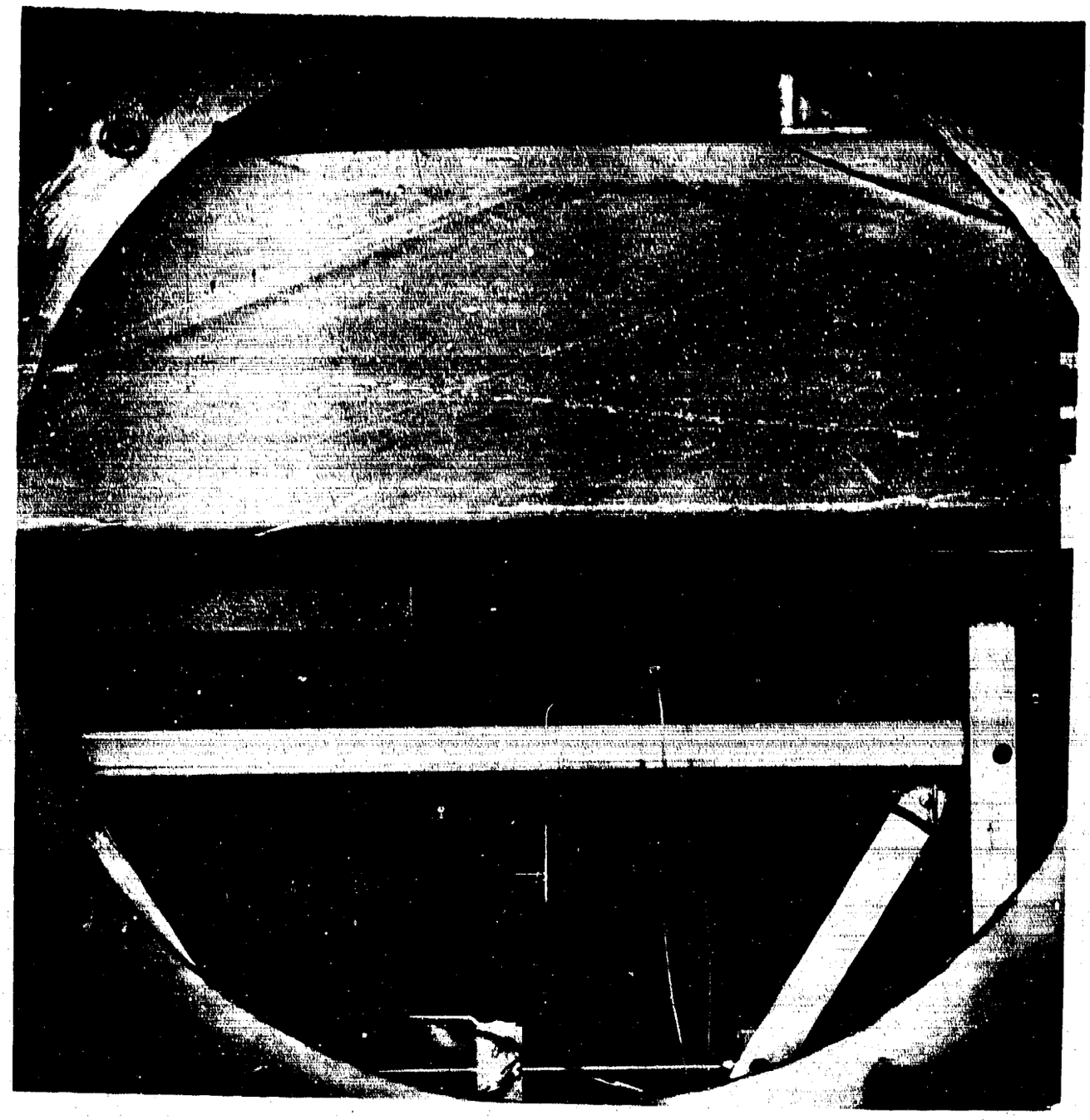

FIGURE 17. SCHLIERENOPTICAL FLOW VISUALIZATION – CLOSED CAVITY; TURBULENT FLOW; M = 3; P_0 = 10 psia.

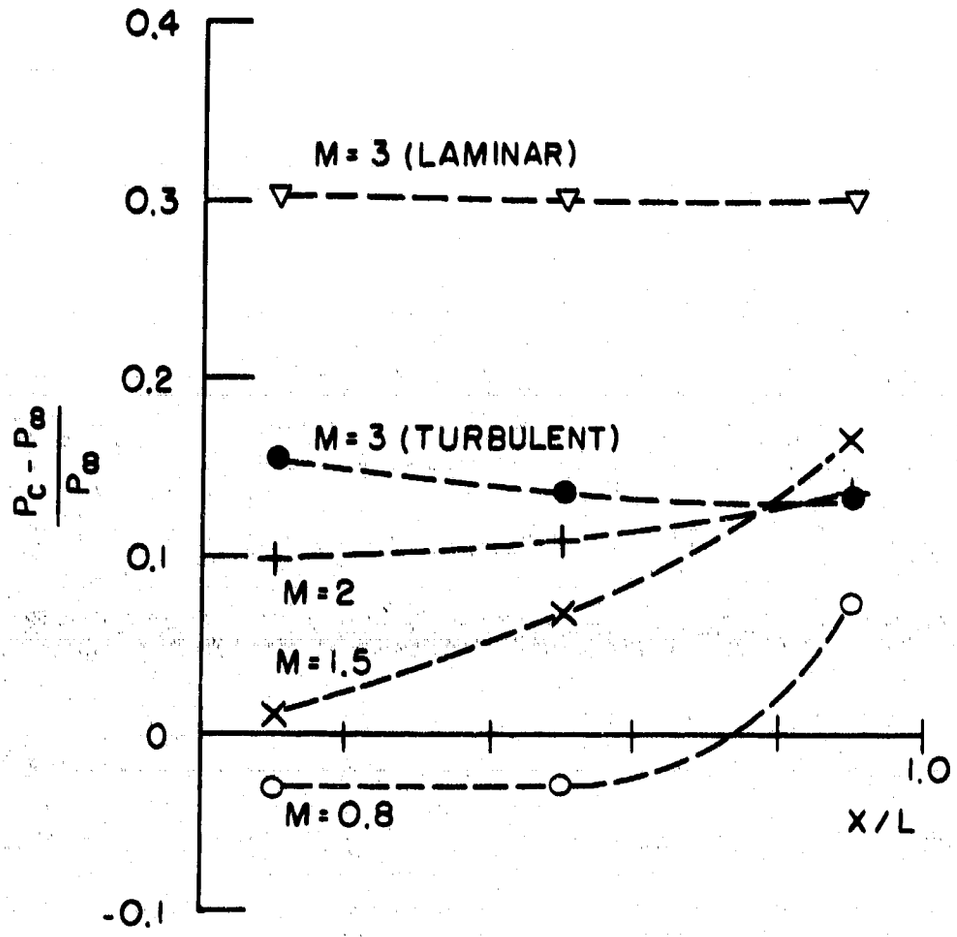

FIGURE 18. VARIATION OF STATIC PRESSURE ALONG CAVITY FLOOR — EMPTY CAVITY; L/D = 4; P_0 = 10 psia.

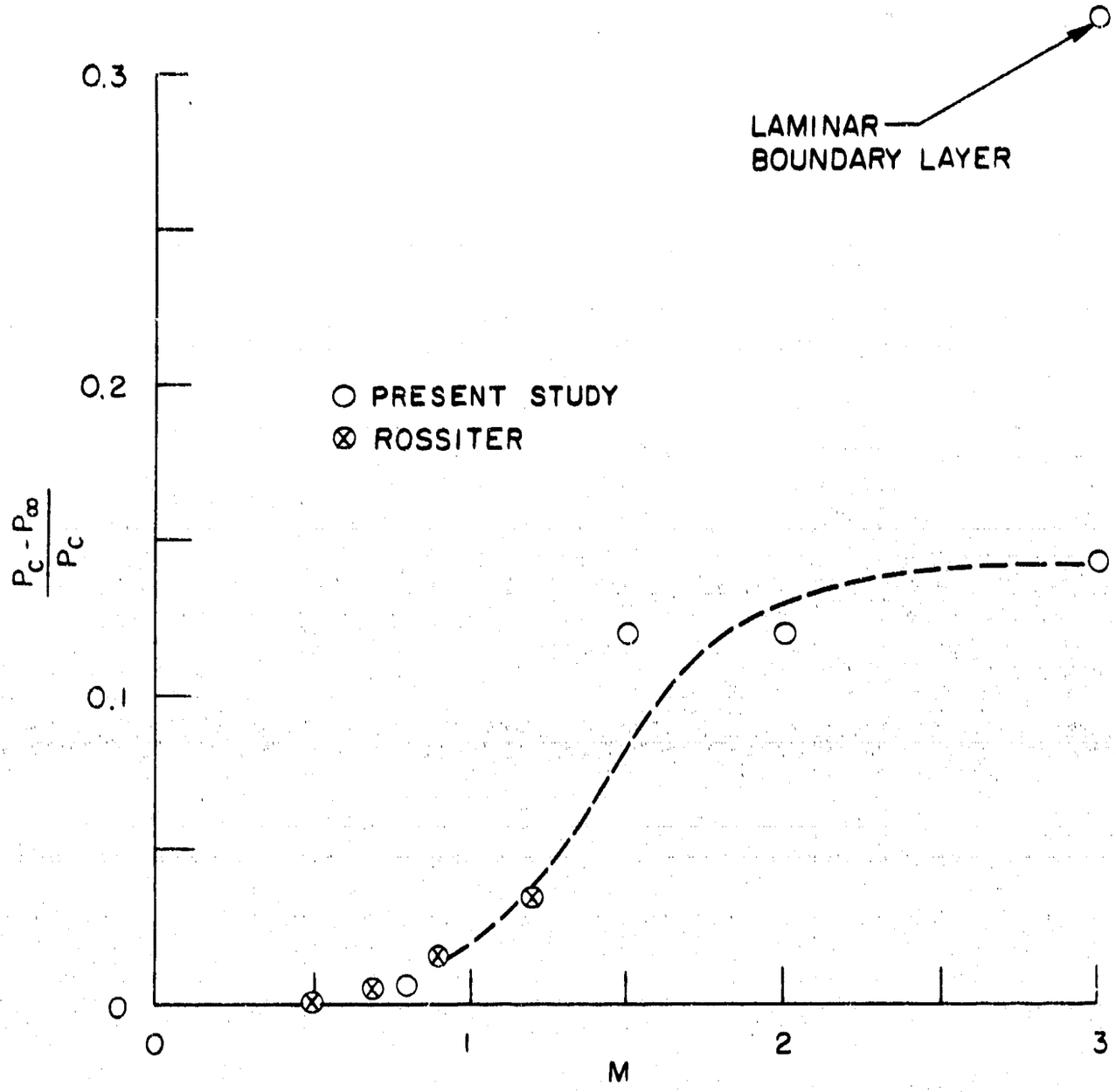

FIGURE 19. MEAN CAVITY STATIC PRESSURE AS FUNCTION OF FREE-STREAM MACH NUMBER.

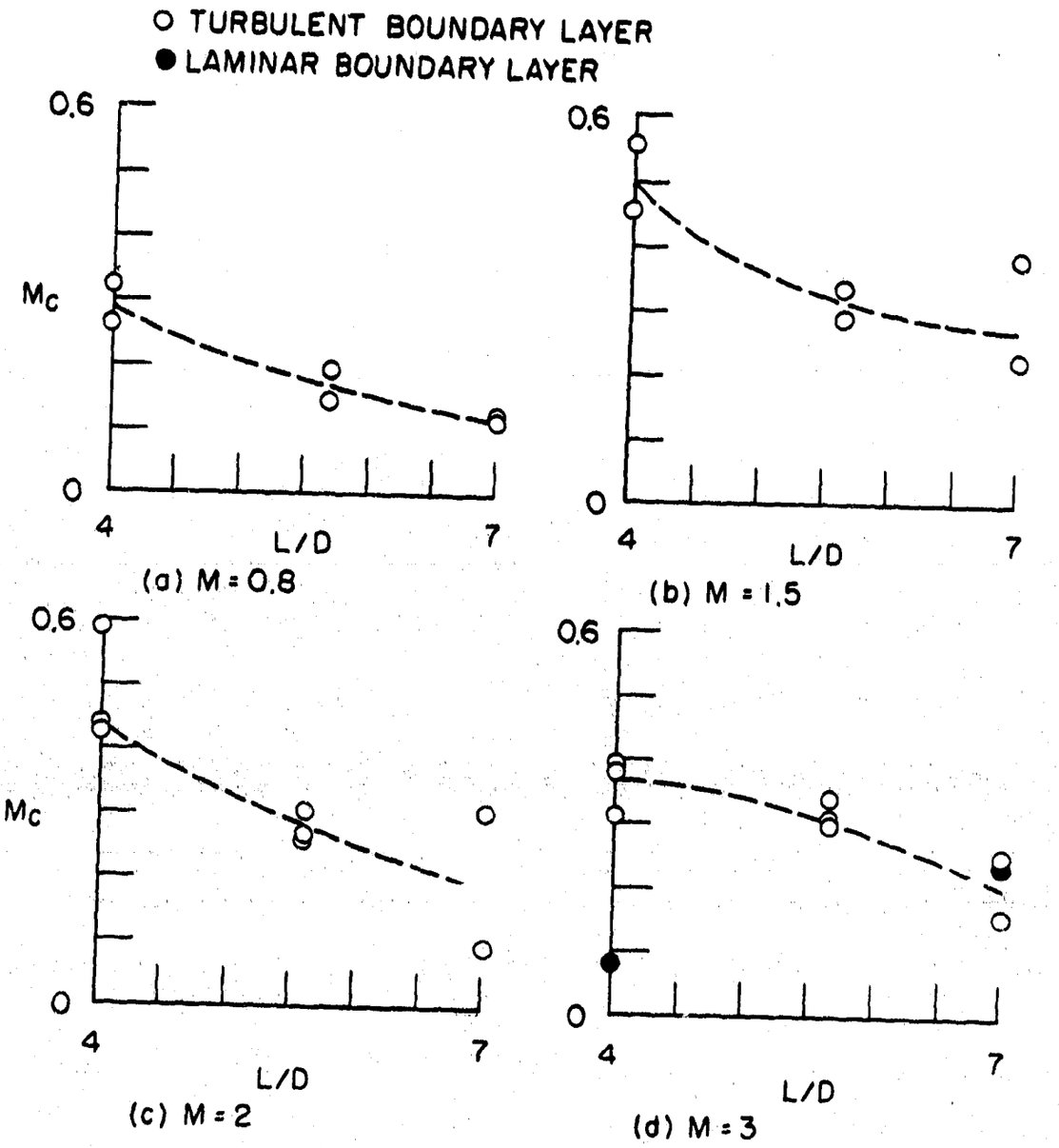

FIGURE 20. RECIRCULATION VELOCITIES.

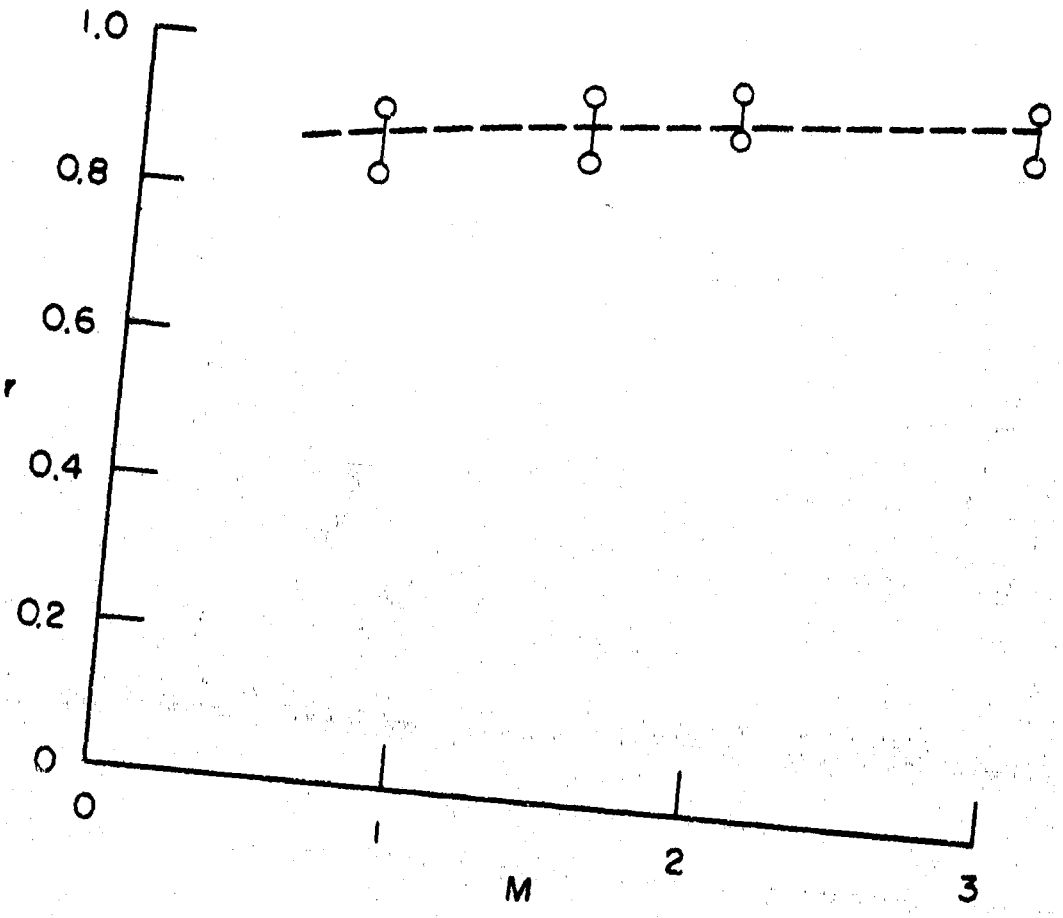

FIGURE 21. RANGE OF CAVITY RECOVERY FACTOR AS FUNCTION OF FREE-STREAM MACH NUMBER.

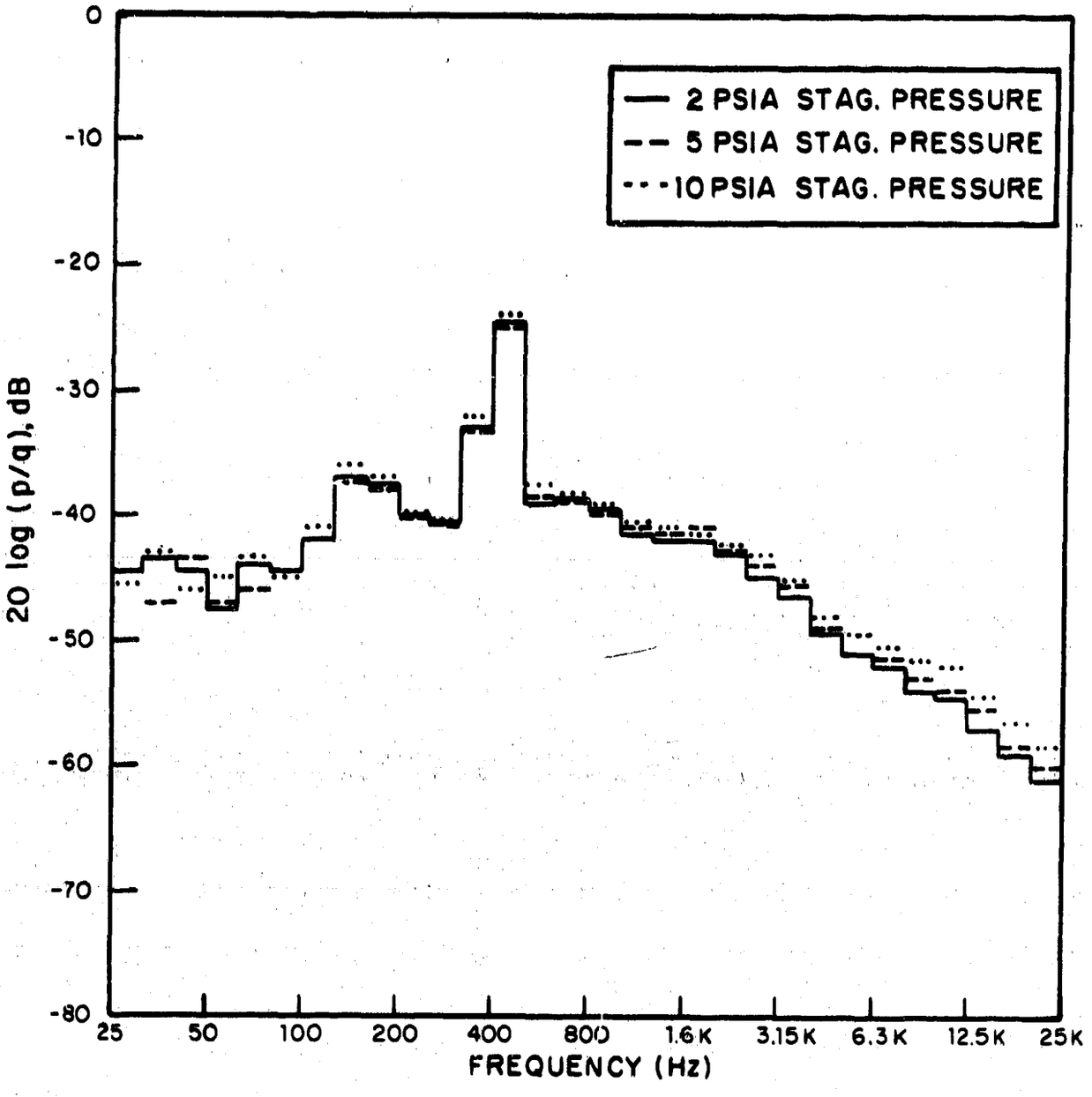

FIGURE 22. EFFECT OF CHANGING DYNAMIC PRESSURE ON SPECTRUM – EMPTY CAVITY; M = 0.8; L/D = 4; MICROPHONE #6.

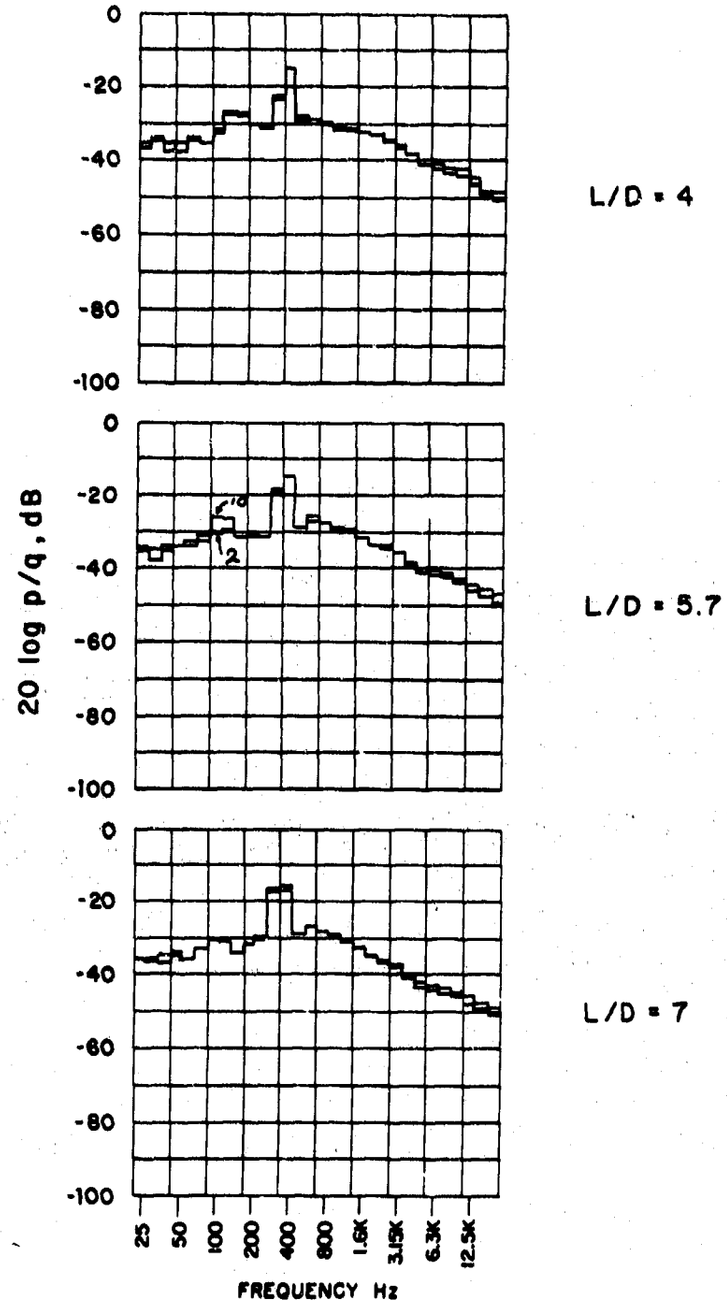

FIGURE 23. THIRD-OCTAVE-BAND SPECTRA — EMPTY CAVITY; M = 0.8; P_0 = 2 and 10 psia MICROPHONE #6.

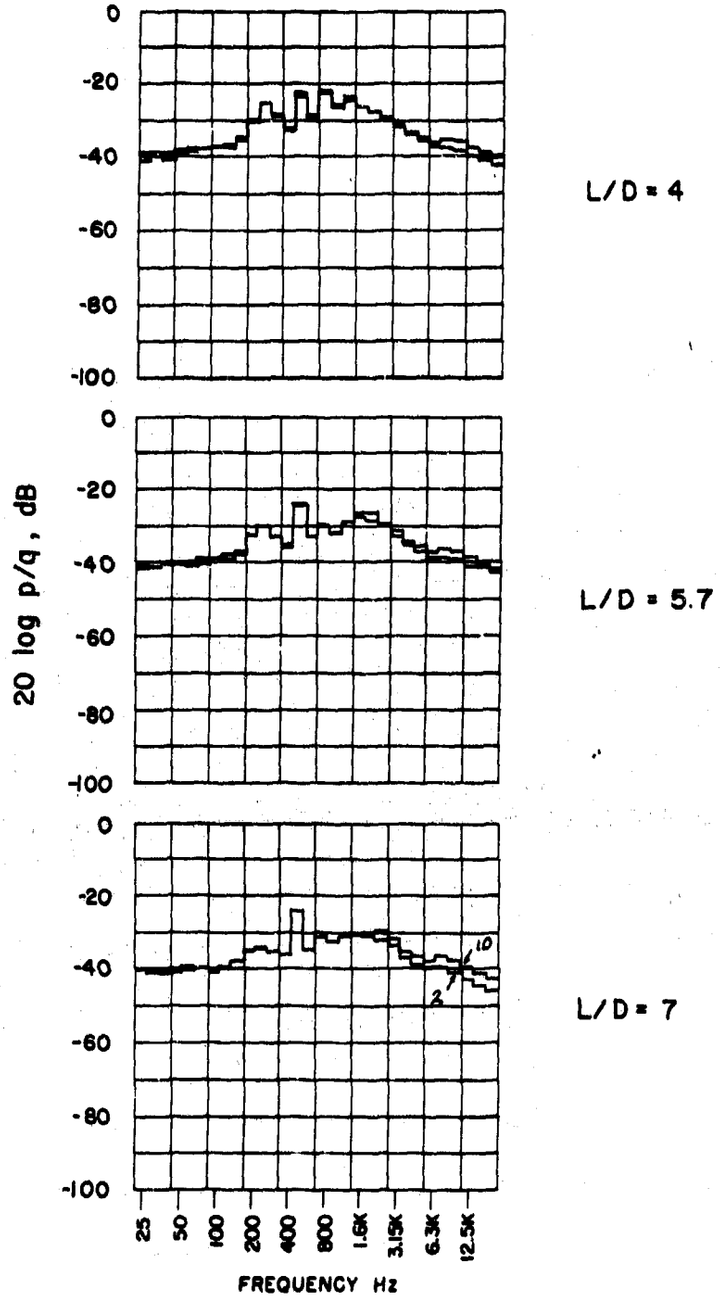

FIGURE 24. THIRD-OCTAVE-BAND SPECTRA – EMPTY CAVITY; M = 1.5; P_0 = 2 and 10 psia MICROPHONE #6.

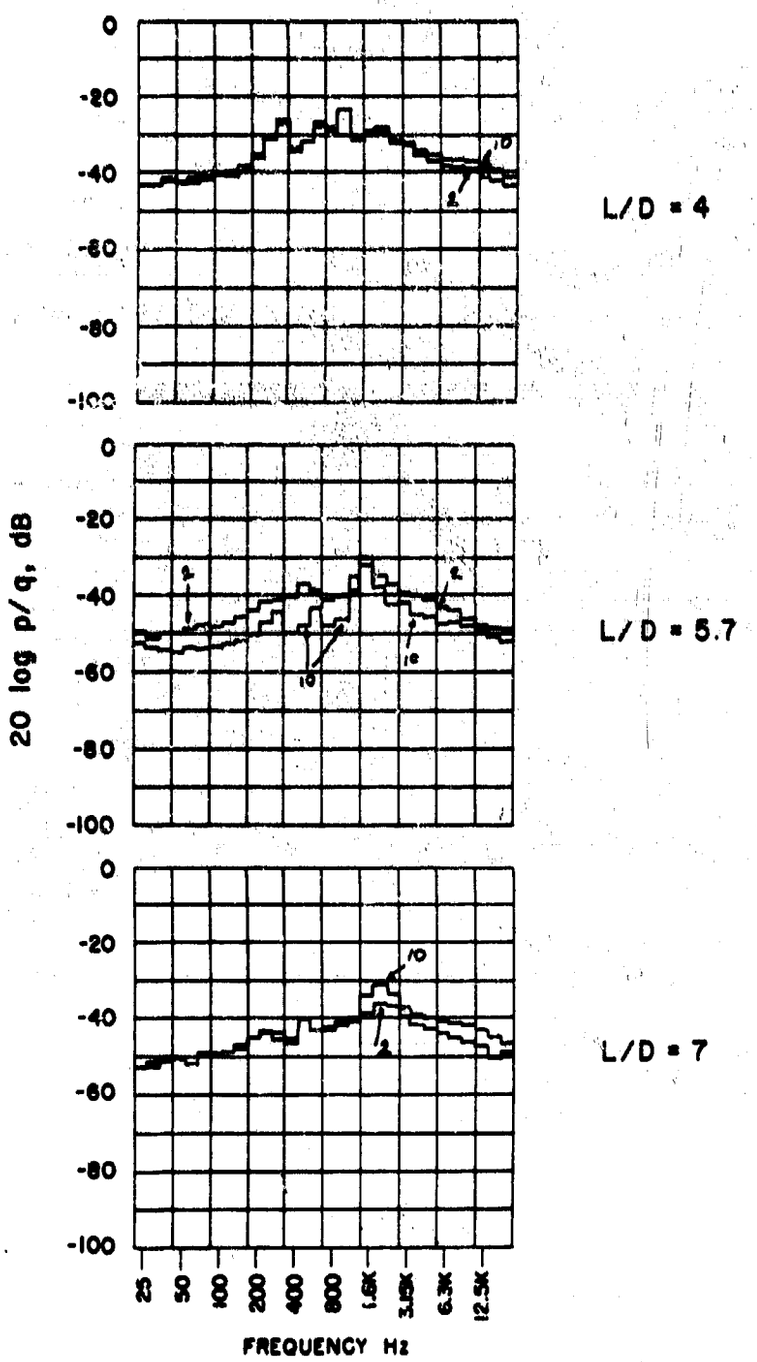

FIGURE 25. THIRD-OCTAVE-BAND SPECTRA — EMPTY CAVITY; M = 2; P_0 = 2 and 10 psia MICROPHONE #6.

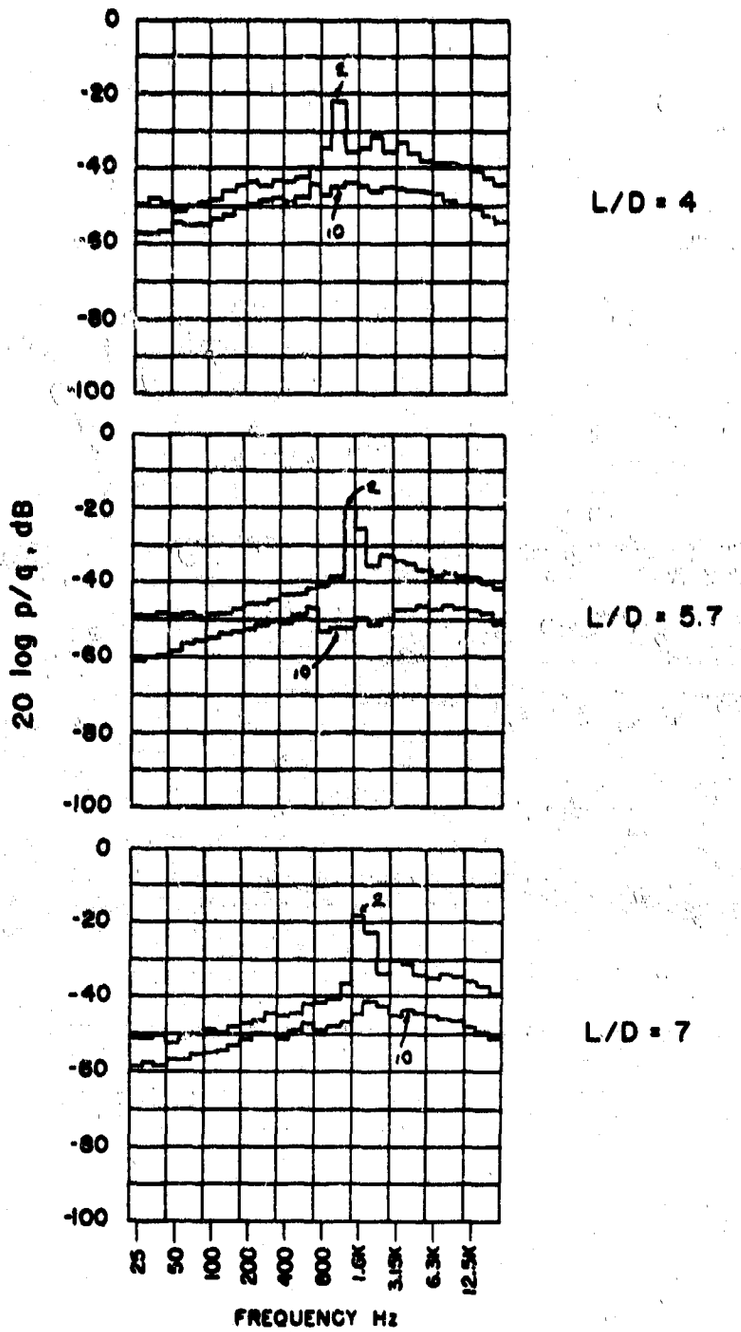

FIGURE 26. THIRD-OCTAVE-BAND SPECTRA – EMPTY CAVITY; M = 3; P_0 = 2 and 10 psia MICROPHONE #6.

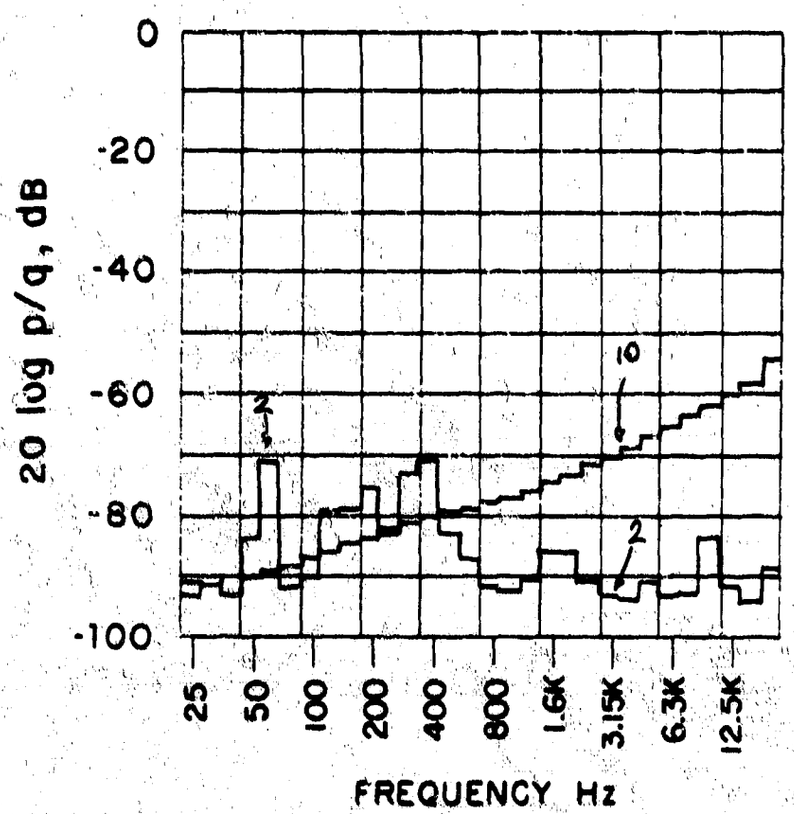

FIGURE 27. THIRD-OCTAVE-BAND SPECTRA — CAVITY CLOSED; M = 3; P_0 = 2 and 10 psia MICROPHONE #1.

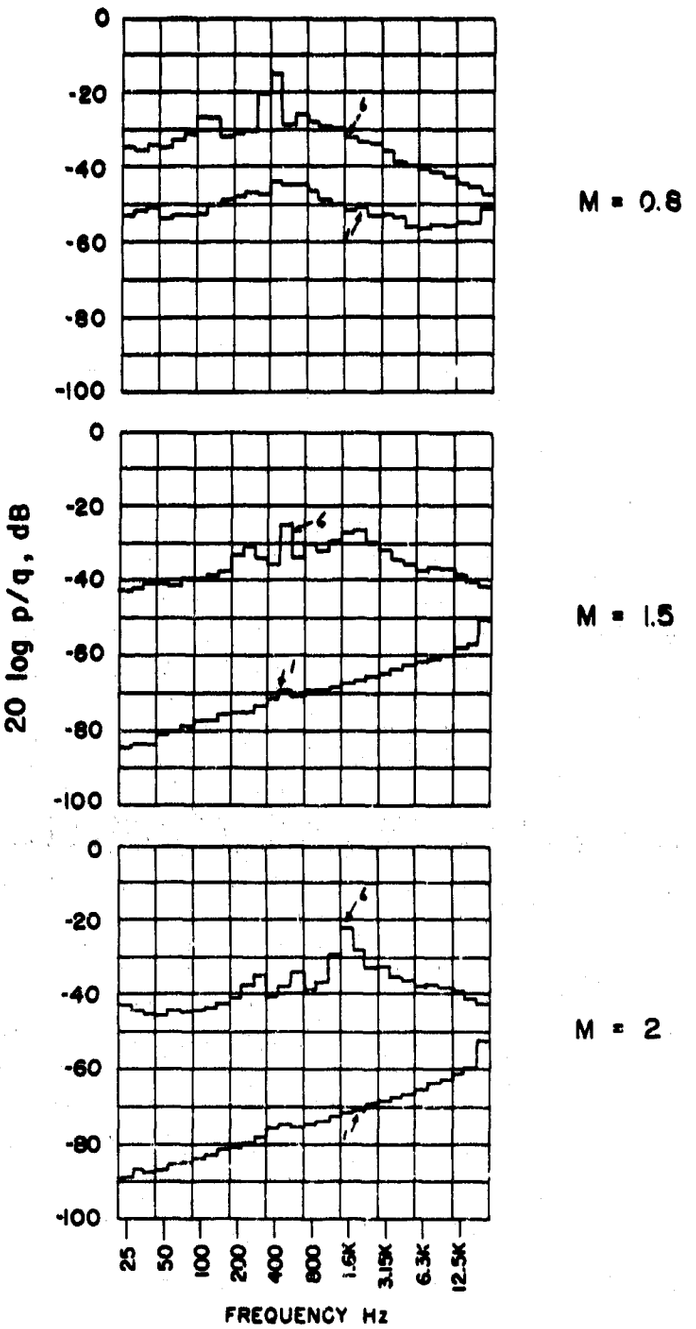

FIGURE 28. THIRD-OCTAVE-BAND SPECTRA — P_0 = 10 psia; L/D = 5.7; MICROPHONE #1 — CLOSED CAVITY; MICROPHONE #6 — EMPTY CAVITY.

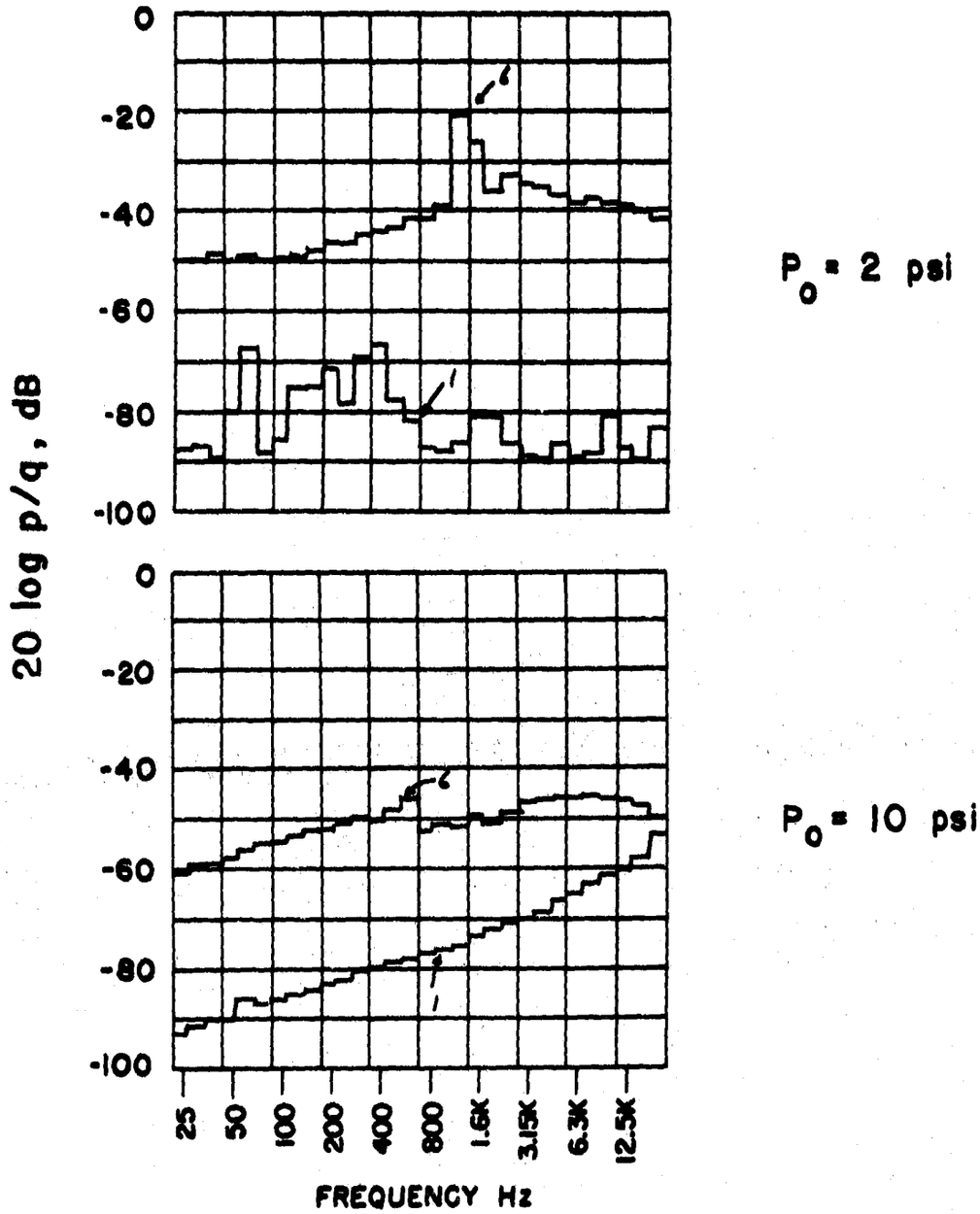

FIGURE 29. THIRD-OCTAVE-BAND SPECTRA — M = 3; L/D = 5.7; MICROPHONE #1 — CLOSED CAVITY; MICROPHONE #6 — EMPTY CAVITY.

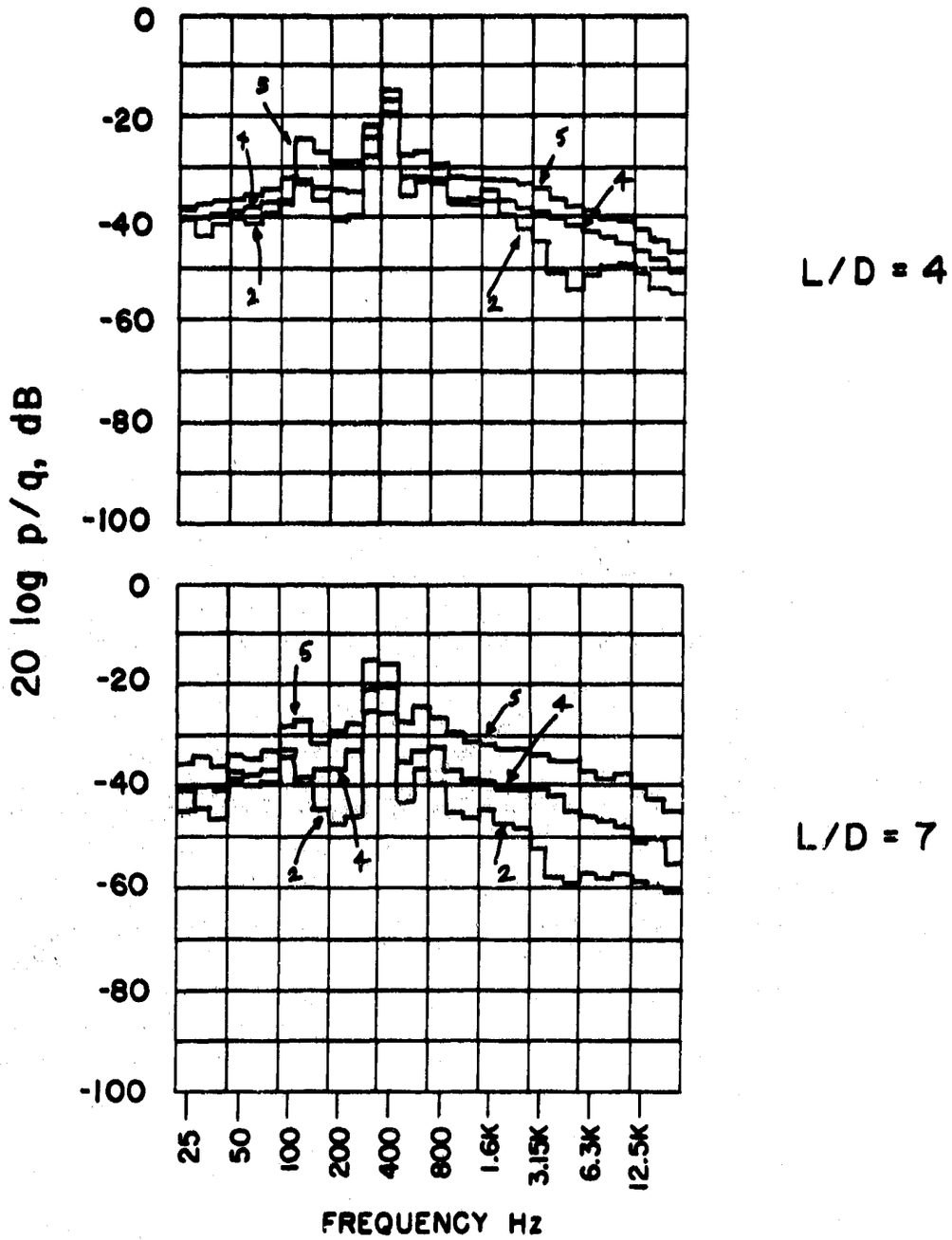

FIGURE 30. THIRD-OCTAVE-BAND SPECTRA — EMPTY CAVIT M = 0.8; P_0 = 10 psia; MICROPHONES #2, #4, #5.

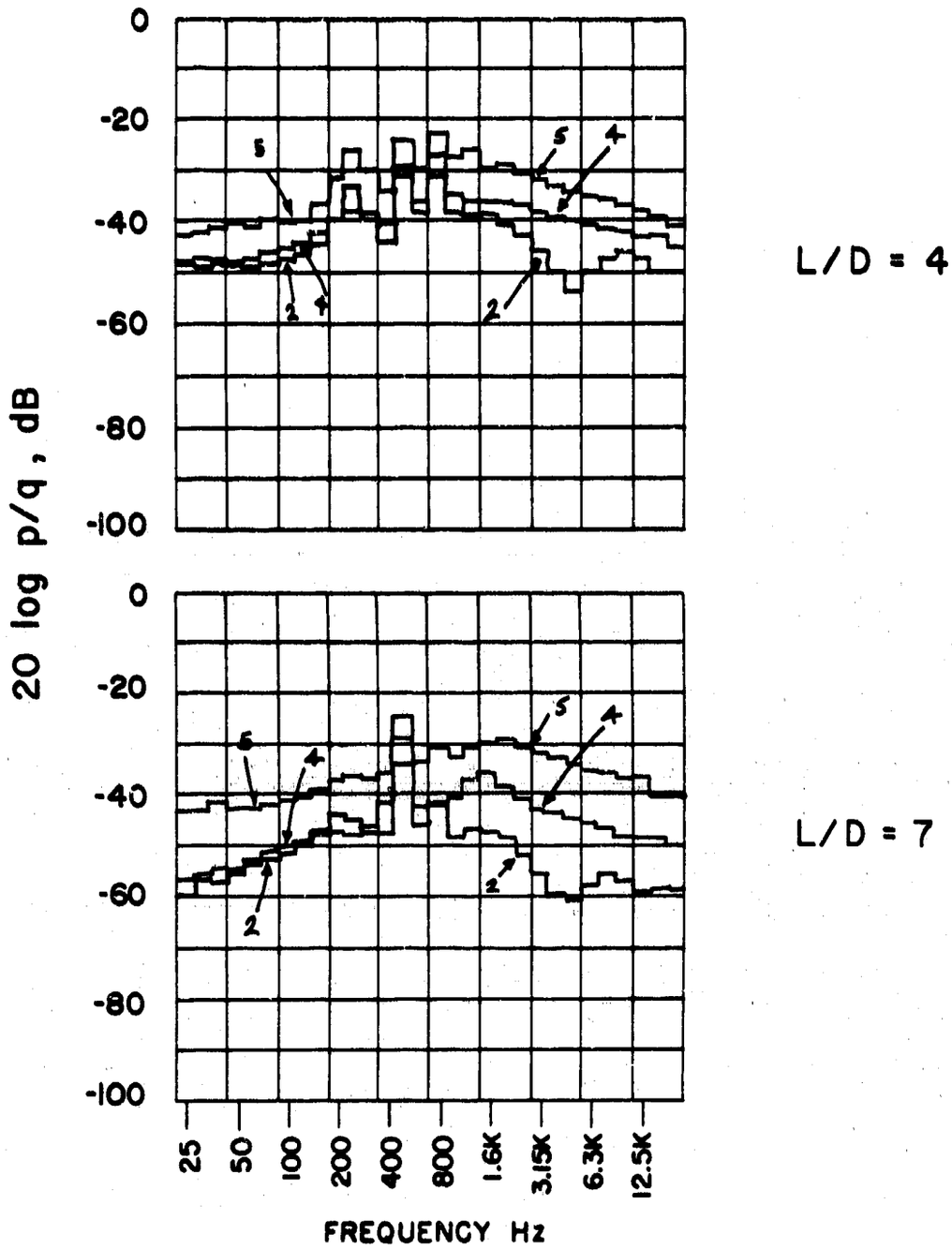

FIGURE 31. THIRD-OCTAVE-BAND SPECTRA — EMPTY CAVITY; M = 1.5; P_0 = 10 psia; MICROPHONES #2, #4, #5.

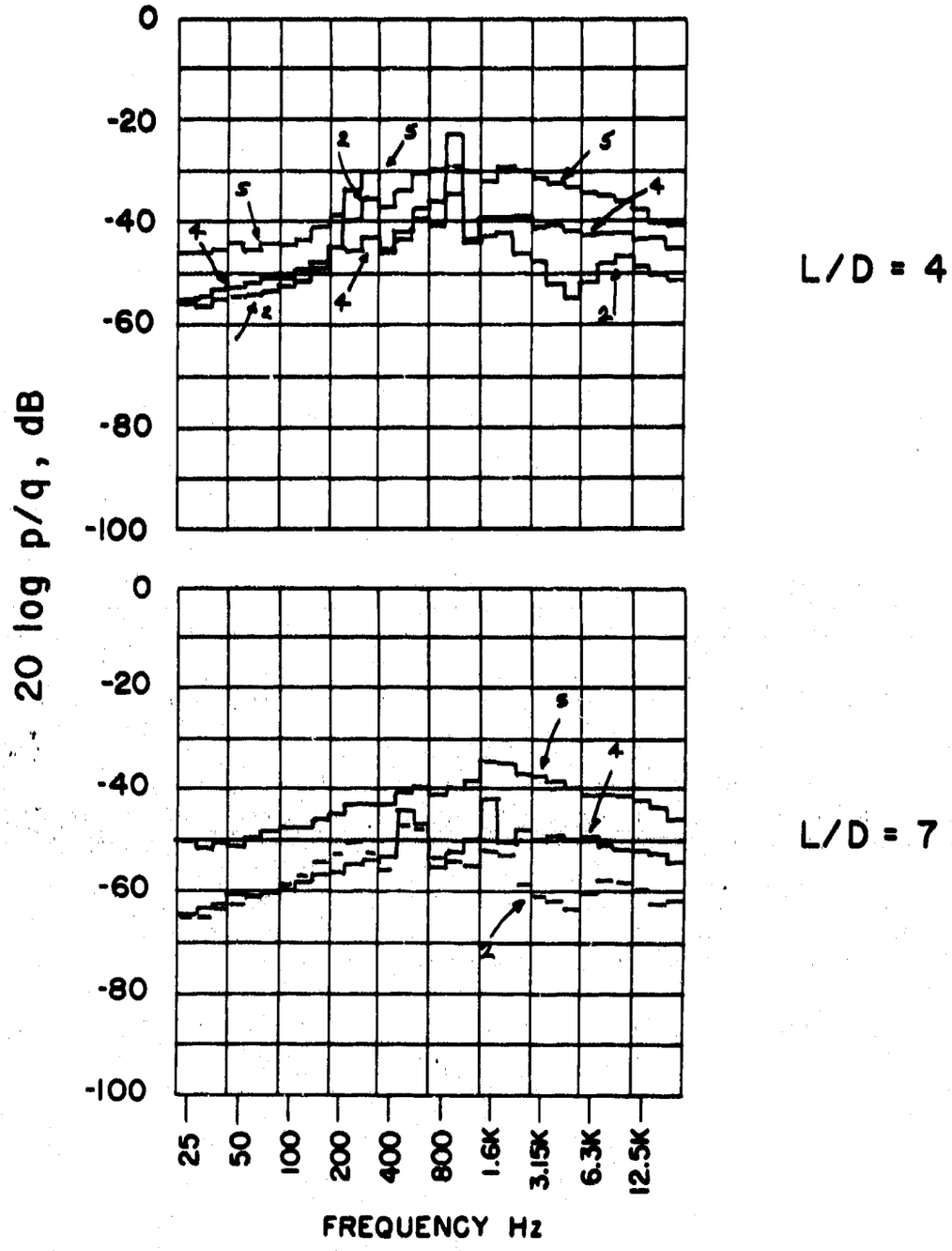

FIGURE 32. THIRD-OCTAVE-BAND SPECTRA — EMPTY CAVITY; M = 2; P_0 = 10 psia; MICROPHONES #2, #4, #5.

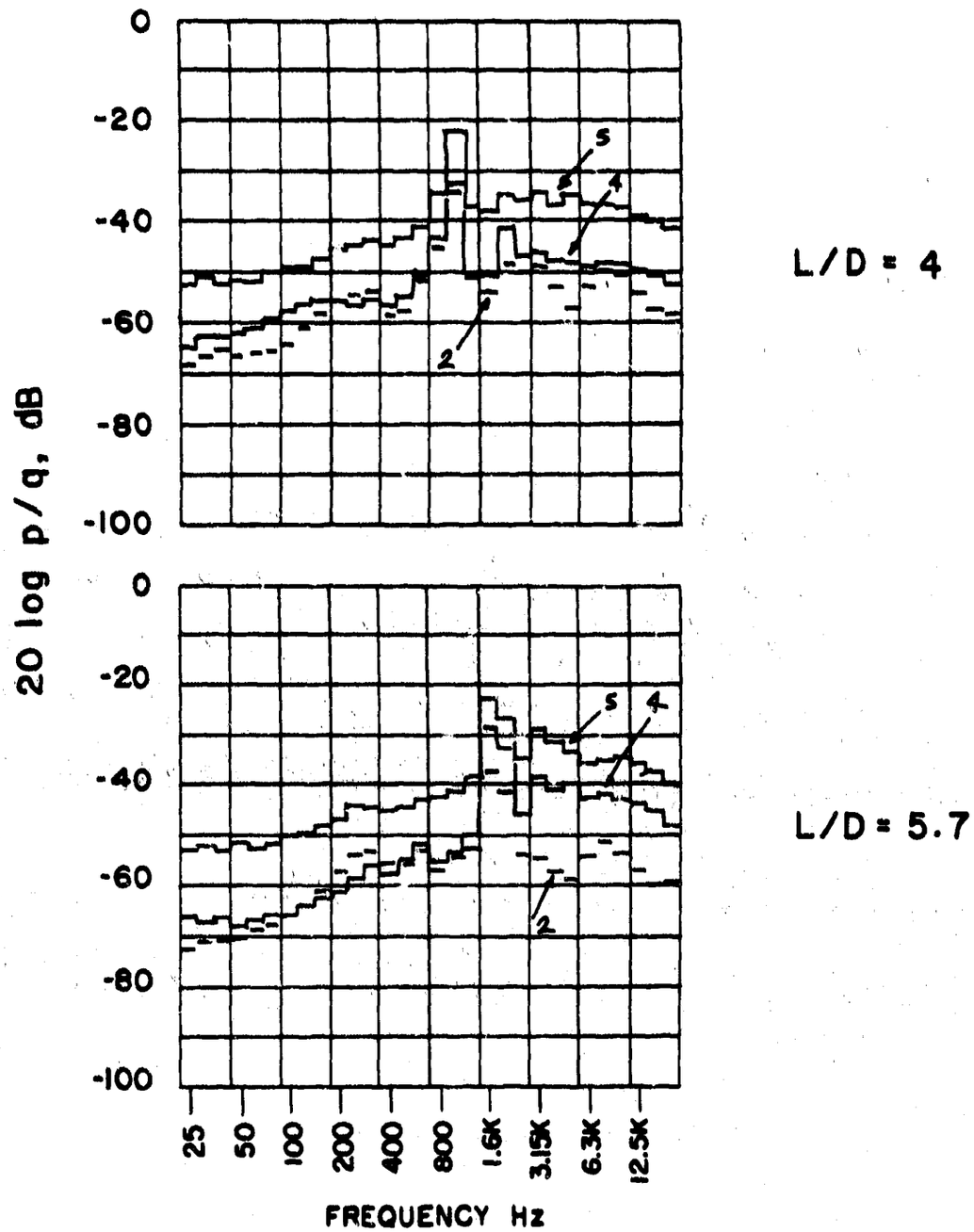

FIGURE 33. THIRD-OCTAVE-BAND SPECTRA – EMPTY CAVITY, M = 3; P_0 = 2 psia; MICROPHONES #2, #4, #5.

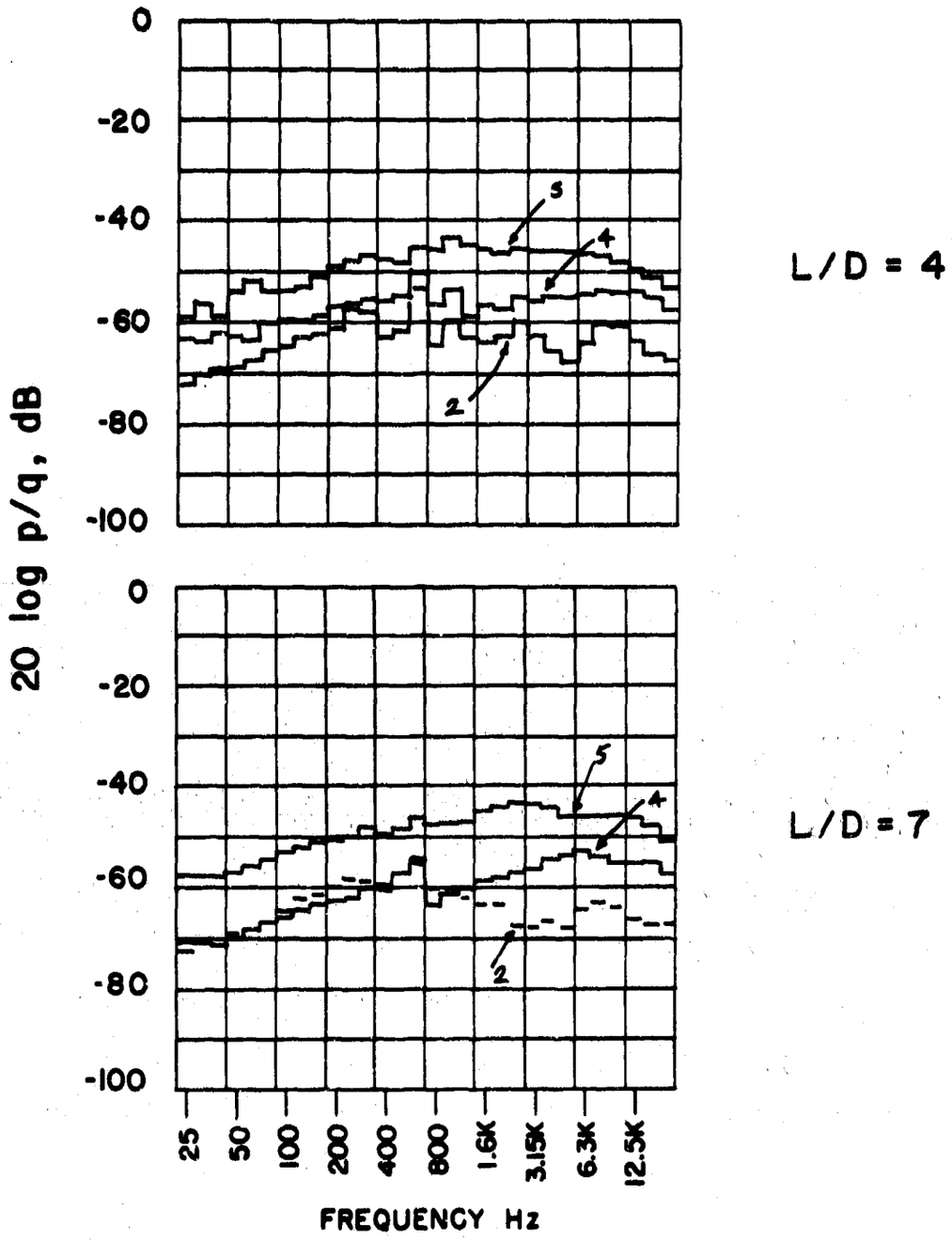

FIGURE 34. THIRD-OCTAVE-BAND SPECTRA – EMPTY CAVITY; M = 3; P_0 = 10 psia; MICROPHONES #2, #4, #5.

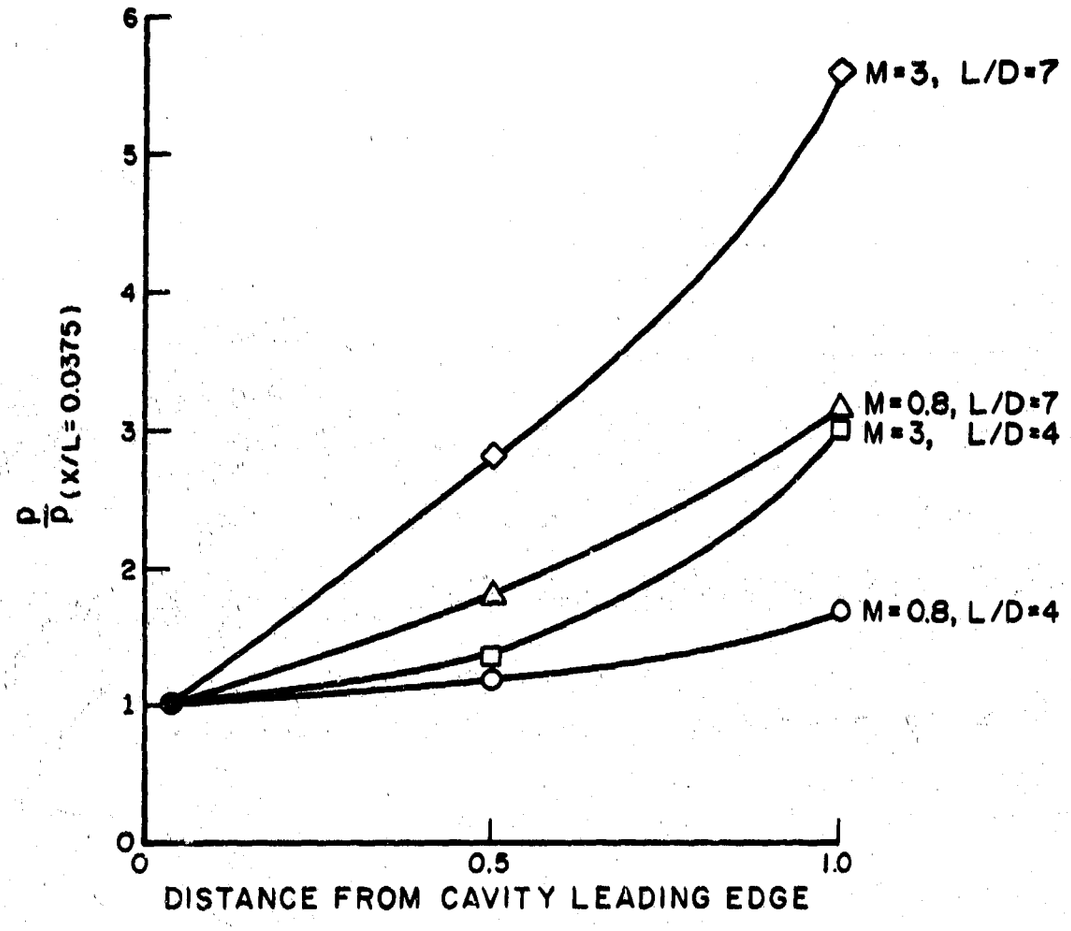

FIGURE 35. LONGITUDINAL ENERGY DISTRIBUTION — M = 0.8 and 3; L/D = 4 and 7.

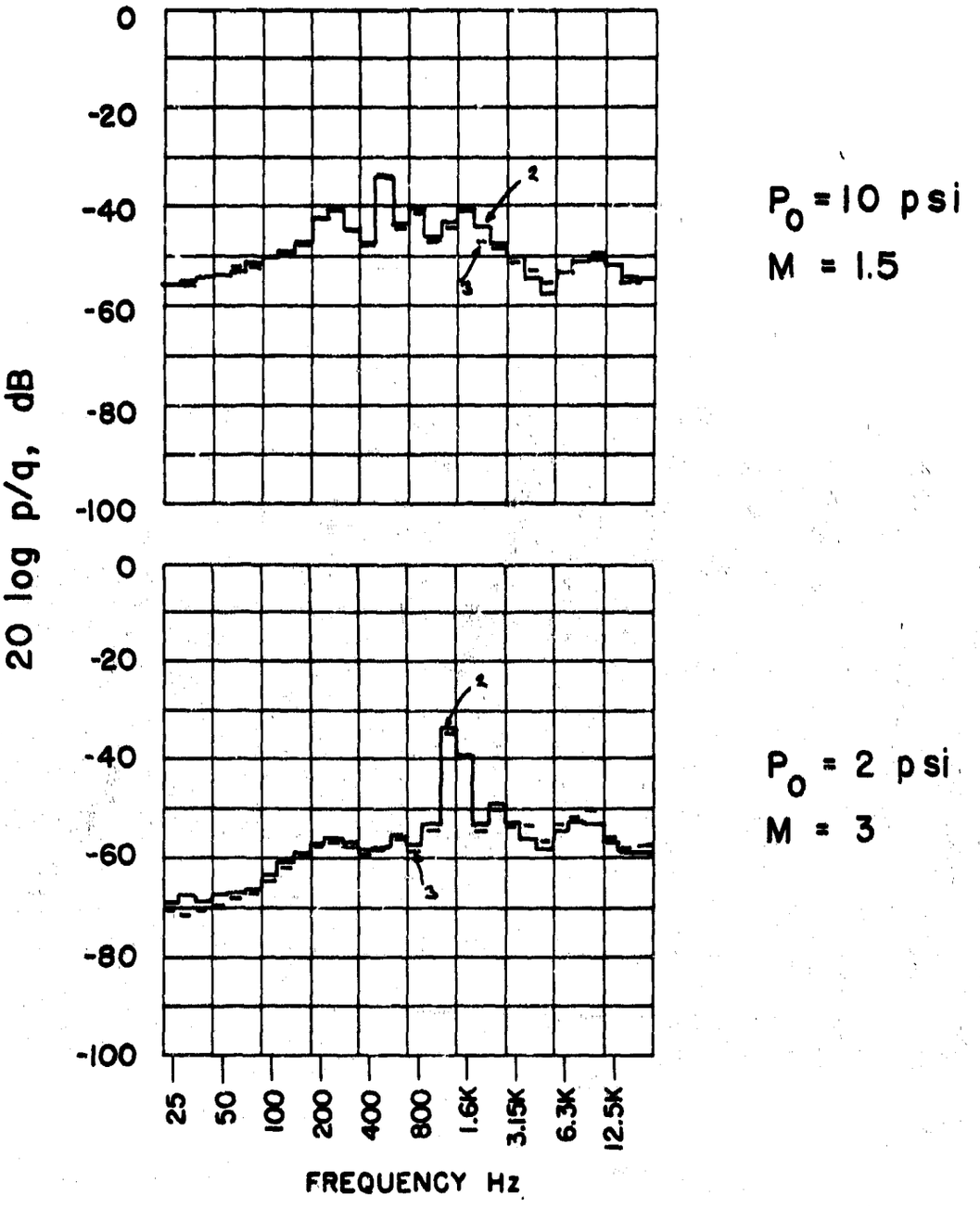

FIGURE 36. THIRD-OCTAVE-BAND SPECTRA — EMPTY CAVITY; L/D = 5.7; MICROPHONES # 2, #3.

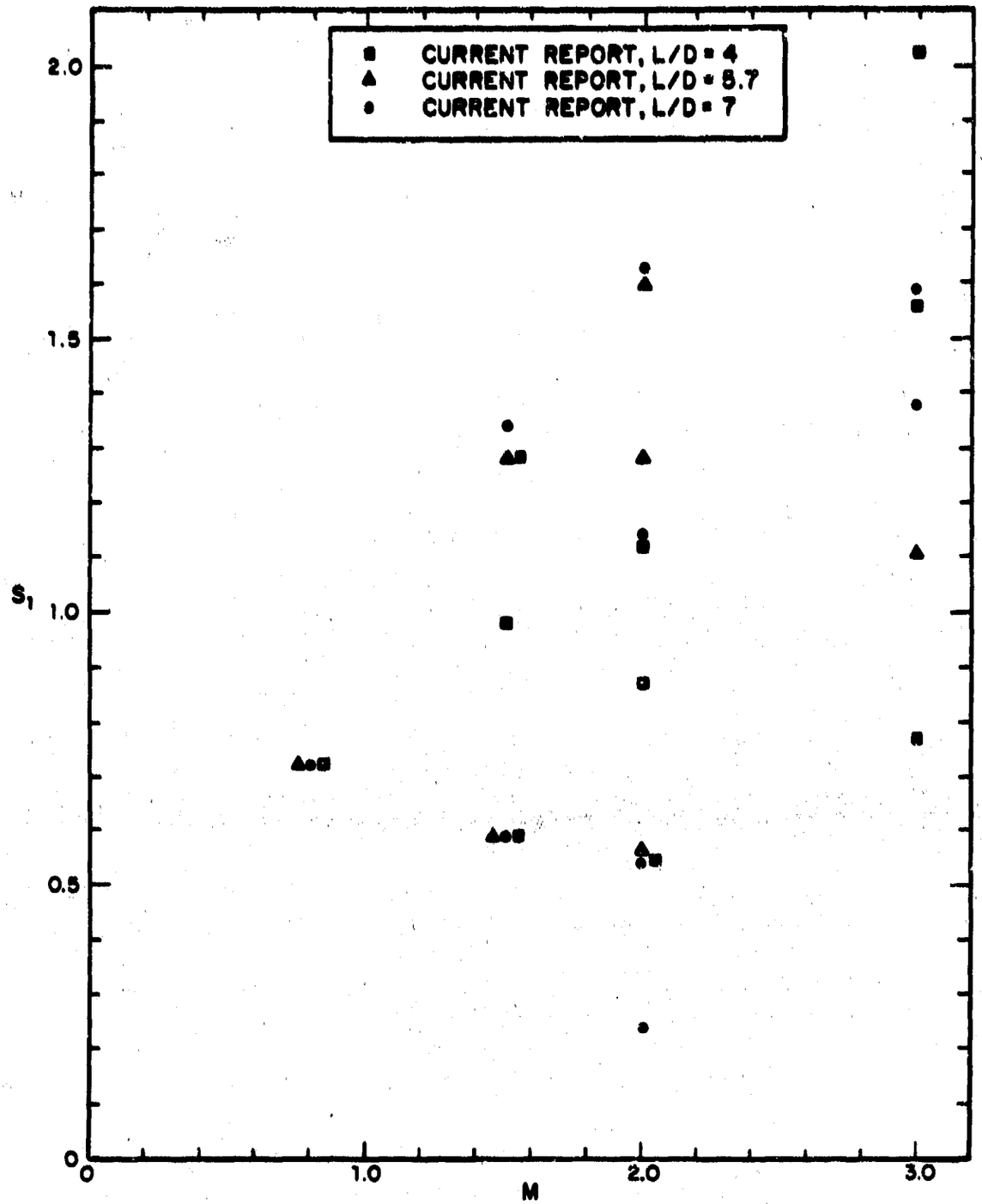

FIGURE 37a. NONDIMENSIONAL RESONANT FREQUENCIES AS A FUNCTION OF MACH NUMBER (CURRENT RESULTS).

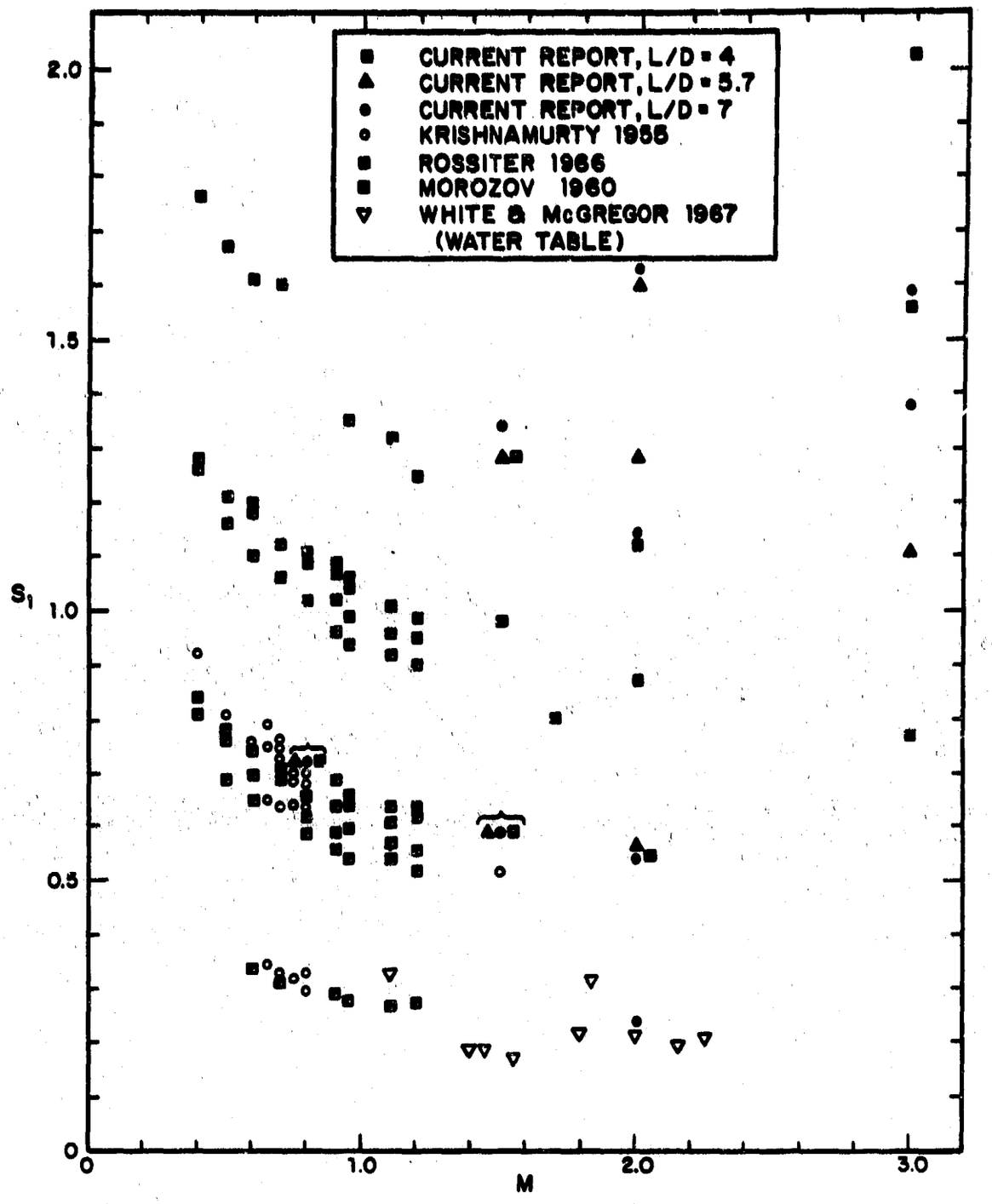

FIGURE 37b. NONDIMENSIONAL RESONANT FREQUENCIES AS A FUNCTION OF MACH NUMBER (CURRENT RESULTS AND OTHER INVESTIGATORS' RESULTS).

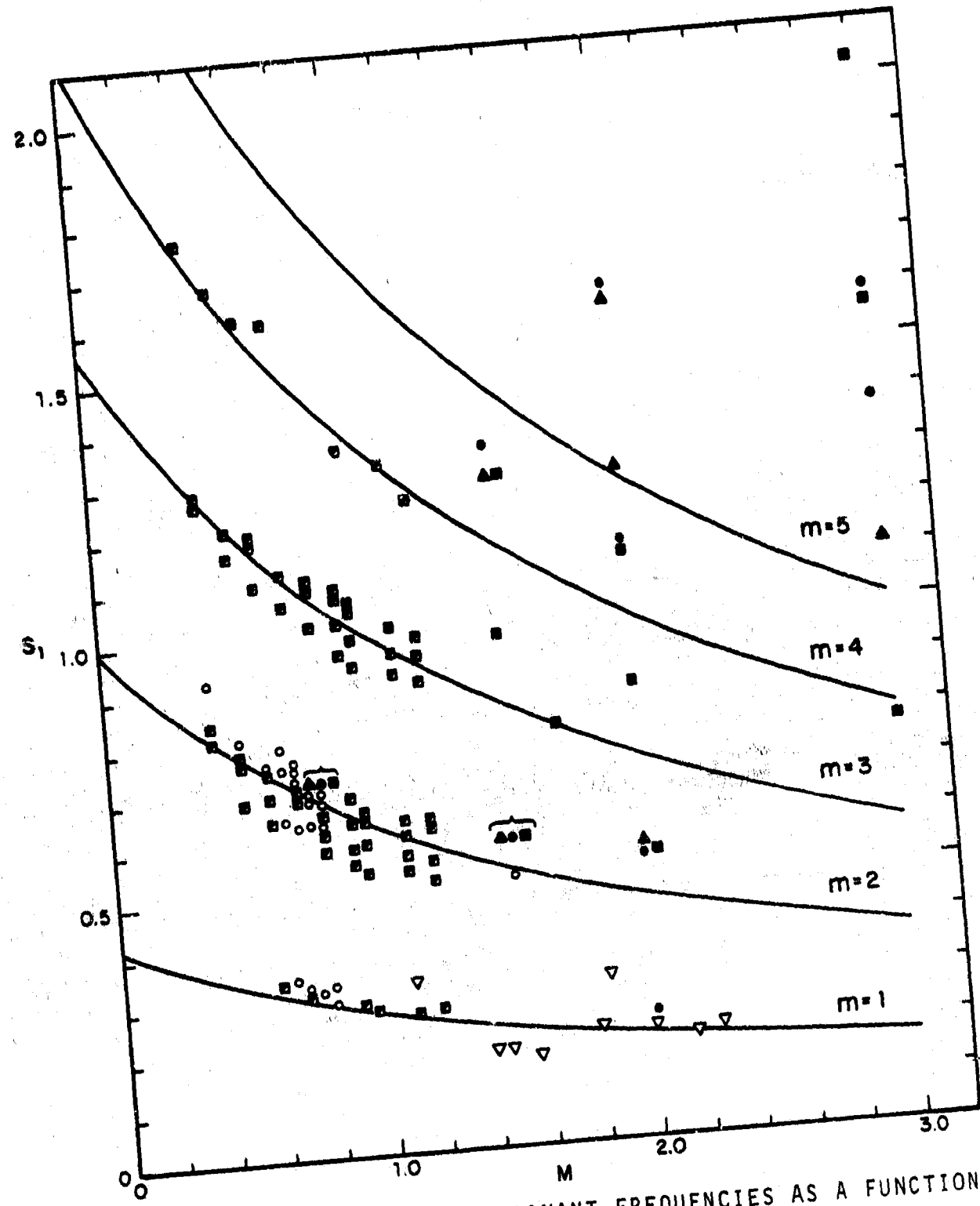

FIGURE 37c. NONDIMENSIONAL RESONANT FREQUENCIES AS A FUNCTION OF MACH NUMBER — IMPLEMENTATION OF ROSSITER's FORMULA.

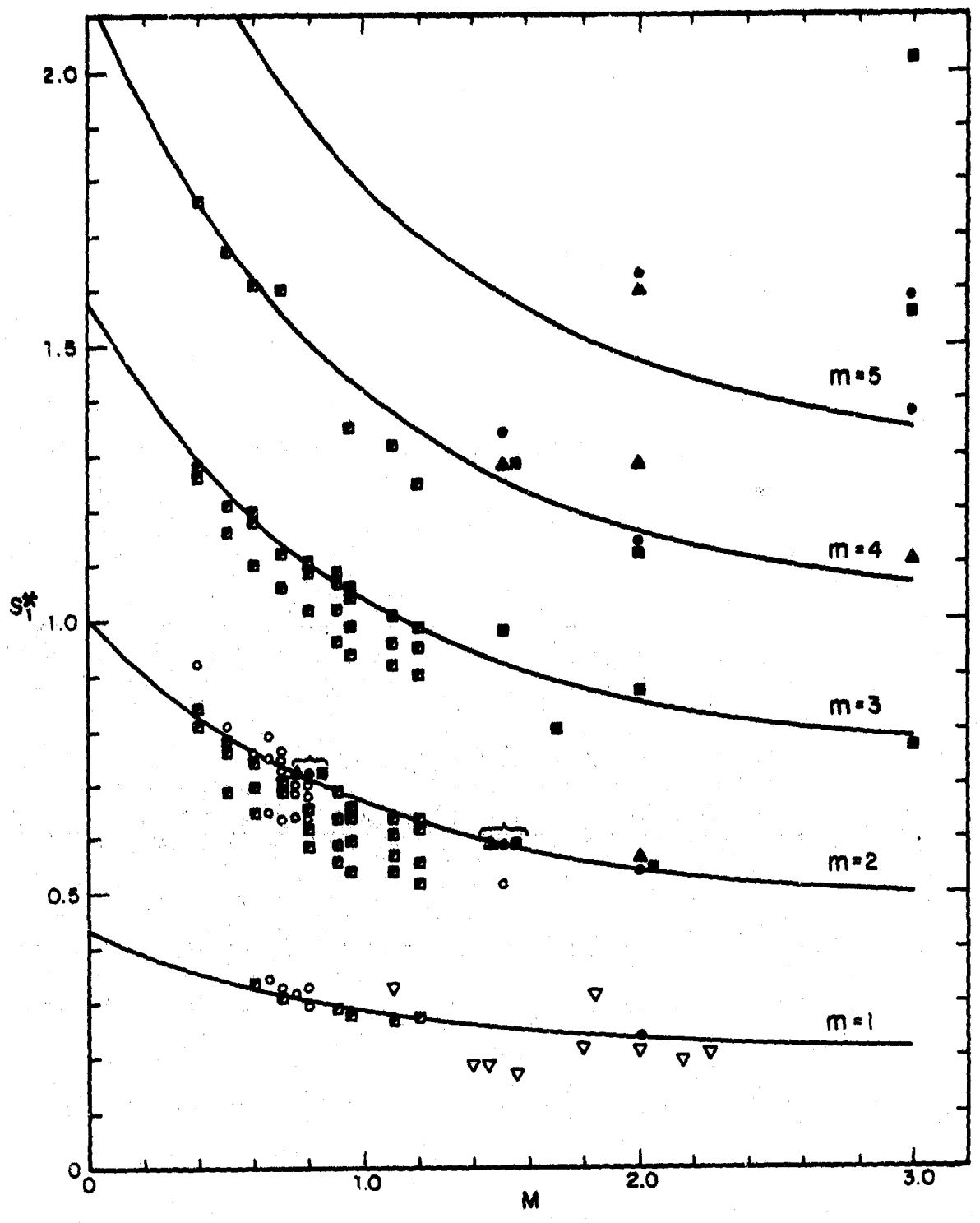

FIGURE 37d. NONDIMENSIONAL RESONANT FREQUENCIES AS A FUNCTION OF MACH NUMBER – IMPLEMENTATION OF MODIFIED ROSSITER FORMULA.

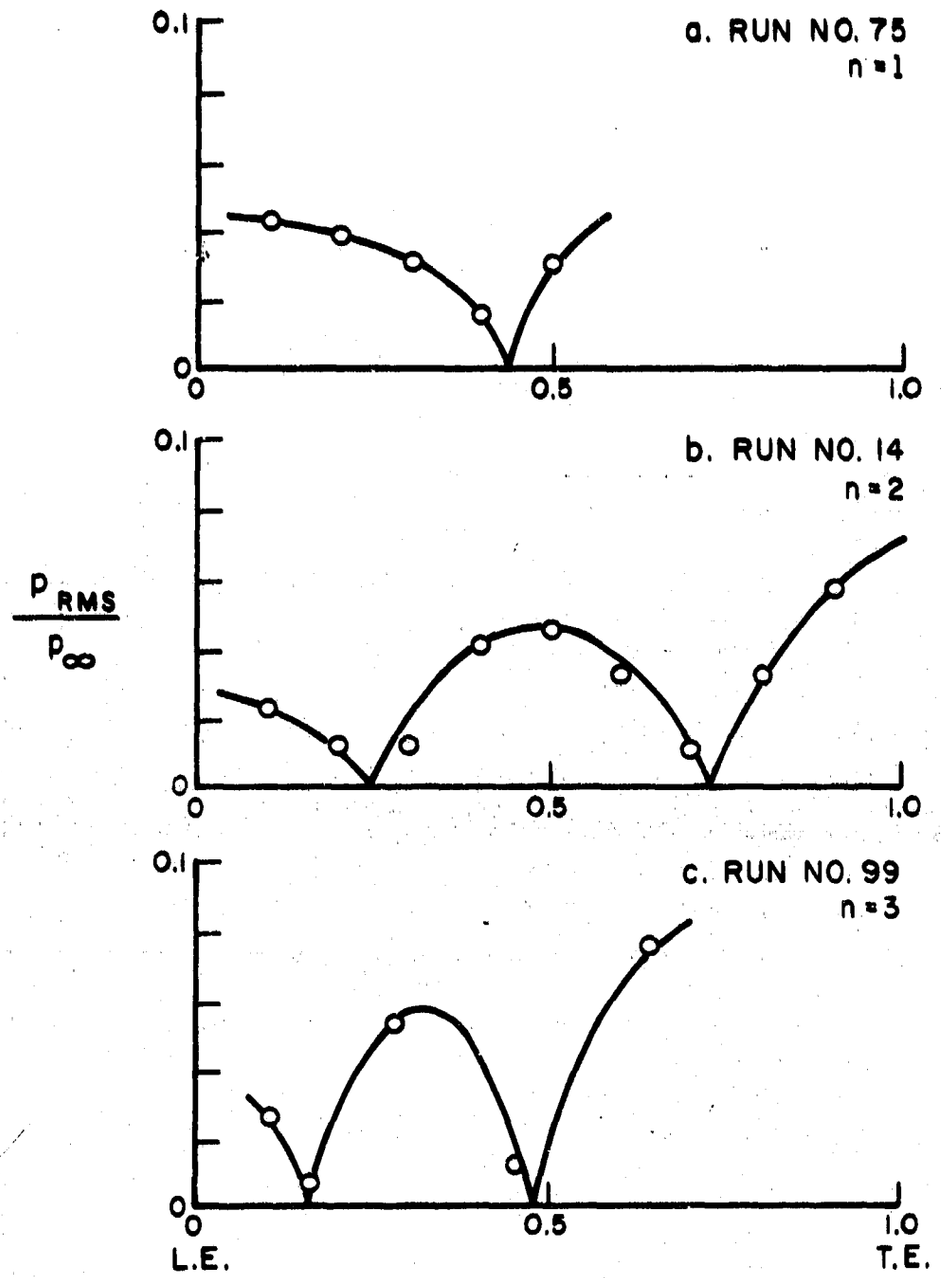

FIGURE 38. SUGGESTED SHAPE FOR FIRST-, SECOND-, AND THIRD-ORDER MODE.

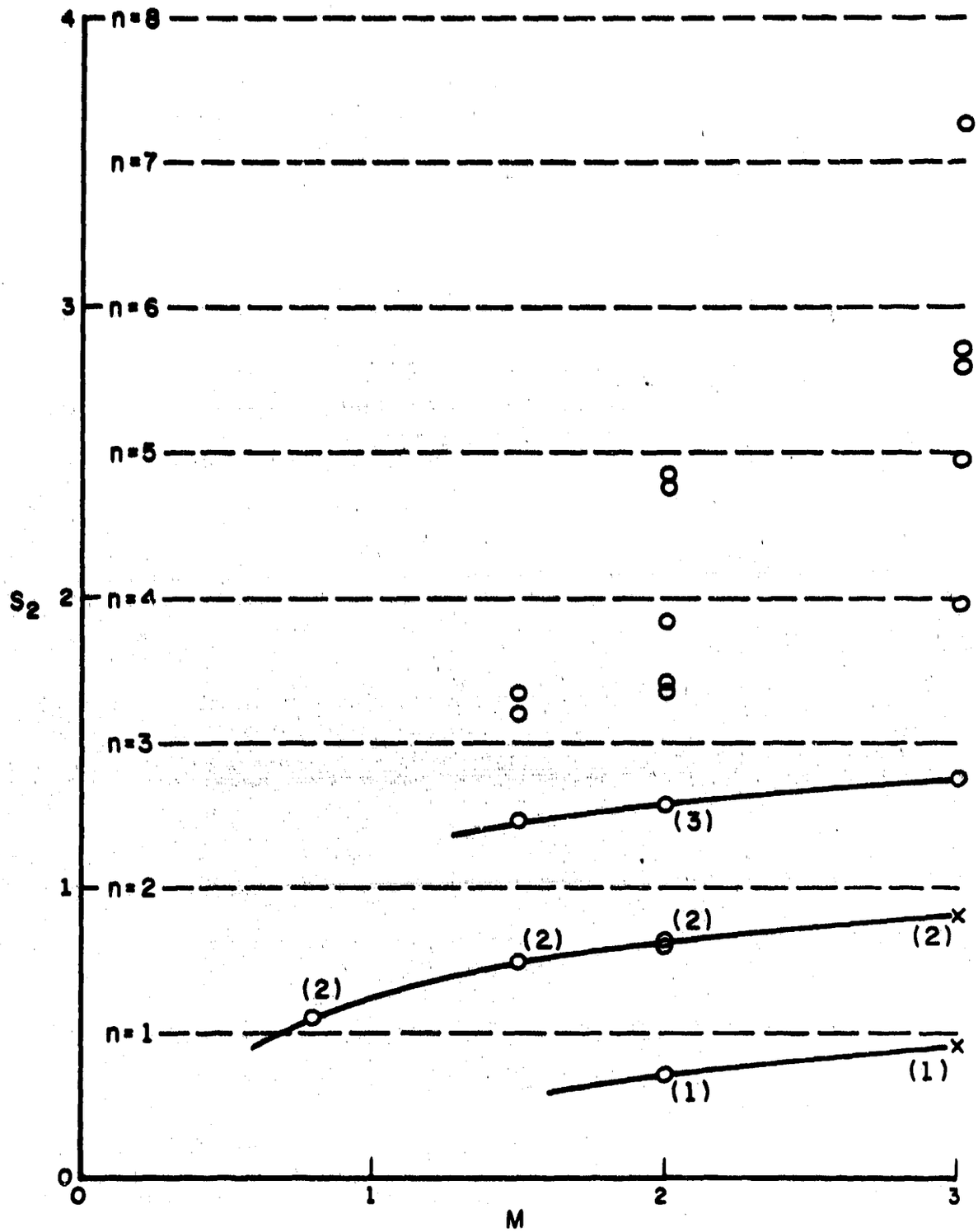

FIGURE 39. STROUHAL NUMBER S_2 AS A FUNCTION OF MACH NUMBER.

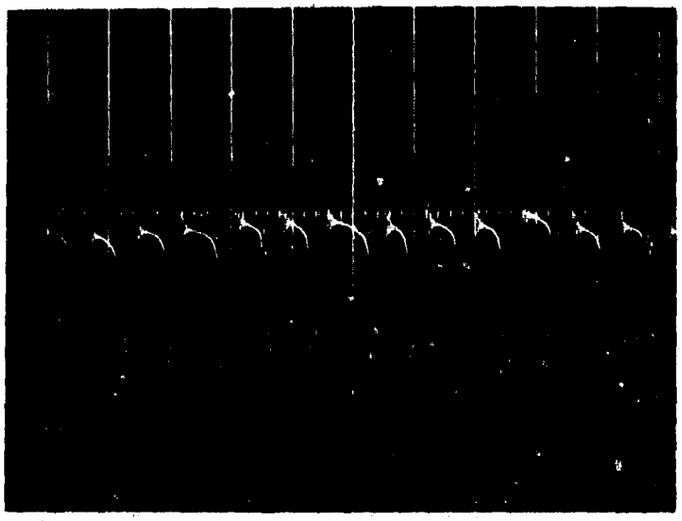

Sweep Rate 1 msec/cm

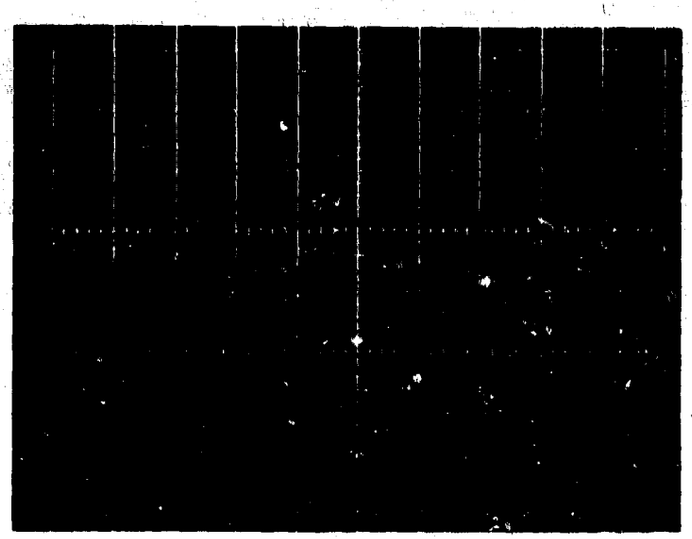

Sweep Rate 0.2 msec/cm

FIGURE 40. TIME HISTORY OF BROADBAND SIGNAL FROM MICROPHONE #6: (a) UNFILTERED SIGNAL; M = 3; L/D = 5.7; P_0 = 2 psia.

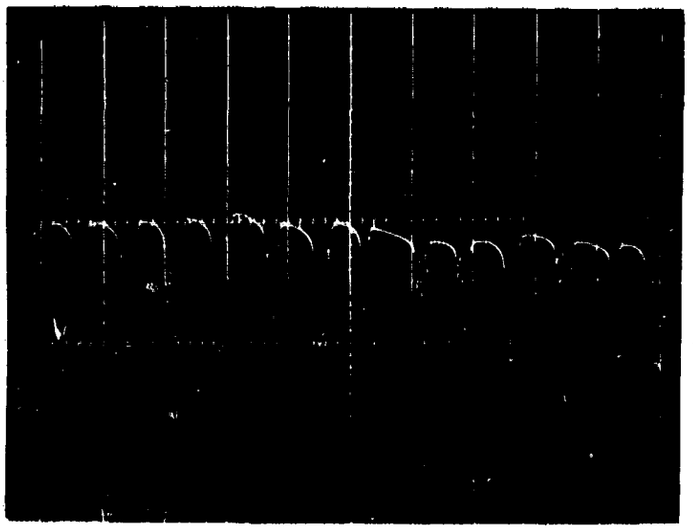

Sweep Rate 1 msec/cm

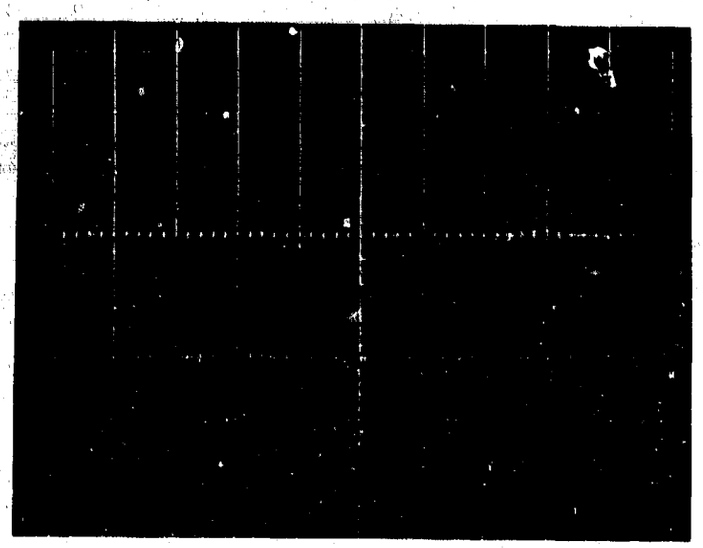

Sweep Rate 0.2 msec/cm

FIGURE 40. CONTINUED:
(b) FILTERED SIGNAL; M = 3; L/D = 5.7; P_0 = 2 psia.

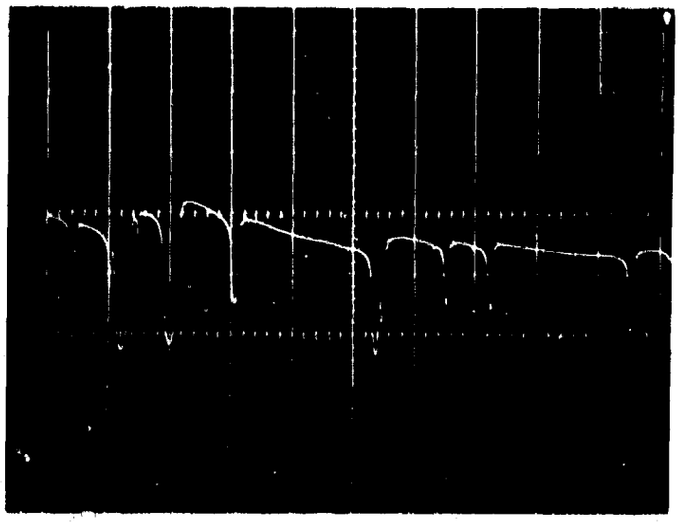

Sweep Rate 1 msec/cm

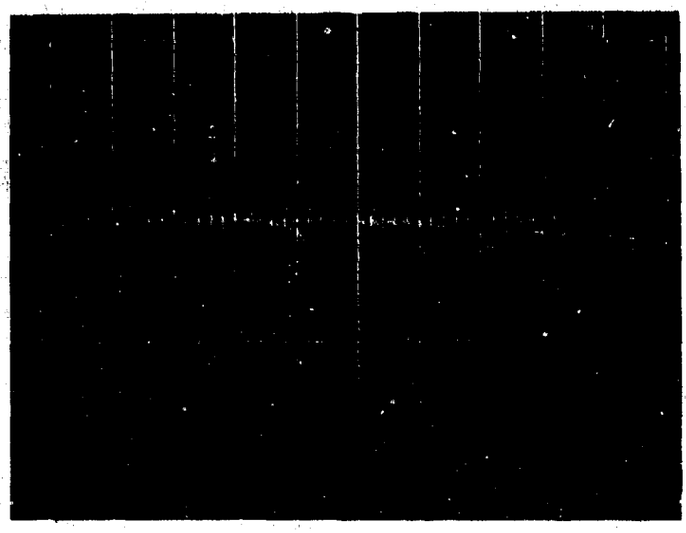

Sweep Rate 0.2 msec/cm

FIGURE 40. CONCLUDED:
(c) FILTERED SIGNAL; M = 3; L/D = 5.7; P_0 = 10 psia.

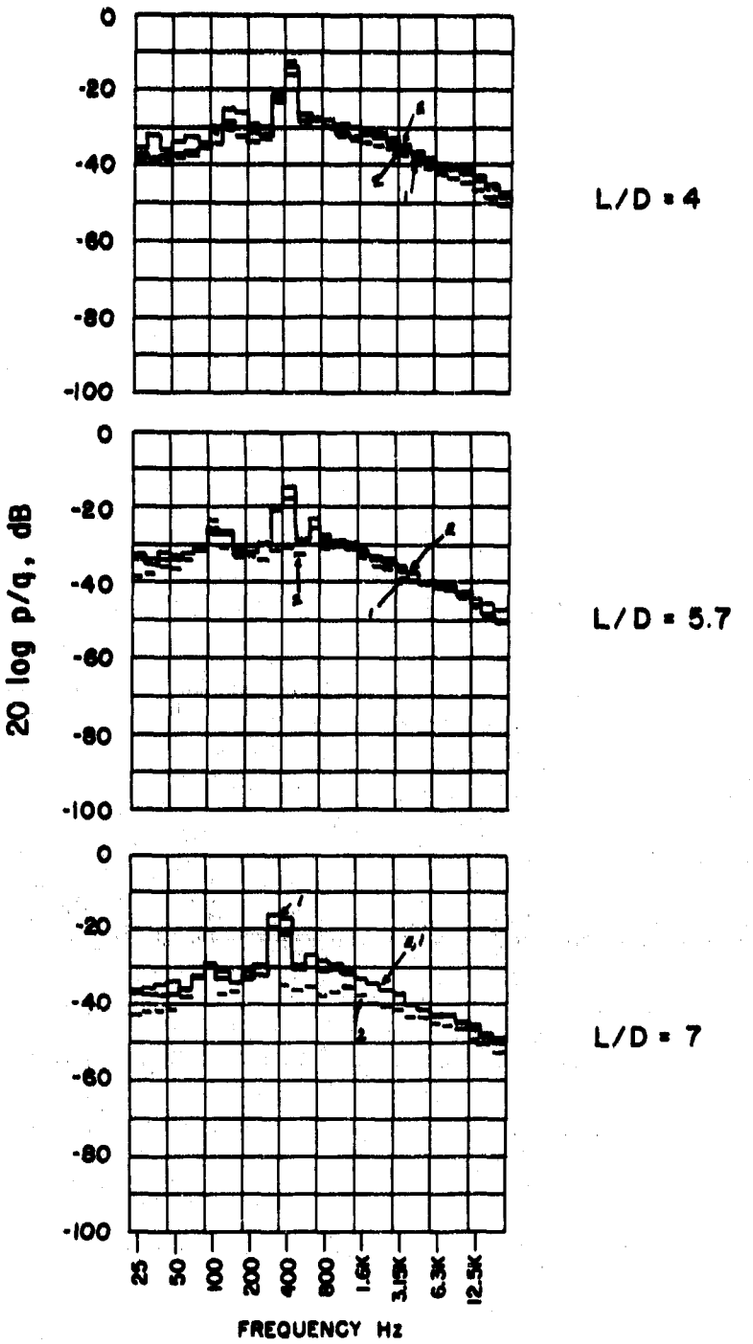

FIGURE 41. THIRD-OCTAVE-BAND SPECTRA — EMPTY CAVITY (E); CAVITY WITH ONE STORE (1), WITH TWO STORES (2); M = 0.8; P_0 = 10 psia; MICROPHONE #6.

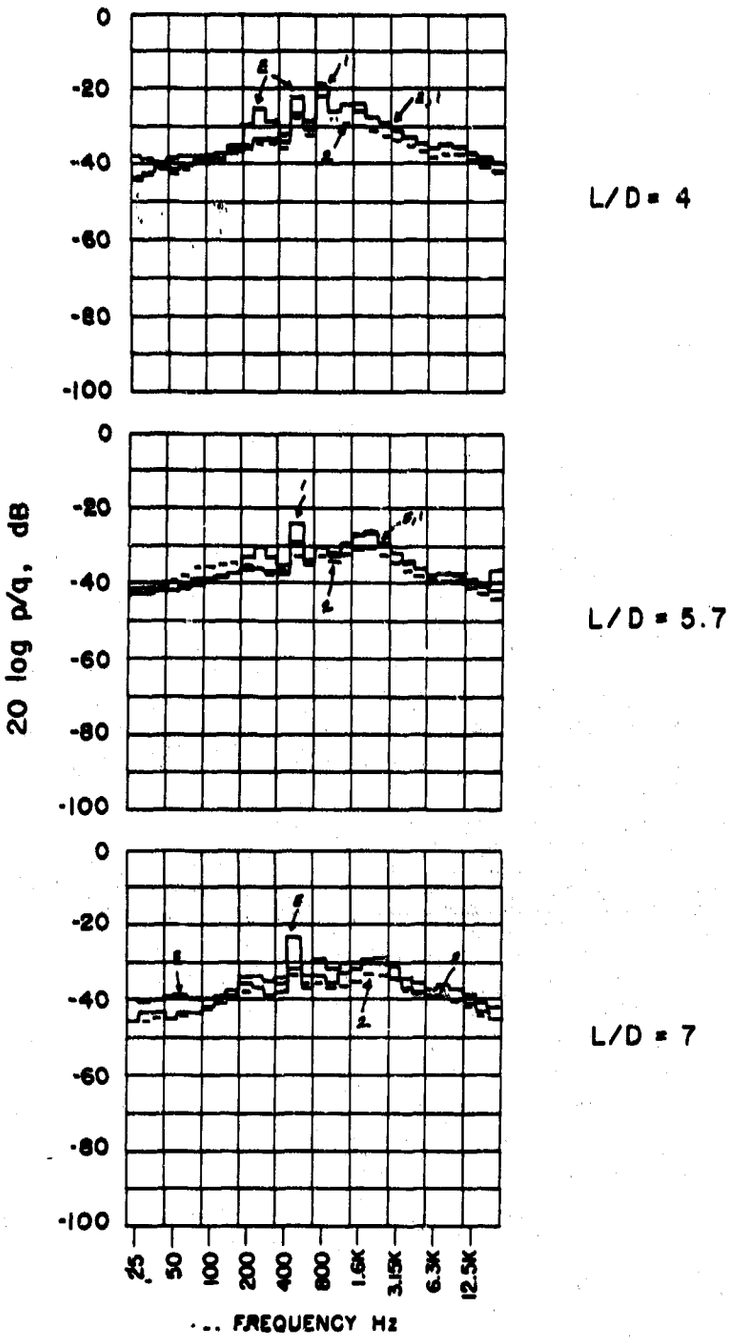

FIGURE 42. THIRD-OCTAVE-BAND SPECTRA – EMPTY CAVITY (E); CAVITY WITH ONE STORE (1), WITH TWO STORES (2); M = 1.5; P_0 = 10 psia; MICROPHONE #6.

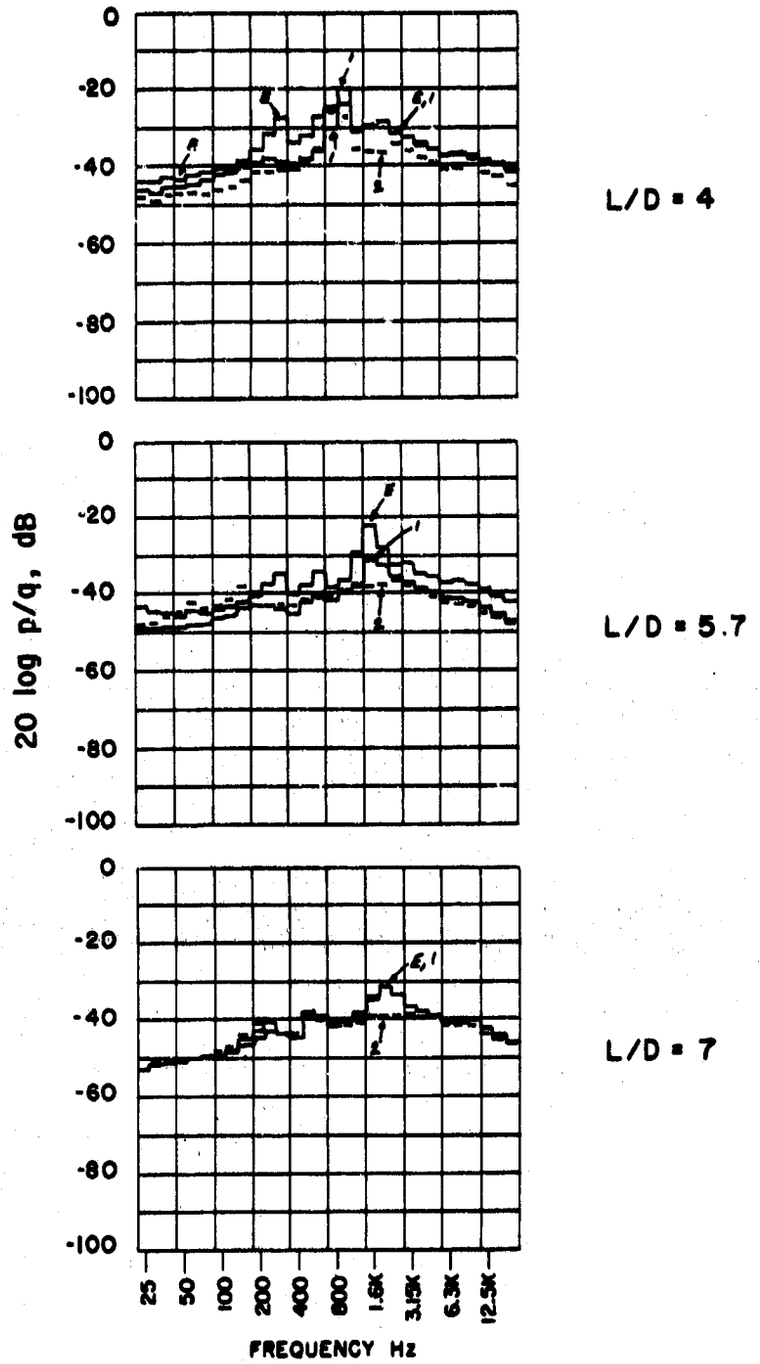

FIGURE 43. THIRD-OCTAVE-BAND SPECTRA — EMPTY CAVITY (E); CAVITY WITH ONE STORE (1), WITH TWO STORES (2); M = 2; P_0 = 10 psia; MICROPHONE #6.

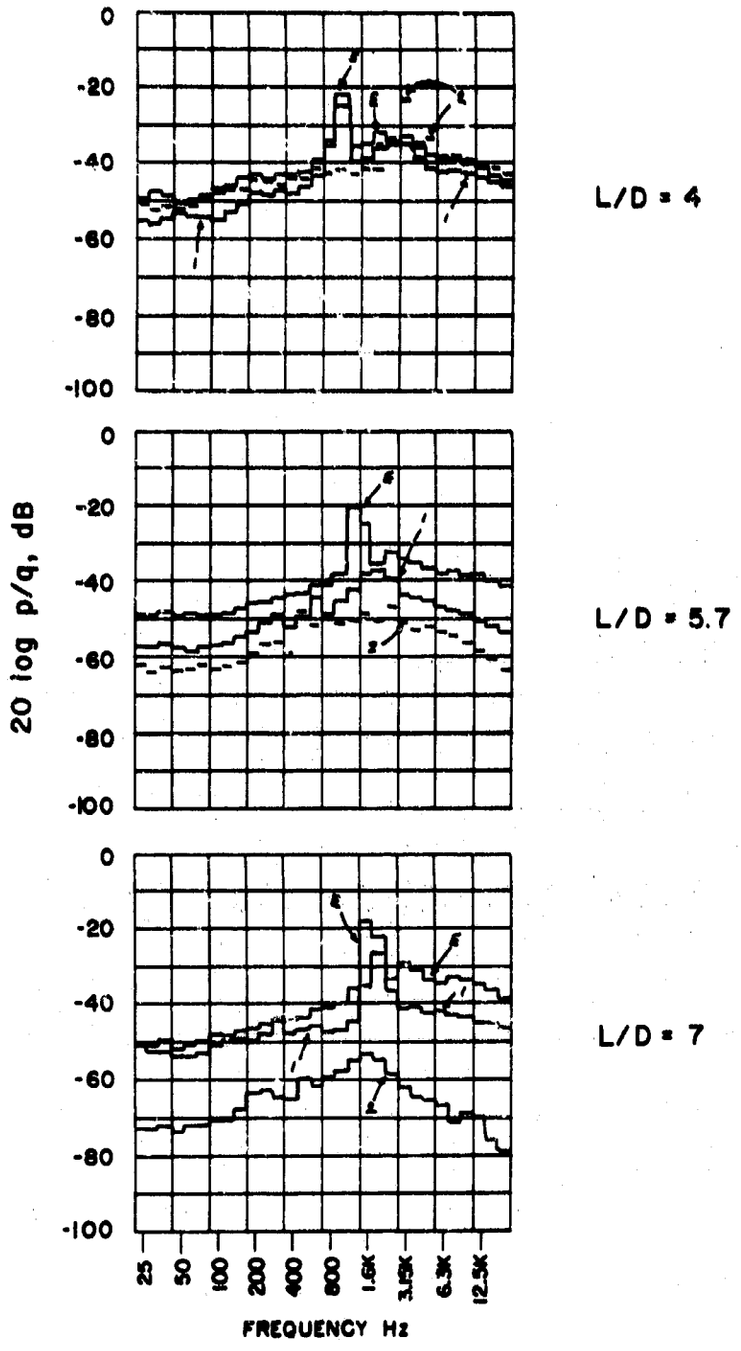

FIGURE 44. THIRD-OCTAVE-BAND SPECTRA — EMPTY CAVITY (E); CAVITY WITH ONE STORE (1), WITH TWO STORES (2); M = 3; P_0 = 2 psia; MICROPHONE #6.

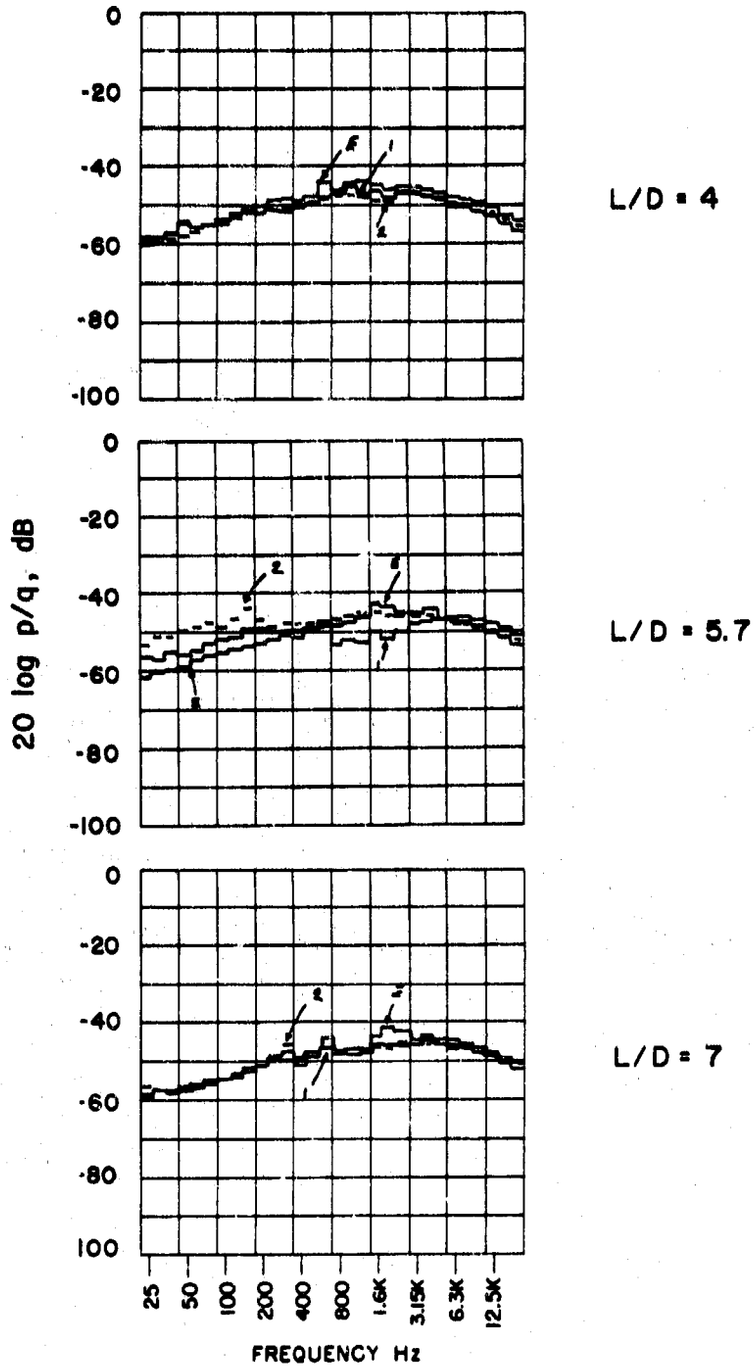

FIGURE 45. THIRD-OCTAVE-BAND SPECTRA — EMPTY CAVITY (E); CAVITY WITH ONE STORE (1), WITH TWO STORES (2); M = 3; P_0 = 10 psia; MICROPHONE #6.

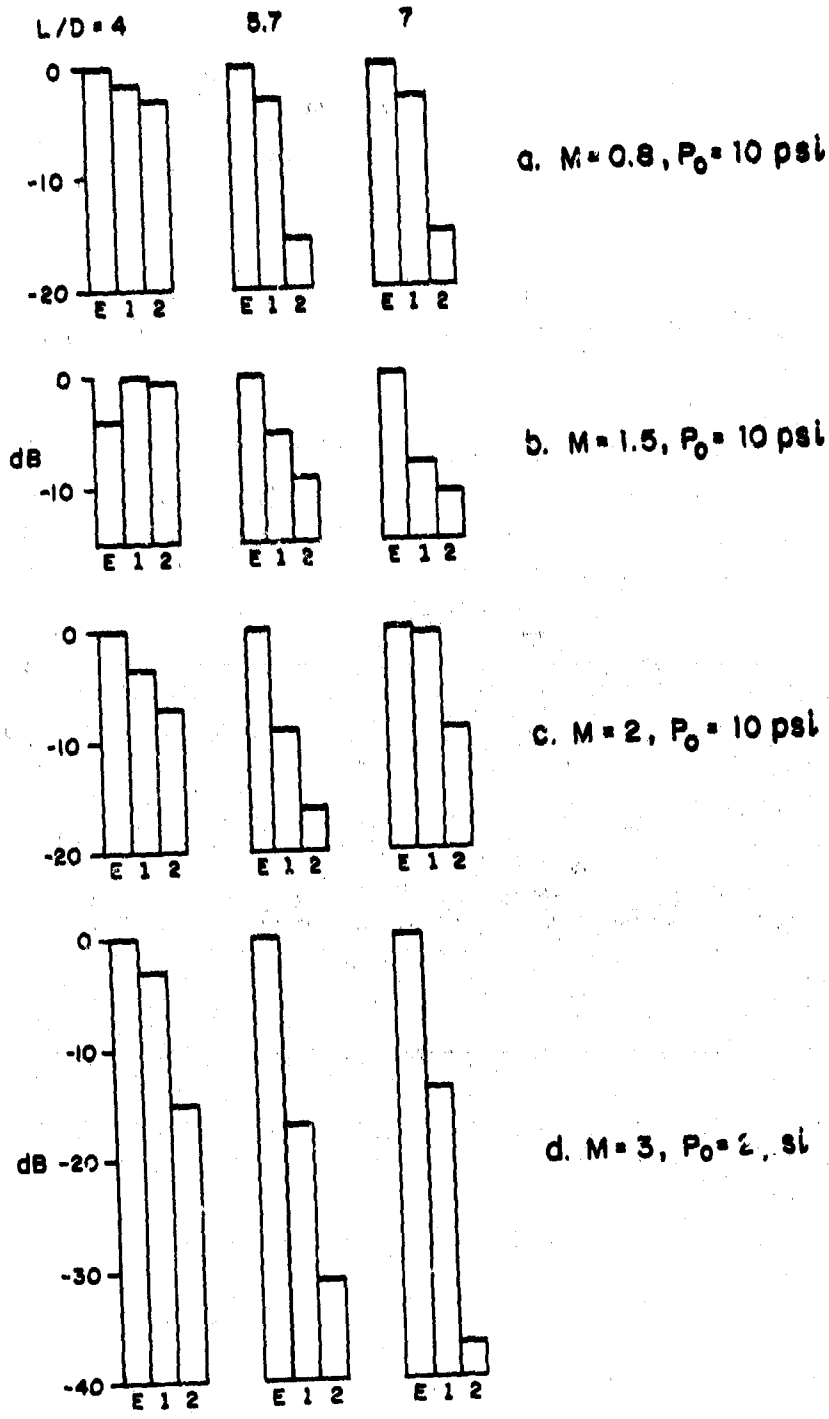

FIGURE 46. RELATIVE CHANGE OF PEAK FLUCTUATING PRESSURE.

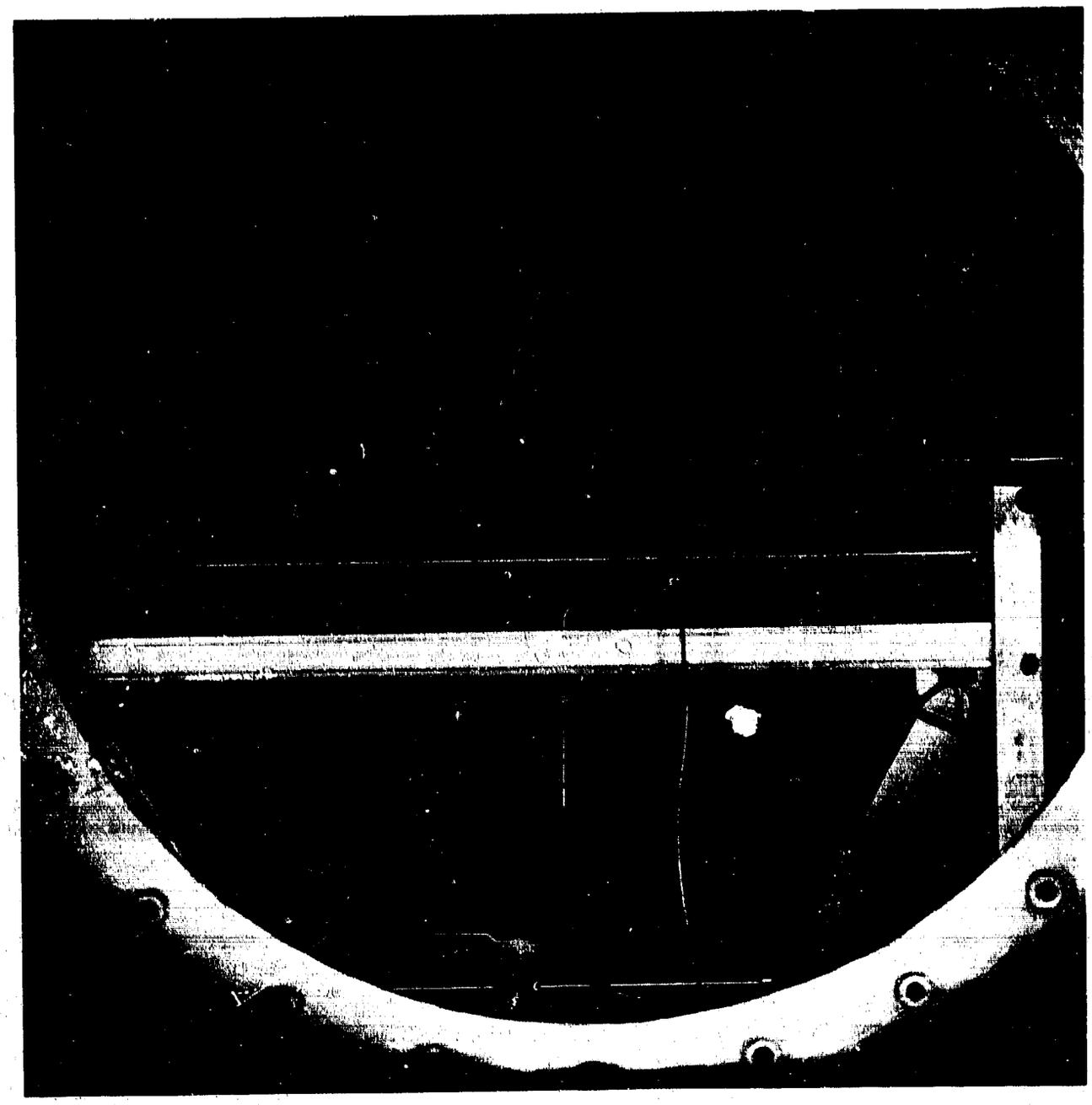

FIGURE 47. SCHLIERENOPTICAL FLOW VISUALIZATION – OSCILLATING LAMINAR BOUNDARY LAYER ABOVE EMPTY CAVITY; M = 3; L/D = 5.7; P_0 = 2 psia.

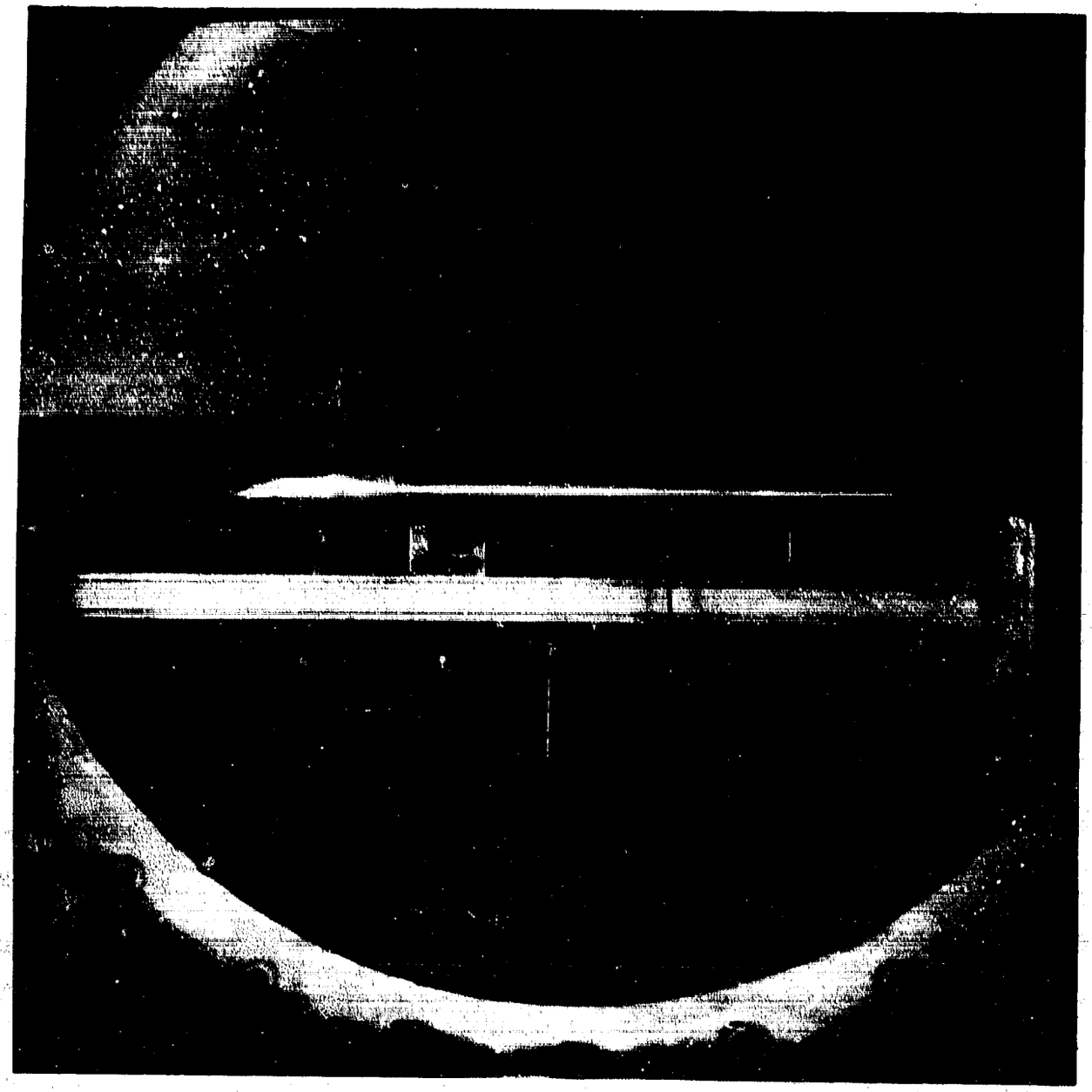

FIGURE 48. SCHLIERENOPTICAL FLOW VISUALIZATION – STABLIZED LAMINAR BOUNDARY LAYER ABOVE STORE-CONTAINING CAVITY; M = 3; L/D = 7; P_0 = 2 psia.

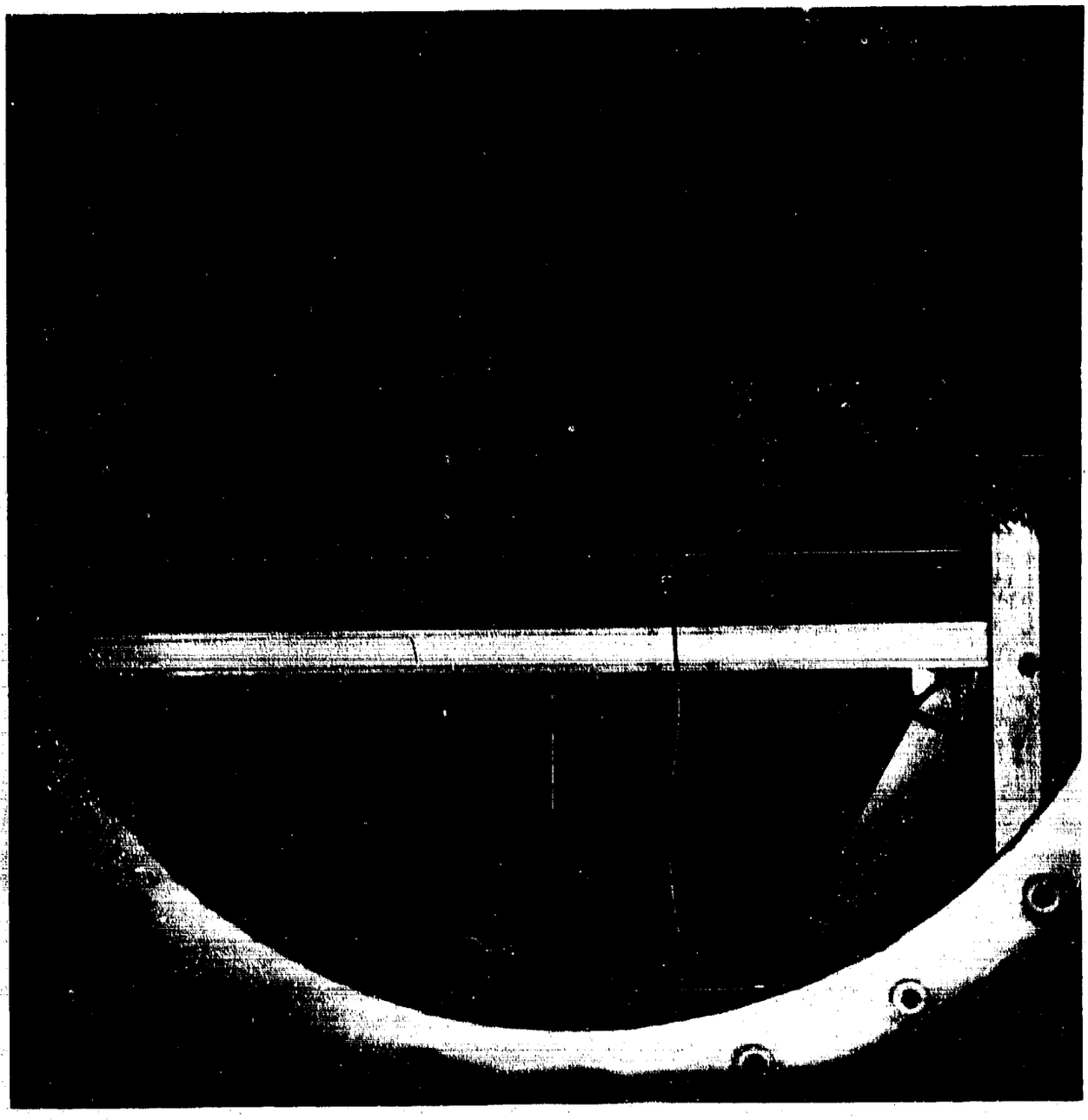

FIGURE 49. SCHLIERENOPTICAL FLOW VISUALIZATION — TURBULENT BOUNDARY LAYER ABOVE EMPTY CAVITY; M = 3; L/D = 5.7; P_0 = 10 psia.

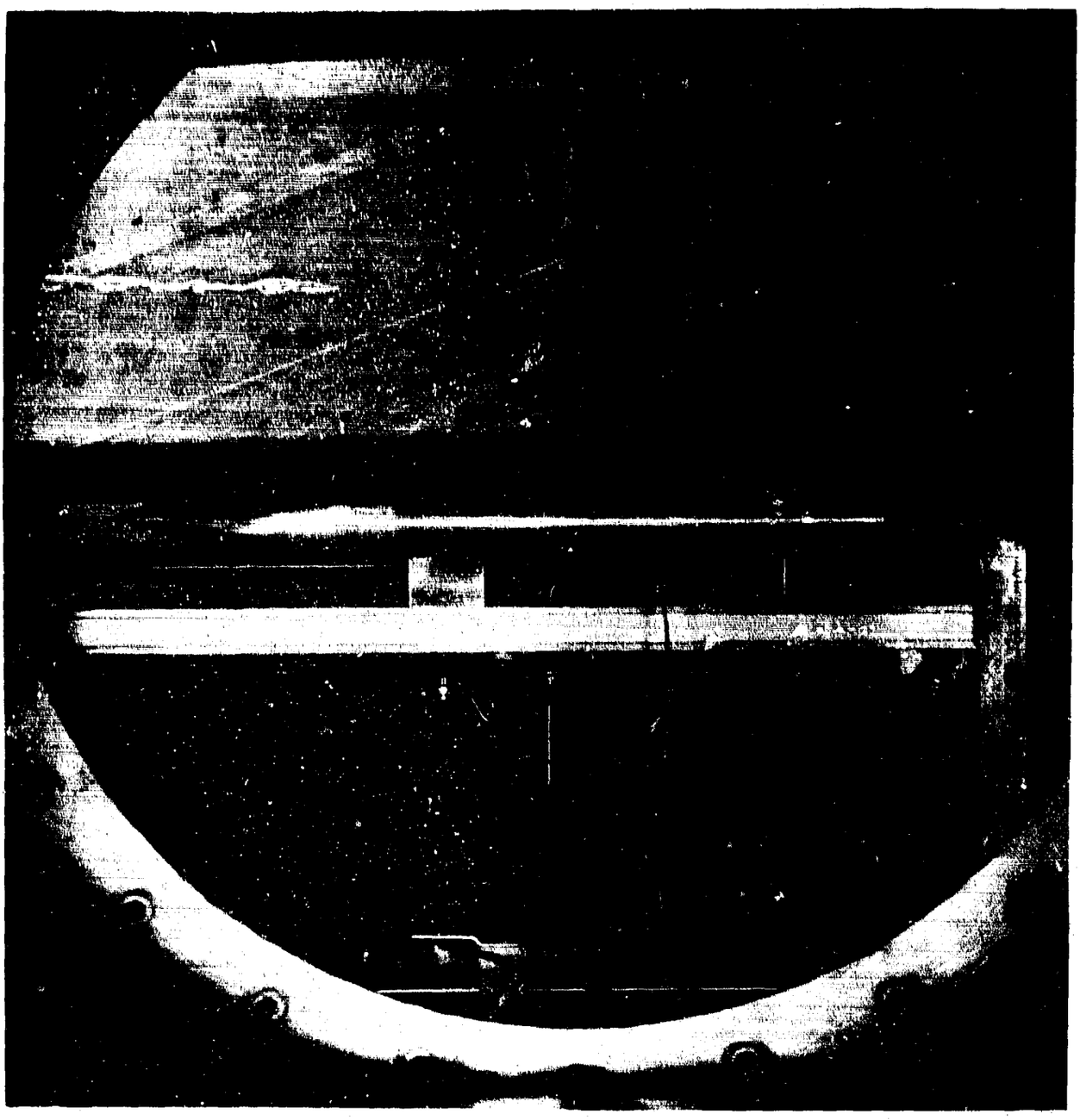

FIGURE 50. SCHLIERENOPTICAL FLOW VISUALIZATION — TURBULENT BOUNDARY LAYER ABOVE STORE-CONTAINING CAVITY; M = 3; L/D = 7; P_0 = 10 psia.

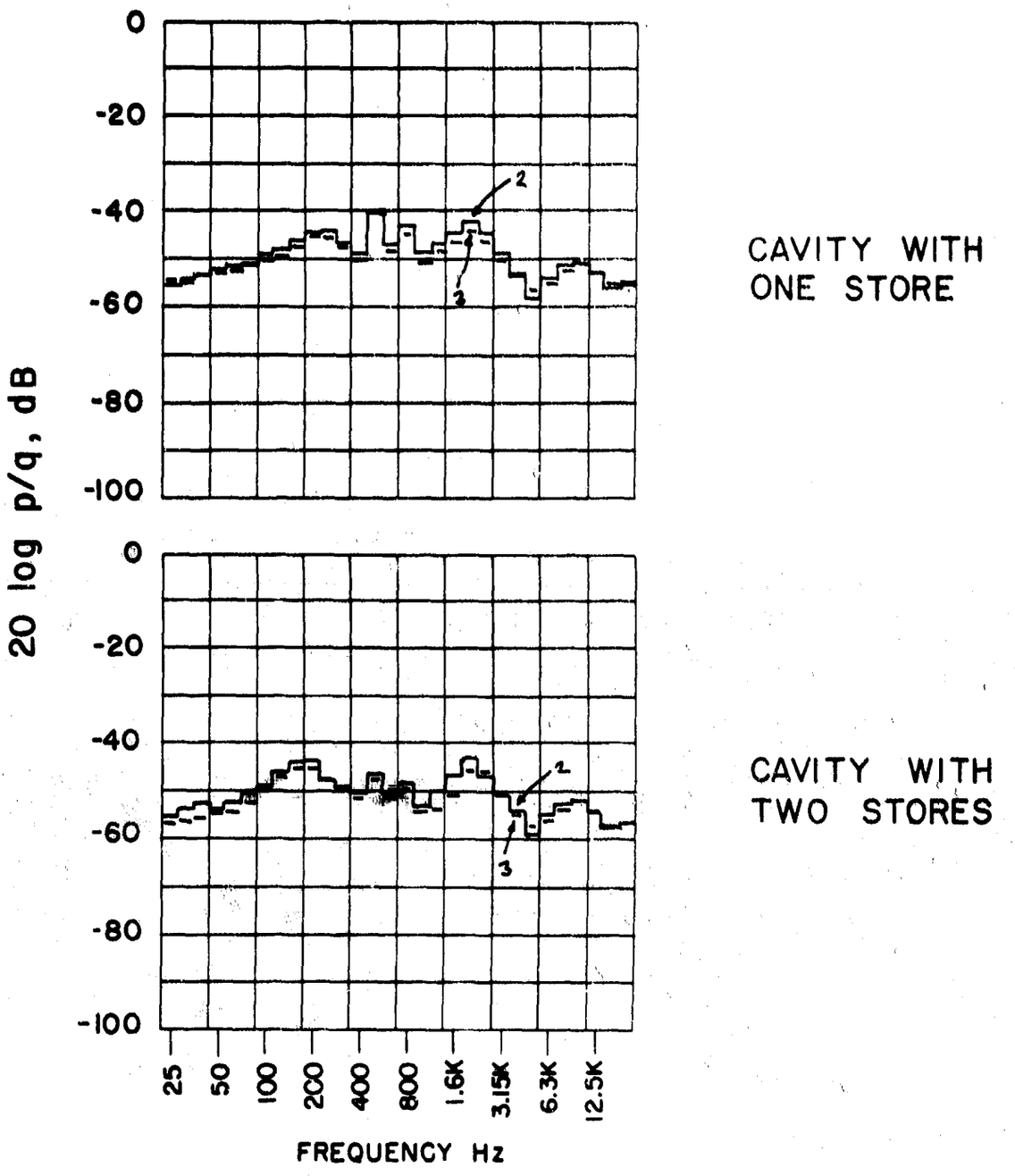

FIGURE 51. THIRD-OCTAVE-BAND SPECTRA — CAVITY WITH ONE STORE (1), WITH TWO STORES (2); M = 1.5; L/D = 5.7; P_0 = 10 psia; MICROPHONES #2, #3.

SECTION IV

PREDICTION SCHEMES

A. Introduction

The prediction procedure advanced in this Section is based solely on wind-tunnel experiments and is not supported by any flight-test results. In fact, the validity of scaling model tests to a real-flight situation for flow-induced pressure oscillations in shallow cavities has not yet been established. However, previous studies[21] indicate that geometric and frequency scaling can be achieved through the use of a Strouhal number and that levels can be scaled with the dynamic pressure.

To determine whether – in a flight situation – the boundary layer is turbulent by the time it reaches the leading edge of an open cavity, one might use Fig. 52, where a transition Reynolds number, $Re_T = \ell \cdot U_0/\nu$, is presented as a function of Mach number. This figure refers to a flat-plate situation, where ℓ is the distance from the leading edge, U_0 is the free-stream flow speed, and ν is the kinematic viscosity. The aircraft-surface region upstream of a cavity, however, is frequently curved, and an adverse pressure gradient tends to encourage flow transition. So, it is probably safe to assume that under those circumstances, the boundary layer is turbulent earlier than predicted by Fig. 52.

As discussed previously, there is probably an effect of the ratio of boundary-layer thickness and cavity depth on the response characteristics of a cavity. However, the experiments in this study were designed to simulate an aircraft situation in that typical boundary-layer dimensions were small compared to the cavity depth.

Assuming a typical distance of the aircraft-nose tip to a cavity leading edge to be 10 ft, then, within a typical flight Reynolds-number range of $10^6 < Re < 10^9$ and a Mach-number range of $0 < M < 3$, the displacement thickness would ordinarily be $0.1 < \delta^*$ in. < 1 and thus will always be small relative to a typical cavity depth. In the current experiments moderate Reynolds-number changes seemed to have no effect on the resonance frequency and thus could be neglected except for determining the stage of the oncoming boundary layer.

An ideal prediction scheme produces, for a given geometry and given flow parameters, nondimensional spectra of the unsteady

pressures at various points in the cavity, as well as some means of correlating the pressure fluctuation at different cavity locations.

It seems possible to characterize the many pressure spectra produced by this investigation as being composed of two parts. One is a broadband "background noise", in which level changes between adjacent bands are small. The other is a set of discrete-frequency tones, which in most cases contain the majority of the fluctuating-pressure energy. In Sec. III-C, it is suggested that these two parts of the spectra may be related; however, barring more positive evidence of this, these prediction schemes are framed with the assumption that these effects are unconnected. The procedure for a prediction scheme is then

(1) estimate the frequencies of the resonant responses of the cavity and determine the associated mode shapes;

(2) estimate the amplitude of the resonant responses; and

(3) estimate the amplitude and shape of the broadband spectrum.

B. Resonant Frequencies

With the modified Rossiter formula of Sec. III-C,

$$S = \frac{fL}{U} = \frac{m - \alpha}{\frac{M}{\left[1 + \frac{\gamma-1}{2}M^2\right]^{\frac{1}{2}}} + \frac{1}{k_v}}$$

where $m = 1,2,3, \ldots$, $\alpha = 0.25$, $k = 0.57$, and $\gamma = 1.4$ the adiabatic exponent. This formula generates a set of frequencies, each of which corresponds to a value of m. Discrete frequencies in the pressure spectrum of the cavity response will have values close to members of this class. It is not possible at present to predict whether these frequencies will actually be observed. As a general guide, the m=1 response is unlikely for Mach numbers much greater than 1; the m=2 response is almost always observed except for high supersonic Mach numbers; the m=3 response is common; the m=4 response seems to be confined largely to high Mach numbers. In any event, responses for $m \geq 4$ become difficult to distinguish from harmonics of lower-order responses.

This formula applies to shallow cavities, where the length to depth ratio is of order 4 or greater. The accuracy of these estimates is limited, as frequencies depend to some extent on cavity configuration and on flow parameters other than Mach number. Perhaps ±10% is an optimistic error bound.

As far as correlations between fluctuations at different points in the cavity are concerned, this investigation has established that each curve of the Rossiter formula corresponds to a different mode shape for the response. For m=1, there is a pressure node at the cavity midpoint, and pressure fluctuations on either side of it are in antiphase. For m=2 there are nodes at 25% and 75% of the cavity length, and so on. In each case there is a 180° phase shift across the node.

C. Pressure Amplitudes

For a *given* cavity geometry, the nondimensional pressure-fluctuation levels will be functions of (1) Mach number, and (2) dynamic pressure.

Cavity geometry, however, is variable. For rectangular cavities the length/depth ratio and the cavity/aspect ratio are parameters; cavities may be nonrectangular and may be cluttered by various store configurations. Also, the upstream-flow geometry could affect the Reynolds number in a determination of the condition of the oncoming boundary layer.

Available experimental data must be used cautiously, with the aim of providing bounds on the expected pressure levels. The bound of engineering interest is the worst case. The goal then is to provide predictions that are conservative — i.e., unlikely to be exceeded — but that make full use of any data that suggest lower fluctuating-pressure levels in a particular case.

1. Discrete frequencies

Examination of the data of Ref. 12 (a discussion of shallow and deep cavities at subsonic and transonic Mach numbers) and comparison of that data with the results from Ref. 3 (a study of deep cavities at the same supersonic Mach numbers as in the present study) indicates that deep-cavity fluctuating-pressure levels tend to be higher than shallow-cavity levels. Accordingly, only shallow-cavity data from Ref. 12 and from the current study are considered below.

It has been noted[7] that at low subsonic Mach numbers the fluctuating-pressure levels scale with the dynamic pressure. At high subsonic Mach numbers, levels appear[12] to rise relative to q and at supersonic Mach numbers, relative levels decline[3]. Thus, there is a strong suggestion of a scaling law for pressures that draws on a steady-state-flow small-perturbation theory:

$$\frac{p_{rms}}{q} \propto \frac{A}{|M^2 - 1|^{\frac{1}{2}}} \quad , \quad M > 1 \tag{24}$$

In this context, p_{rms} is to be taken as some measure of the overall rms pressure, or of the rms pressure in the most intense 1/3-octave band. It is not to be anticipated that all experimental data collapse onto one curve represented by some choice of the proportionally constant A; variations in level at a given Mach number are of the same order as variations with Mach number of p_{rms}/q computed with this formula. This formula also does not provide a means to calculate the variation of p_{rms}/q with Mach number for a given configuration. The only objective, in fact, is a choice of the constant A to give a useful upper bound on the data.

Figure 53 shows data from the present report and from Ref. 12 for $L/D > 4$. Levels in the most intense 1/3-octave band are shown, and each pair of points represents the range of peak values observed at each Mach number. Spectra were presented in Ref. 12 with a narrower bandwidth on the analyzer, but they have been corrected to a 1/3-octave bandwidth assuming peak values to be single-frequency signals superimposed on a broad background. The curve shown is the formula above with the constant A chosen as $10^{-0.85}$, i.e.,

$$20 \log \frac{p}{q} = -(17 + 10 \log|M^2 - 1|) \tag{25}$$

Note that the intensities recorded in Ref. 12 at low Mach numbers (0.4 and 0.7) lie well below the curve. (As pointed out above, shallow cavities are ineffective resonators, but their Q-factor must increase at higher Mach numbers, when the impedance presented by the outer flow increases.)

Note also the data at Mach number 3 — where worst-case results were determined for laminar and turbulent boundary layers — are widely different. Accordingly, the constant A is a function

of the boundary-layer stage. In this context, the flight-test data will be of great value in determining whether or not peak pressure-fluctuation levels vary with boundary layer parameters.

With these qualifications about low Mach numbers and boundary layer similarity, the above formula is advanced as a simple estimation procedure for the upper-bound peak fluctuating pressure; thus, the highest discrete-frequency levels can be computed. Since spectra of cavity-pressure oscillations frequently exhibit discrete frequency, or, at least, narrowband energy, the above formula can be used to compute pressure levels of resonant frequencies.

The value of this formula would be greatly increased by any observations on circumstances in which lower-peak levels might be achieved; for example,

Effect of Dynamic Pressure or Reynolds Number

These effects are discussed above, in relation to the choice of the constant A.

Effect of L/D

For the L/D range in this investigation ($4 < L/D < 7$), the peak pressure-fluctuation level generally does not vary greatly with L/D. Exceptions occur when a change in L/D either suppresses a pre-existing resonance or excites a new one. (See, for example, Fig. 25.) Without a more complete theoretical model, no definite predictions can be made. Very shallow cavities, however, tend to show a broad, less intense response[12].

Effect of Aspect Ratio

Reference 12 gives results of testing cavities at various aspect ratios. Results are inconsistent: a doubling of the cavity span at a given Mach number can increase by 10 dB the intensity of one component frequency of the cavity and lower the intensity of another by a similar amount. An understanding of this process awaits successful theoretical models.

Effect of Stores

Stores can greatly attenuate pressure fluctuations when they are close enough to the surface to interfere with the shear layer over the cavity mouth.

Other Effects

Reference 12 shows that a spoiler placed ahead of the cavity can greatly reduce pressure fluctuations. This effect is readily explained. Cavity oscillations, driven by an essentially two-dimensional instability of the shear layer over the cavity mouth, produce organized perturbations in almost the entire *spanwise* vorticity of the shear layer. The very small spoilers found to be effective in Ref. 12 produce strong *streamwise* vorticity, perturbing the two-dimensional organization of the vorticity. Any device that can put a streamwise vorticity into a shear layer should reduce fluctuating-pressure levels considerably. In a practical context, conventional or ramp-like vortex generators ought to be very effective with a smaller drag penalty than a spoiler.

2. Broadband spectrum

Figures 54 and 55 show the range of broadband spectra observed at each Mach number. The curves are obtained by plotting on a single sheet all microphone #6 spectra for a given Mach number. Obvious *discrete* frequencies are omitted, and an envelope is drawn embracing all the data. The spread at Mach numbers 0.8 and 1.5 is remarkably small. The reasons for the greater spread at Mach number 2, and for the laminar case at Mach number 3, are not known. Nor is the great difference spread between laminar and turbulent cases at Mach 3 explained. (See Sec. III B however.)

Figure 56 represents an attempt to correlate the broadband data. Contours of the upper bound of the broadband envelopes are plotted in a Strouhal number vs Mach number diagram. The result is not intended to be very quantitative but rather to give a general idea of the form of the data. Note the decline in maximum broadband level with increasing Mach number and the shift to higher Strouhal frequencies.

In the sample calculation below, Fig. 56 is used to estimate the broadband spectrum.

D. Sample Calculation

Consider the case of an airplane flying at Mach number 1.5 close to sea level and containing an open cavity of closely rectangular shape (12-ft-long and 2-ft-deep). At standard sea-level conditions, $U_\infty = 1675$ ft/sec, and $Re/ft = 1.07 \times 10^7$. The Strouhal

numbers corresponding to m = 1,2,3, are, respectively, 0.25, 0.58, and 0.92. Corresponding frequencies are 35, 81, and 128 Hz.

The dynamic pressure under these conditions is 3,340 lbs/ft^2, or 23.2 psia, corresponding to 198 dB re .0002 μbar. Thus, from Fig. 53 the expected worst-case 1/3-octave band fluctuating-pressure level is approximately 180 dB – i.e., 18 dB below the dynamic-pressure level. The broadband fluctuating-pressure levels can also be estimated from Fig. 56. One-third-octave band levels peak at a Strouhal number of about 1.5, corresponding to 280 Hz, with intensity roughly -28 dB relative to q. Levels are -40 dB at Strouhal number 15 (i.e., 2100 Hz) and -35 dB at Strouhal number 0.08 (i.e., 11 Hz).

The above information permits construction of a hypothetical 1/3-octave-band spectrum. (Fig. 57.) Note that both peak and broadband intensities are *worst-case* values.

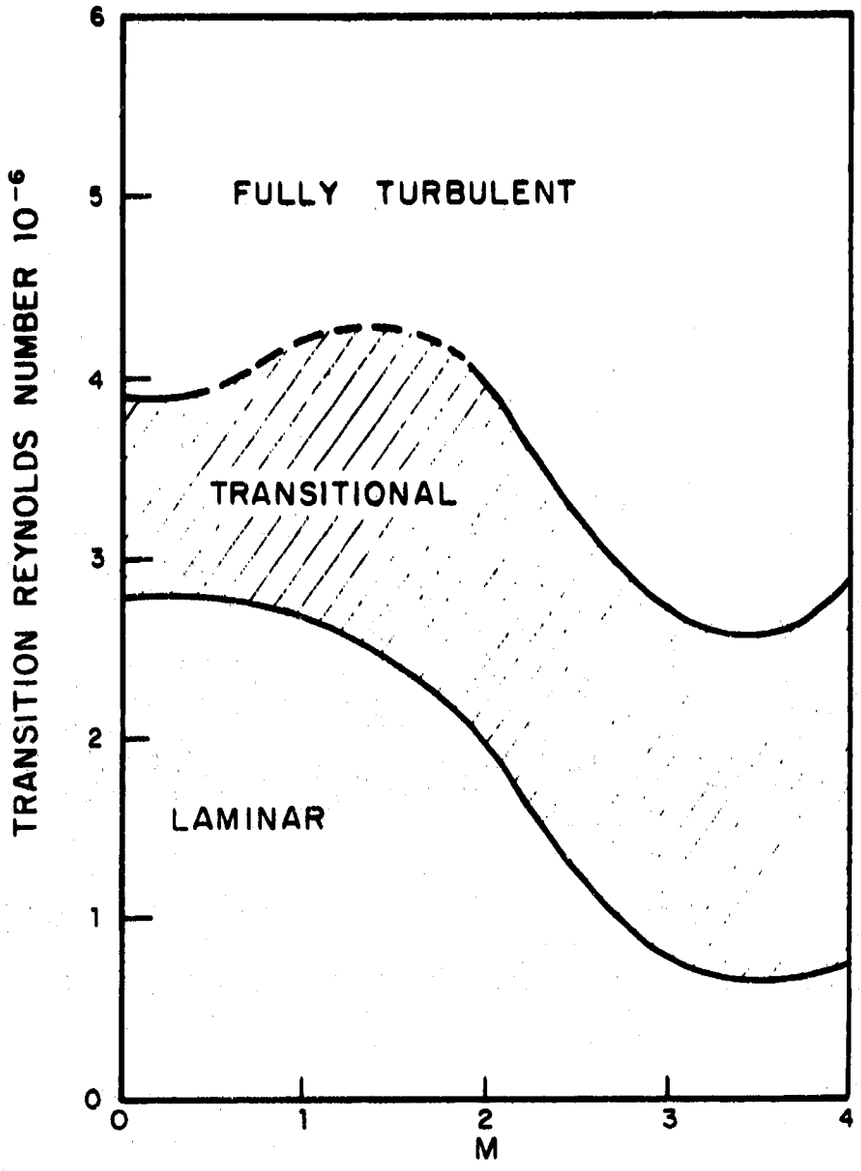

FIGURE 52. TRANSITION REYNOLDS NUMBER AS A FUNCTION OF MACH NUMBER.

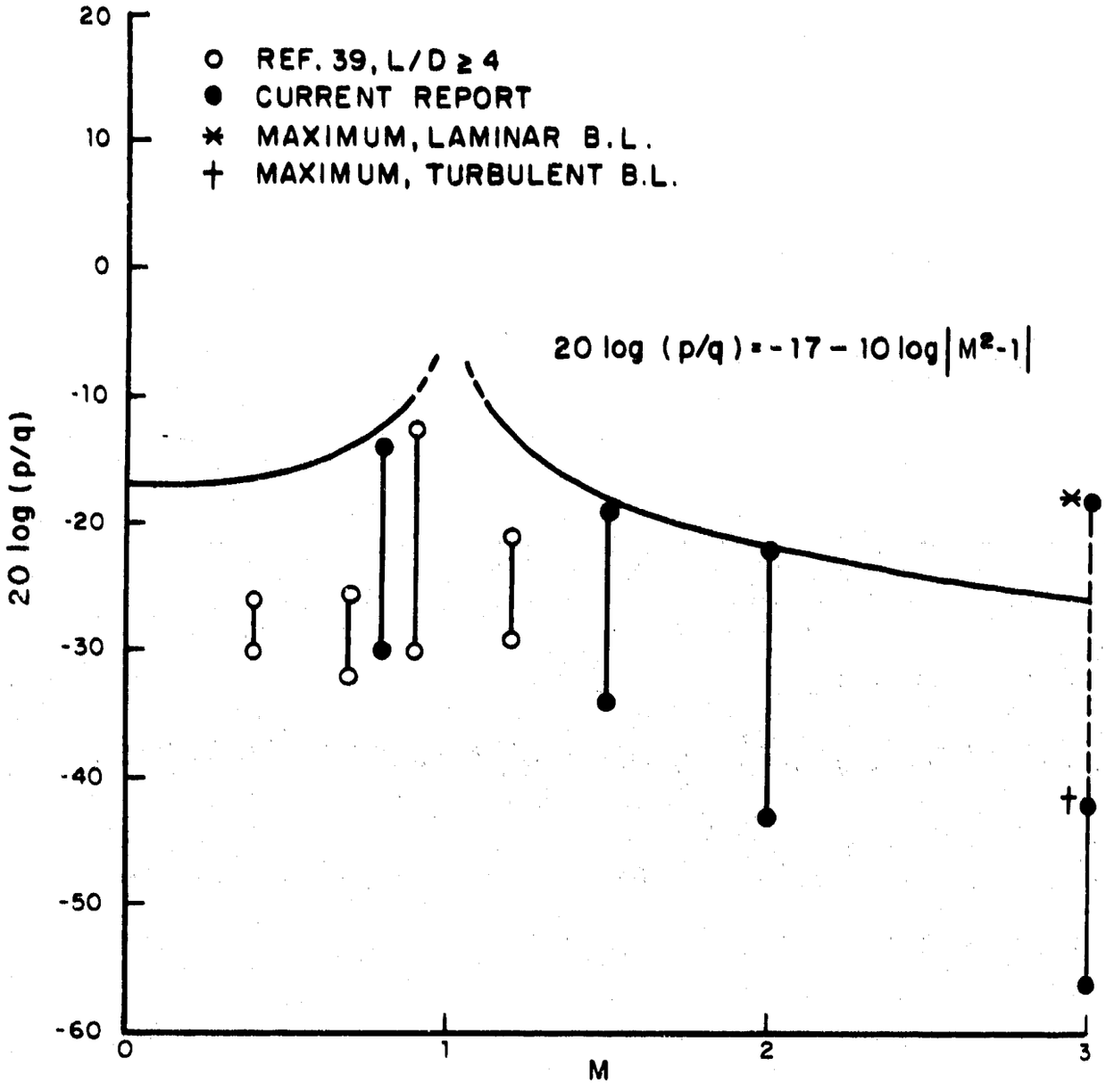

FIGURE 53. PEAK SOUND-PRESSURE LEVEL AS A FUNCTION OF MACH NUMBER.

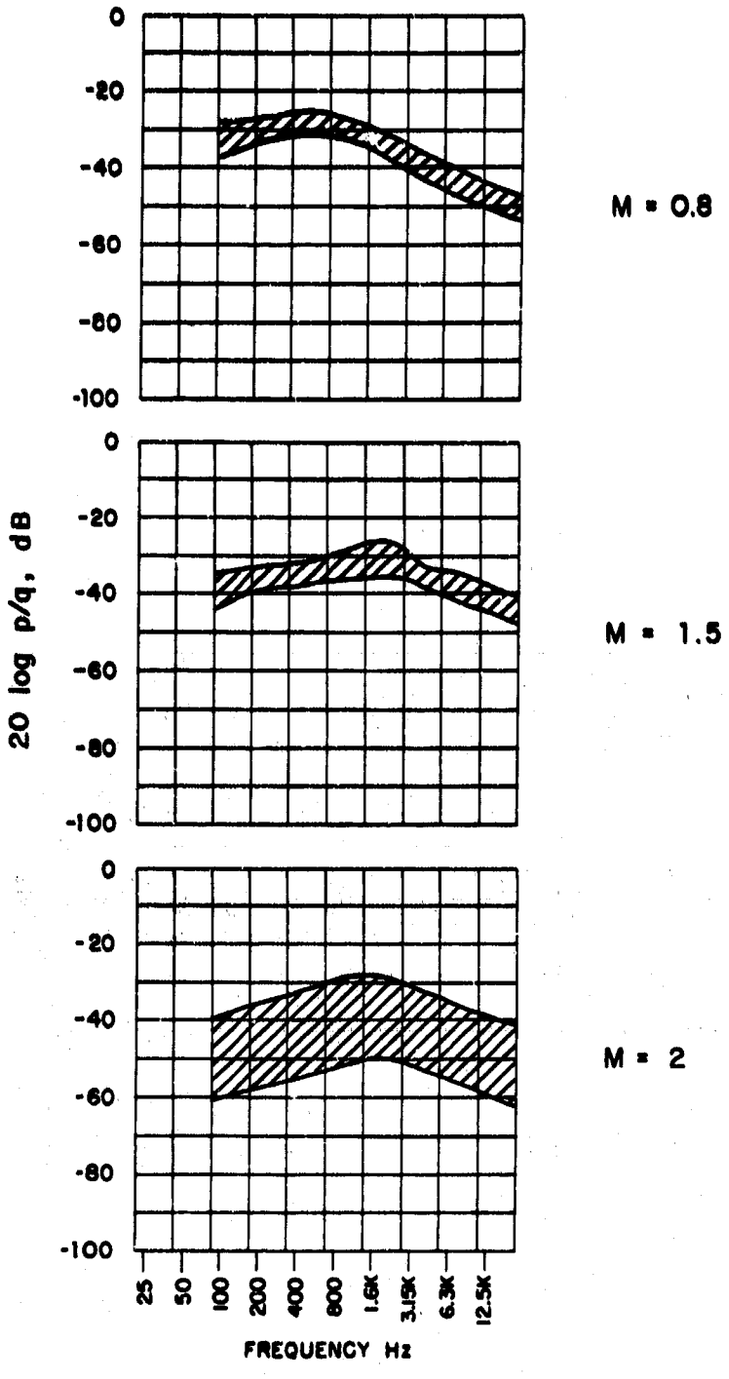

FIGURE 54. RANGE OF THIRD-OCTAVE-BAND SPECTRA — BROADBAND PART ONLY — CAVITY WITH AND WITHOUT STORE; MICROPHONE #6.

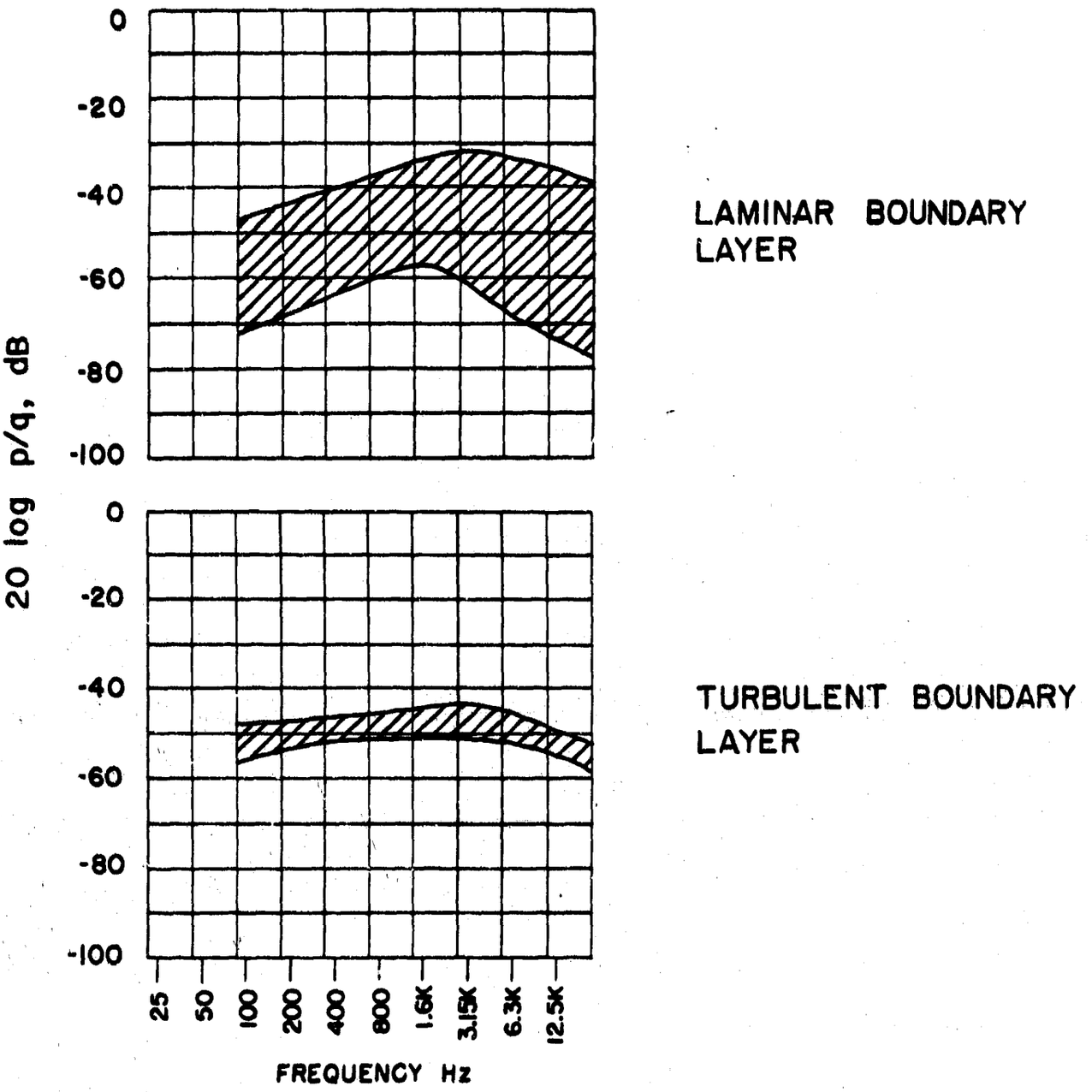

FIGURE 55. RANGE OF THIRD-OCTAVE-BAND SPECTRA — BROADBAND PART ONLY — CAVITY WITH AND WITHOUT STORE; M = 3; MICROPHONE #6.

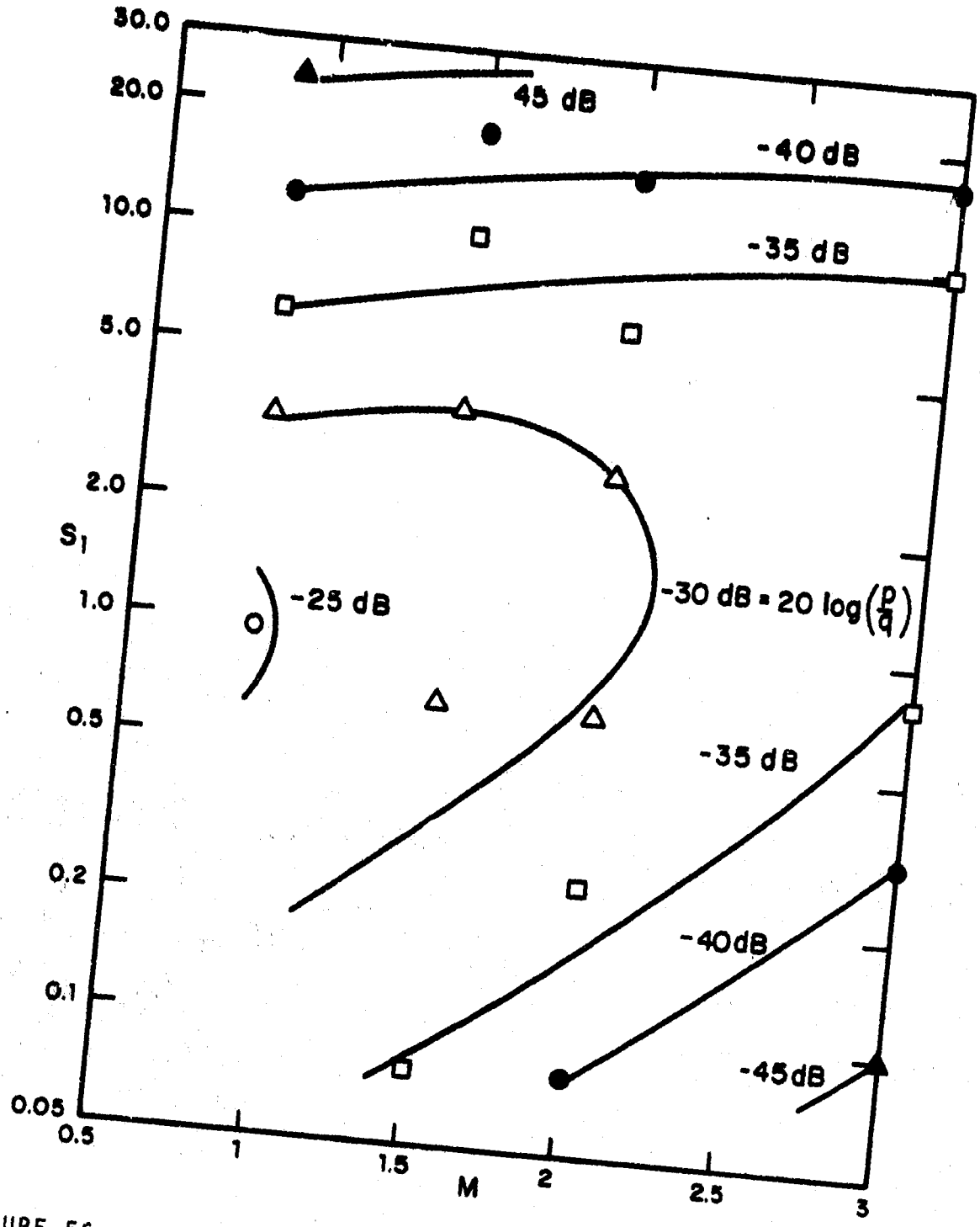

FIGURE 56. CONTOURS OF EQUAL FLUCTUATING-PRESSURE LEVELS RELATIVE TO FREE-STREAM DYNAMIC PRESSURE.

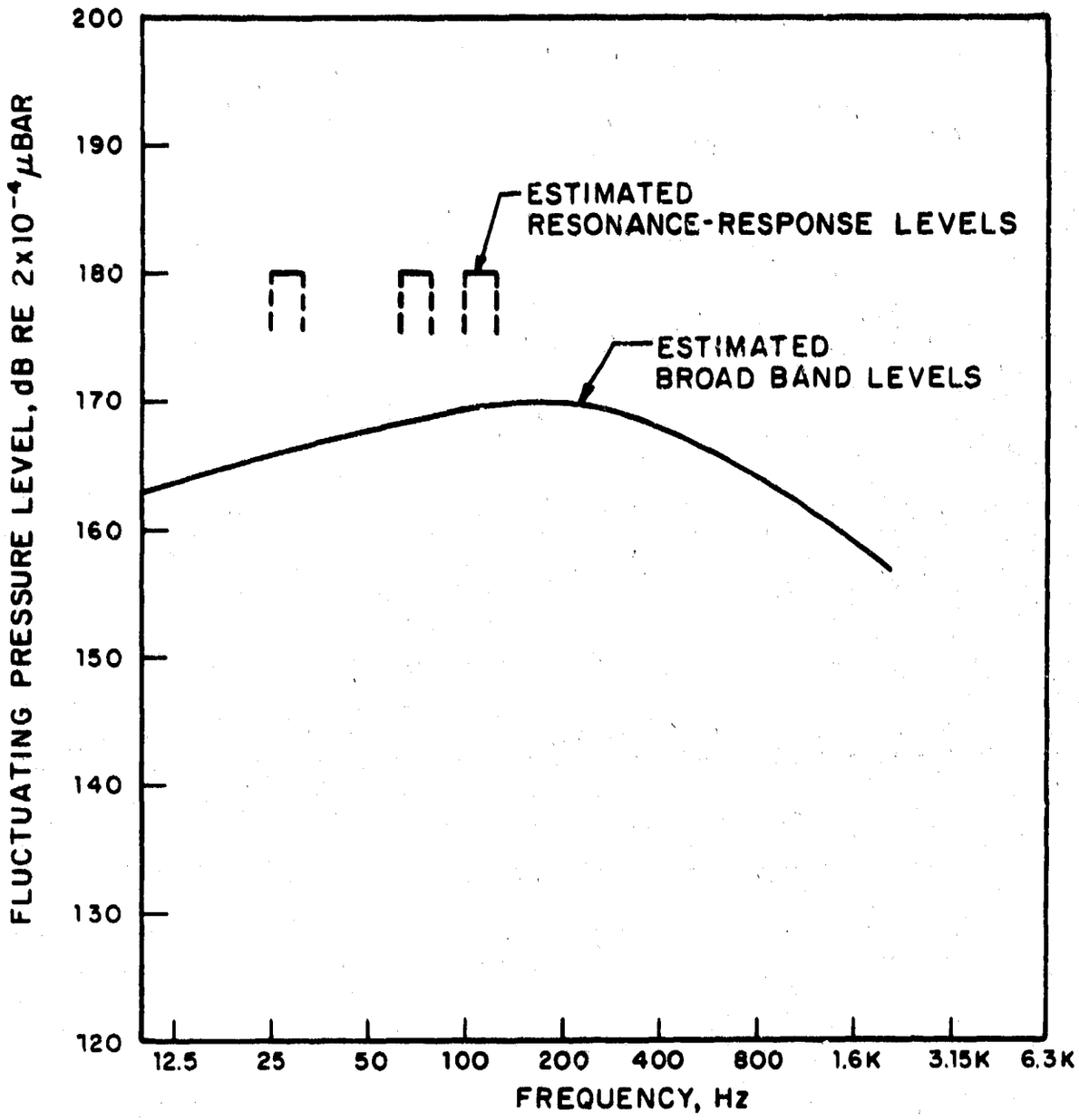

FIGURE 57. RESULT OF SAMPLE CALCULATIONS: ESTIMATED WORST CASE THIRD-OCTAVE-BAND SPECTRUM; M = 1.5; L = 12 ft; SEA-LEVEL CONDITIONS.

SECTION V

EVALUATION AND DISCUSSION

As the various experimental results were presented throughout this Report, data were interpreted *ad hoo* and related to information available in the literature. In this evaluation of the entire research program, however, all important results are summarized.

The research program was broadly divided into studies of the empty cavity and of the store-containing cavity. The available literature made it quite clear that the current understanding of cavity phenomena — particularly of those related to empty cavities — was insufficient. Therefore, the major portion of the effort went into studying the experimental cavity in its empty configuration; full use was made of the available extensive instrumentation and configuration versatility. Many of the results obtained with the empty-cavity configuration are directly applicable to those of a store-containing cavity. Essential differences will be pointed out below.

The major features of the experimental results are summarized below. (Note that there results pertain to shallow cavities only.)

1. The principal practical result of this study is an improvement of Rossiter's formula for the calculation of resonance frequencies of open shallow cavities in a free-stream Mach-number range covering at least 0.5 to 3.0. The generalization of this formula is

$$S_1^* = \frac{f_m \cdot L}{U_0} = \frac{m - 0.25}{\frac{M}{\left[1 + \frac{\gamma-1}{2} M^2\right]^{\frac{1}{2}}} + 1.75}$$

for m = 1, 2, 3 .. pertaining to the order of mode.

By means of this equation, possible resonance frequencies can be computed; however, such frequencies do not necessarily have to occur. In fact, the cavity may not resonate at all.

2. The longitudinal energy distribution of resonant-frequency oscillations suggests the occurrence of definite pressure modes – as could be expected between a hard front and rear wall – up to at least the fifth order, but very likely to even higher orders.

3. Higher-order modes tend to prefer the higher Mach-number range. Only in one instance could a first-order mode be detected at a Mach number of 2. It seems generally safe to assume that first-order modes are extremely unlikely to occur at Mach numbers above one.

4. Resonant-mode frequencies seem to approach "closed-box" type frequencies at hypersonic Mach numbers. At these Mach numbers the shear layer atop the cavity represents a high impedance, thus an acoustic closing, for the open mouth of the cavity. At low supersonic Mach numbers, and even more so at subsonic Mach numbers, the cavity-mouth area is better characterized by assuming an open, or pressure-release, surface boundary. Resonant frequencies, in fact, deviate from the ideal closed-box resonance frequencies by a factor of 2 or more at low subsonic Mach numbers.

5. Cavities of L/D ratios from 4 to 7 did not exhibit any significant depth modes.

6. Cavities of this same L/D ratio did not exhibit any transverse-pressure oscillations.

7. Maximum pressure levels of resonant frequencies – as measured at an antinode in a rearward corner of the cavity – ranged from 12 to 56 dB below the reference dynamic pressure of the free stream. Empirical correlation of resonant-frequency levels with Mach number suggest an upper bound that can be formalized as $20 \log p/q = -(17 + 10 \log|M^2-1|)$.

   Resonant-frequency levels can reach this upper bound, but they are often much lower. Qualitatively speaking, levels are highest in the transonic flow-speed range.

8. Cavity-internal broadband fluctuating-pressure energy increases towards the rear end of the cavity. The increase depends for a given Mach number on the shallowness of the cavity and for a given geometry on the free-stream flow speed; the shallower the cavity and the higher the free-stream flow speed, the larger will be the relative increase.

9. The broadband part of the pressure spectra, when represented in one-third-octave bands, exhibits a very shallow haystack-shape. The spectra peak at a nondimensional Strouhal frequency S equal to $f \cdot L/U_0$ of 1.6 ± 0.4.

10. Schlierenoptical flow visualization supports the theory that the shear layer oscillates above the cavity in a periodic manner at cavity resonant conditions. The magnitude of the shear-layer disturbance grows towards the downstream end of the cavity mouth. Still inconclusive results suggest a periodic mass entrainment and ejection; such a process would provide a nonlinear loss-mechanism that could explain the amplitude limitations.

11. The response of a cavity is totally different for approaching laminar and approaching turbulent boundary layers. At the one experimental instant when a laminar boundary layer could be obtained, the cavity response was on the order of 25 dB above the equivalent turbulent boundary-layer case.

12. Although the stage of the approaching boundary-layer strongly affects the cavity response, no obvious relationship of the upstream fluctuating-pressure spectrum and the cavity-response spectrum could be established; however, such a relationship cannot *a priori* be denied.

13. Insertion of store, in either an asymmetric or a symmetric location, has no effect on the resonance frequencies and only a minor effect on their levels – as long as the store does not physically interfere with the shear layer. When such interference does occur, the shear layer stabilizes, effectively killing discrete-frequency resonances. The broadband portion of the spectrum is not very much affected by the presence or the absence of store.

14. Even in the asymmetric (one-store) configuration, no transverse oscillations were observed; thus there appears to be no strong excitation in the transverse direction.

15. In general, the present study revealed that shallow cavities have a low Q-factor and do not respond as classical acoustic resonators; however, they can certainly be driven at definite frequencies.

16. Shallow cavities are driven by an energy input near their trailing edge. This result could support the edgetone/cavity interaction mechanism suggested by other investigators.

17. A large captive vortex is driven within a shallow cavity. For the first time, recirculation velocities were measured; these velocities range from Mach numbers of 0.5 to 0.1, for decreasing depth of a cavity. Absolute velocities are rather insensitive to free-stream Mach-number changes. The internal-vortex strength, as inferred from the fluid Mach number near the floor of the cavity, is strongly dependent upon whether the boundary layer is laminar or turbulent, but not very strongly dependent upon the Reynolds number. There seems to be a difference between subsonic flow and supersonic flow.

18. Changes in free-stream Reynolds number seemed to have no effect on the response frequencies.

19. Internal-cavity temperatures were measured for the first time. Results indicate that internal temperatures approach the free-stream stagnation temperature – in contrast to the assumption of other investigators who used free-stream static temperature as relevant internal temperature.

APPENDIX I

WALL INTERFERENCE EFFECTS AT MACH NUMBER 0.8

I-1. Introduction

Cavity tests at Mach number 0.8 produced an undesired high-frequency shock pattern moving upstream in the wind-tunnel test section. It is shown that the shocks correspond to a waveguide mode of the test section with effectively zero group velocity. The energy of the mode does not propagate out of the test section, and the amplitude increases until the shock system is established.

The following features of the subsonic results are significant here:

1. All tests at Mach number 0.8 showed spectra of the unsteady pressures with a dominant peak close to 375 Hz.

2. This peak corresponds to a Strouhal number based on a cavity length of 0.72. Previous investigators[1, 10, 11, 12] indicate that this corresponds to a resonant mode of the cavity.

3. Schlieren photographs taken of tests at Mach number 0.8 always show oblique shocks in the test section - Fig. 10 is typical. At this subsonic Mach number such shocks cannot be stationary. In fact the position of the shock pattern varies from photograph to photograph, and the shocks cannot be seen when the Schlieren image is viewed with the naked eye. (The exposure time of the photographs is of order one μsec only.)

4. The shocks observed form a system of oblique shocks reflecting off the tunnel roof and floor and from the shock/boundary-layer interactions, visible in the photographs, propagating upstream.

5. In tests with the cavity replaced by a flat plate, the shock system does not appear and is thus not caused by a shortcoming of the test facility.

In Section I-2 it will be shown that the shocks are associated with the strong cavity resonance at 375 Hz; in Section I-3 a reason is advanced for this interaction between the resonant mode of the cavity and the tunnel walls.

I-2. Shock Geometry

One can estimate the velocity with which such a system of shocks moves through the test section. Figure 58a shows a schematic picture. U_s is the velocity with which the shocks propagate normal to themselves in still air; H is the height of the test section; and λ is the wavelength of the shock pattern. If the free-stream velocity were zero, the shock pattern would advance a distance BC while an element of wavefront travels from A to B. The downstream velocity, U_p, of the shock pattern is therefore

$$U_p = U_s \, BC/AB$$

$$= - U_s/\cos \theta$$

Allowing for the free stream,

$$U_p = a_o(M - M_s/\cos \theta) \qquad \text{(I-1)}$$

M_s is the shock-propagation Mach number, and M is the free-stream Mach number. The velocity with which an element of wavefront travels downstream is

$$U_g = U_o - U_s \cos \theta$$

$$= A_o(M - M_s \cos \theta) \qquad \text{(I-2)}$$

U_p and U_g are in the relationship of phase and group velocity (see Sec. I-3).

The frequency of this shock pattern as seen by a stationary observer is

$$f = |U_p|/\lambda$$

$$= |U_p|/2H \tan \Theta$$

$$f = a_o(M_s - M \cos \Theta)/2H \sin \Theta \qquad (I\text{-}3)$$

Here, $M = 0.8$, $H = 1$ ft, $a_o = 1070$ ft/sec (80° F stagnation temperature). Θ is roughly 40 degrees. Microphone data suggest that the pressure ratio across a shock is about 1.1, giving $M_s = 1.05$, whence $f = 345$ Hz. This frequency is within 10% of the observed frequency of 375 Hz. An accurate estimate of Θ is unnecessary, since the right-hand side of Eq. I-3 has a broad minimum in the region where $\Theta = 30$ to 50 degrees. The estimate for f could be improved by assuming that the shocks reflect, not at the wall, but at some distance away in the boundary layer. This assumption reduces the effective distance H and increases f proportionately.

For values for $\Theta = 40$ degrees and for $H = 1$ ft, the wavelength, λ, becomes 1.68 ft - almost exactly the cavity length of 1.67 ft. Note that the value for Θ is approximate; values measured from photographs vary over a range of 10 degrees, leading to estimates for λ ranging from 1.4 ft to 2.0 ft. These correspondences - that the observed frequency is the calculated frequency caused by the passage of the shocks and that the wavelength of the shock system is the length of the cavity - indicate that we are observing an interaction between a resonant response of the cavity and the rectangular duct formed by the test section. A reason for this interaction is advanced below in an analysis based on an assumed coincidence of the *wavelength* of disturbances in the duct and in the cavity length. The same conclusions could equally be drawn from a coincidence of cavity and duct response *frequencies*.

I-3. The Test Section as a Waveguide

The shocks observed in the test section are weak and propagate with a normal velocity only a few percent greater than the sound speed. Shocks of vanishingly small strength can be regarded as reversible compression waves. This suggests that the shock pattern might be treated as an isentropic wave motion in the test section, and this approach provides an explanation for the appearance of this interference effect.

The theory of acoustic waves in a rectangular duct can be adapted from any of the standard references (e.g., *Theoretical Acoustics*, by Morse and Ingard) by adding to any solution a uniform downstream convection velocity U_o. Considering only two-dimensional disturbances in a vertical plane, the phase velocity of a mode of wavelength λ is

$$U_p = a_o \left[M \pm (1 + n^2\lambda^2/4H^2)^{\frac{1}{2}}\right] \qquad \text{(I-4)}$$

U_p is positive downstream. For $n = 1$, this equation represents a single acoustic wave reflecting off the test-section roof and floor (Fig. 58b); for $n = 2$, a pair of acoustic waves (Fig. I-58c), and so on. When $n = 1$, Eq. I-4 is the limiting, isentropic form of Eq. I-1, where $\lambda/H = 2 \tan \theta$.

Since the phase velocity is a function of wavelength, the group velocity differs from the phase velocity and is given by

$$U_g = U_p - \lambda \, dU_p/d$$

(See, for example, Lamb's *Hydrodynamics*, p 381.) Thus,

$$U_g = a_o\left[M \pm (1 + n^2\lambda^2/4H^2)^{-\frac{1}{2}}\right] \qquad \text{(I-5)}$$

For $n = 1$, Eq. I-5 is the isentropic form of Eq. I-2. The group velocity is the velocity with which a package of waves moves through the duct. It is also the velocity with which the energy of a wave pattern propagates through the duct. It is possible to show directly for this class of waves that the group velocity, energy density, and intensity are related by (Intensity) = (Energy Density) × (Group Velocity).

Figure 59 shows a plot of nondimensional group velocity ($M_g = U_g/a_o$) against H/n for two values of m, 0.2 and 0.8. Point A shows the value of M_g corresponding to the shock pattern of Figure 58: M = 0.8, n = 1, /H = 1.67, upstream propagation. The reason for the formation of the shock pattern is clear; one of the resonant modes of the cavity feeds energy into a duct mode in the test section with almost zero group velocity. The energy is unable to escape and the disturbances increase until dissipation appears in the form of shock waves.

Before this explanation was available, an attempt was made to eliminate the shock pattern by testing a smaller cavity. A simple modification produced a cavity with length 0.57 of the full scale. The group velocities of the corresponding duct modes, point B for n = 1, point C for n = 2, are shown in Fig. 59. It appears that both modes are subject to poor energy propagation. Figure 60 shows a typical Schlieren photograph of the flow field around this approximately half-scale cavity. There is strong evidence in the intersecting shocks of the duct mode corresponding to n = 2. The reason for the appearance of only the n = 2 mode, when both modes have poor propagation, is that the Strouhal number of the n = 2 mode is that corresponding to the full-scale cavity resonance. If it is assumed that λ is equal to L, the cavity length, then

$$S = FL/U_o = U_p|/U_o|$$

$$= 0.73 \ (n = 2)$$

$$= 0.39 \ (n = 1) \qquad \text{(I-6)}$$

Thus switching to a half-scale cavity merely coupled the cavity resonance to a different, but still poorly propagating, duct mode.

I-4. Conclusions

The wall-interference effects described above may occur whenever unsteady-flow situations are tested at combinations of free-stream Mach number, disturbance frequency, and disturbance wavelength that excite test-section duct modes having group velocities near zero. This is a phenomenon of high-subsonic and low-supersonic Mach numbers. Supersonically, for all modes the energy escapes downstream (although the phase velocity may be supersonic, and waves downstream of the model may appear to propagate upstream). At low-subsonic Mach numbers (Fig. 59), poor propagation can occur only for very small $H/n\lambda$ - i.e., for very large models or for high-order duct modes which are less likely to be excited since they have high Strouhal frequencies.

It is this phenomenon that will set the upper-subsonic and lower-supersonic Mach-number limits for testing unsteady flows in conventional wind tunnels. As can be seen from Figure 59, at Mach numbers close to one decreasing model size (increasing $H/n\lambda$) has a small effect on the group velocity. Extra-large models (small values of $H/n\lambda$) would permit free downstream propagation but would introduce other transonic interference effects.

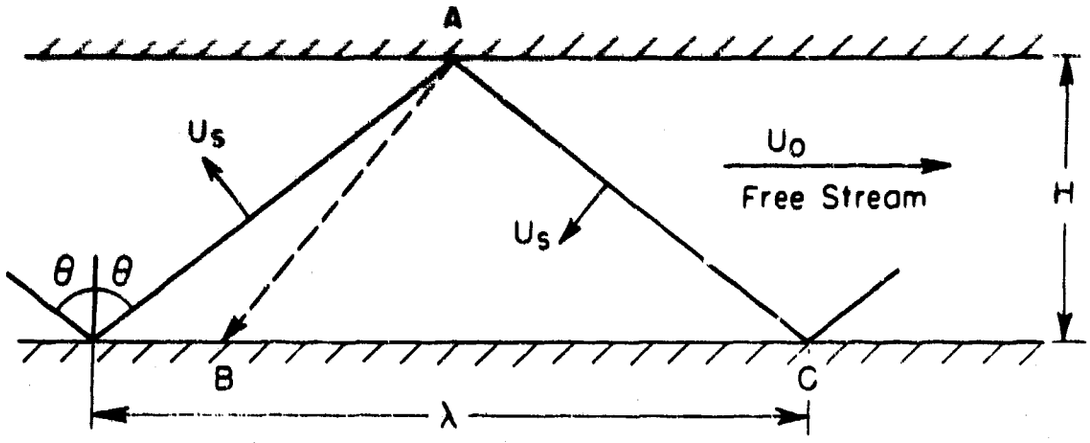

a. SCHEMATIC SHOCK PATTERN.

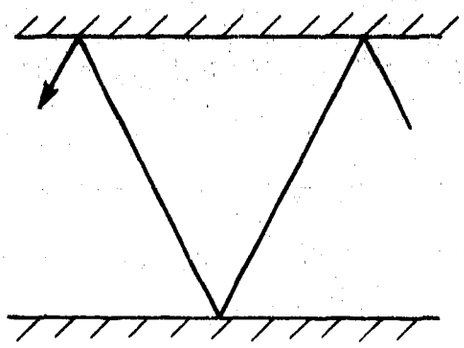

b. DUCT MODE FOR n = 1.

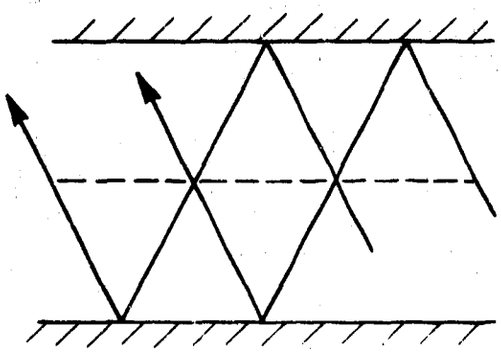

c. DUCT MODE FOR n = 2.

FIGURE 58. SCHEMATIC OF SHOCK PATTERN IN WIND-TUNNEL TEST SECTION AT SUBSONIC SPEEDS.

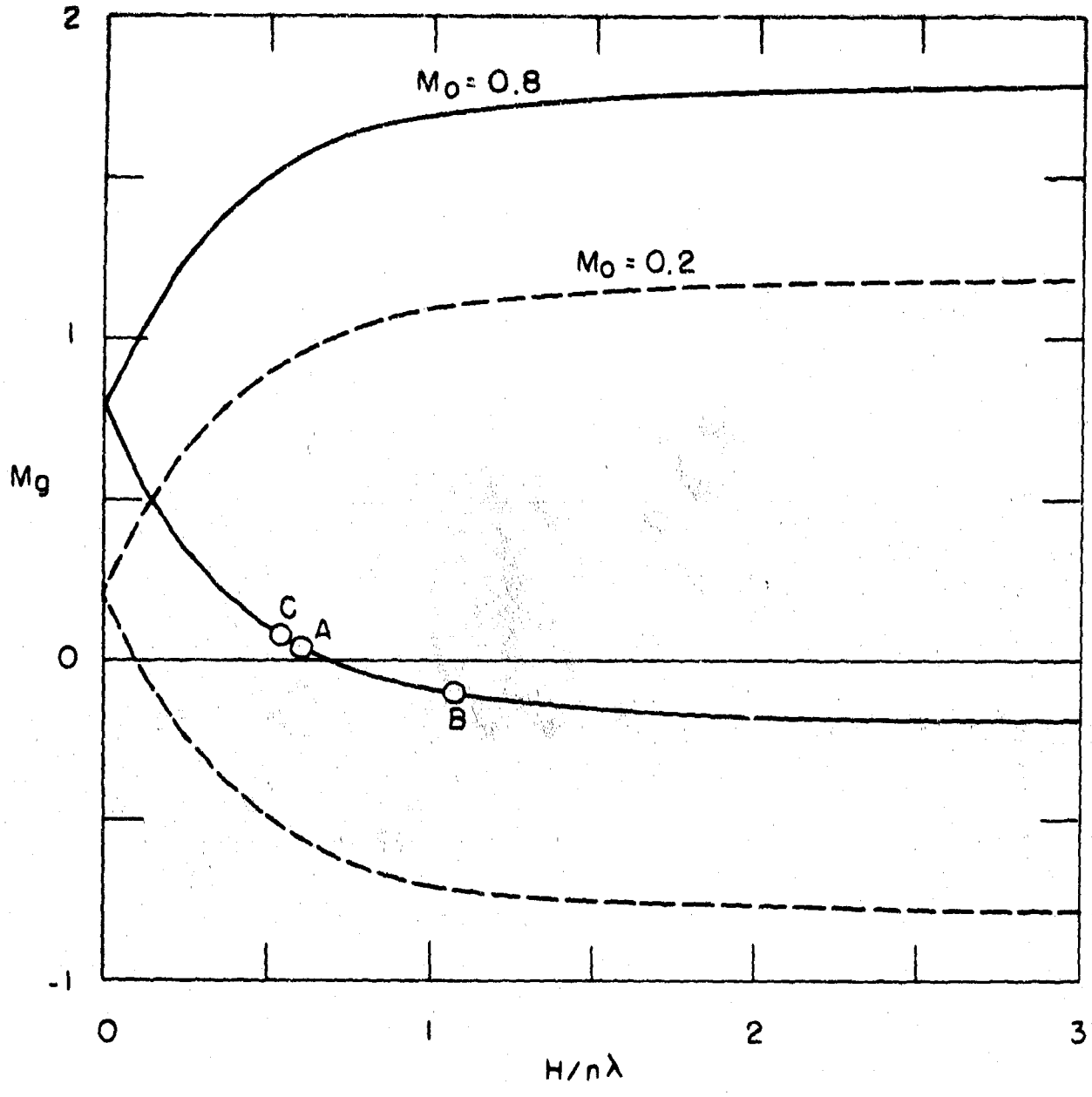

FIGURE 59. GROUP VELOCITY AS A FUNCTION OF WAVELENGTH.

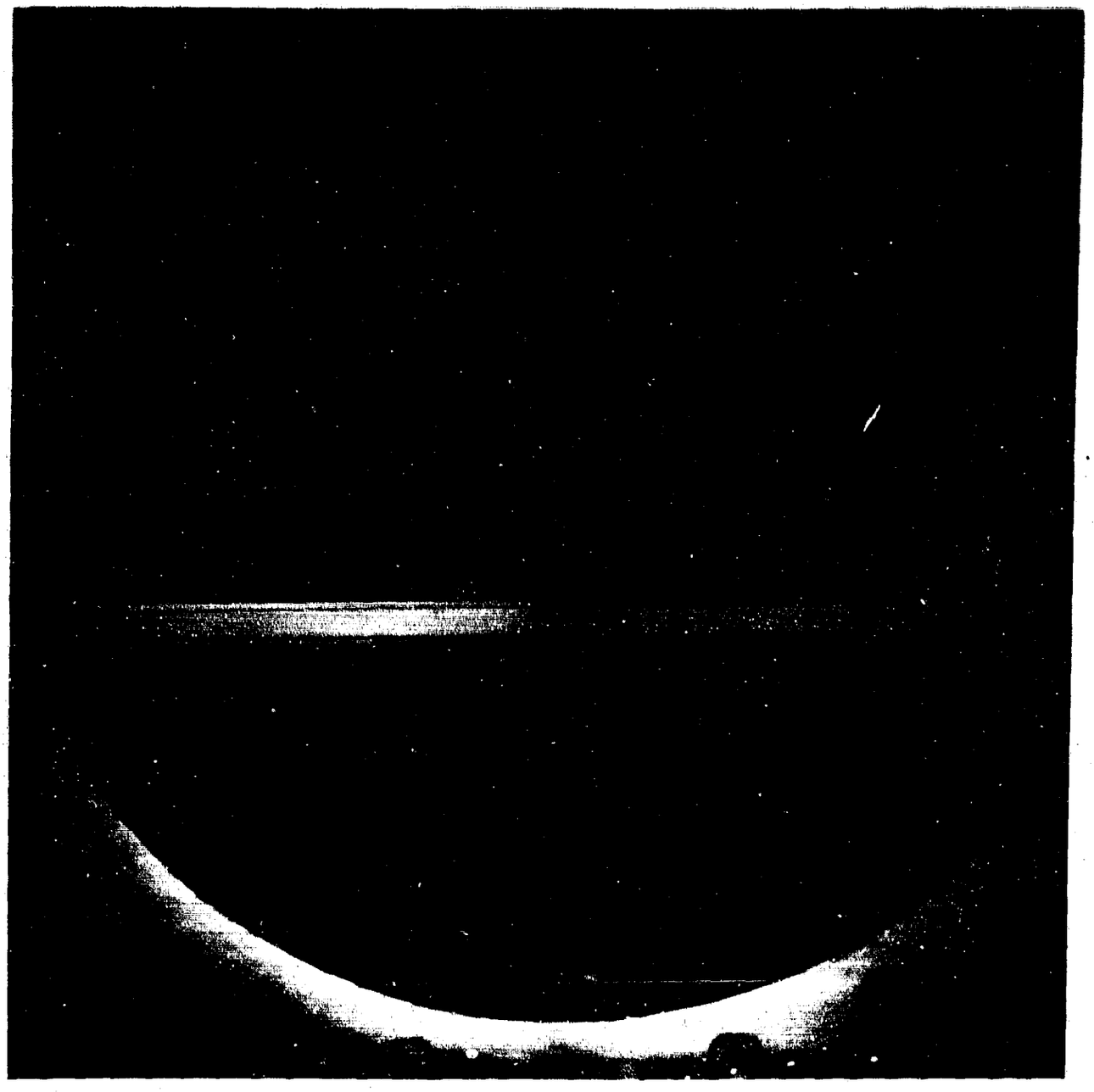

FIGURE 60. SCHLIERENOPTICAL FLOW VISUALIZATION OF SHOCK PATTERN; HALF-SCALE EMPTY CAVITY; M = 0.8; L/D = 4; P_0 = 10 psia.

APPENDIX II

VIBRATION LEVELS

An accelerometer, attached to the underside of the cavity floor close to the center was used to monitor structural vibration during the tests. During each test run, one spectrum was taken with the same instrumentation as that used with the microphones.

Figures 61a and b show four typical spectra of the vertical acceleration of the center point of the cavity floor. The reference level in each case is 1 g, the acceleration due to gravity. The Figures present spectra taken for one-store, L/D = 4, 10 psia stagnation pressure, and all Mach numbers. The spectra are typical in that they differ widely in intensity and generally show peaks in the same frequency bands as the fluctuating pressures.

It is necessary to determine how far these vibration levels are acceptable — i.e., how far the structure response modifies the acoustic response of the cavity. An order of magnitude estimate follows.

The measure of acceptability chosen is (energy-exchange/cycle between structure and air mass) divided by (energy stored in the acoustic oscillation). Let p be a typical rms pressure and s be the acceleration of the cavity floor. Then the energy exchange/cycle is $O(pLs/\omega^2)$. L is the cavity length, ω is the dominant circular frequency. The energy stored is $O(p^2LD/\rho_0 a_0^2)$. D is the cavity depth; ρ_c and a_c are cavity air density and sound speed. Thus, if ξ is the acceptability parameter defined above,

$$\xi = O\left(\frac{s\rho_c a_c^2}{pD\omega^2}\right) \qquad \text{(II-1)}$$

Known quantities are $Q_1 = p/q$, where q is the dynamic pressure, and $Q_2 = s/q$.

Thus

$$\xi = O\left(\frac{Q_2}{Q_1} \cdot \frac{g\rho_c a_c^2}{q \cdot D\omega^2}\right) \qquad \text{(II-2)}$$

Now $\rho_c a_c^2 = \gamma p_c = \gamma p_\infty$, and $q = \gamma M^2 p_\infty / 2$, where subscript ∞ refers to free-stream conditions. Finally,

$$\xi = O\left(\frac{Q_2}{Q_1} \cdot \frac{2g}{\gamma M^2 D \omega^2}\right) \qquad \text{(II-3)}$$

Estimates of this parameter for the two high-level cases shown in Figs. 61a and b are 0.5×10^{-2} and 1.6×10^{-6}. Both of these numbers are small.

The above analysis does not indicate how large a value of ξ is unacceptable. A conservative guess might be that a value of 1/2% is just acceptable, and one or two parts in a million certainly so. Accordingly, in the discussions of the experimental results given above, it is assumed that vibration of the cavity structure has an insignificant effect. The vibration levels are also insignificant with respect to the microphones' vibratory sensitivity.

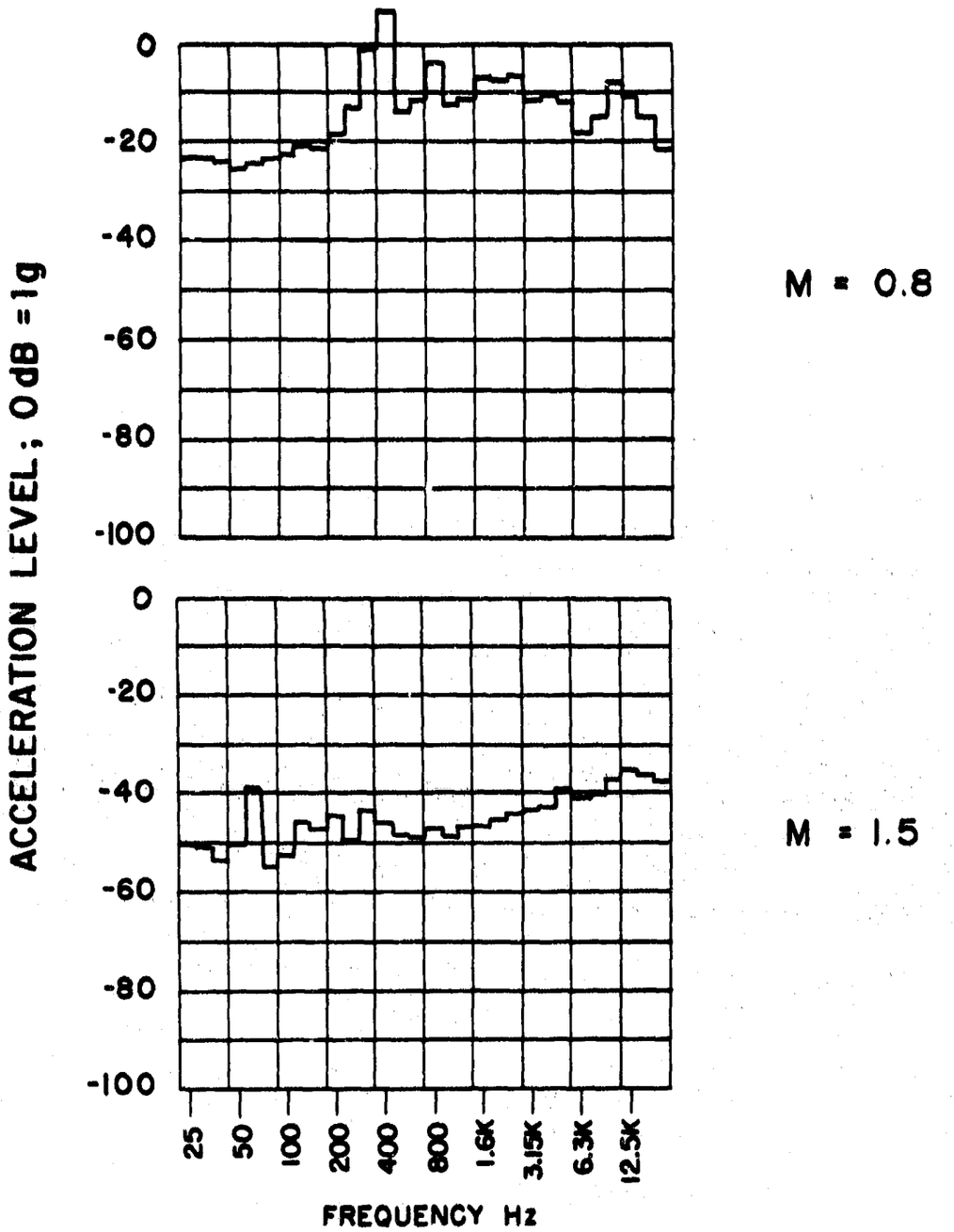

FIGURE 61a. ACCELERATION SPECTRUM AT CENTER LOCATION OF CAVITY FLOOR – CAVITY WITH ONE STORE; L/D = 4; P_0 = 10 psia.

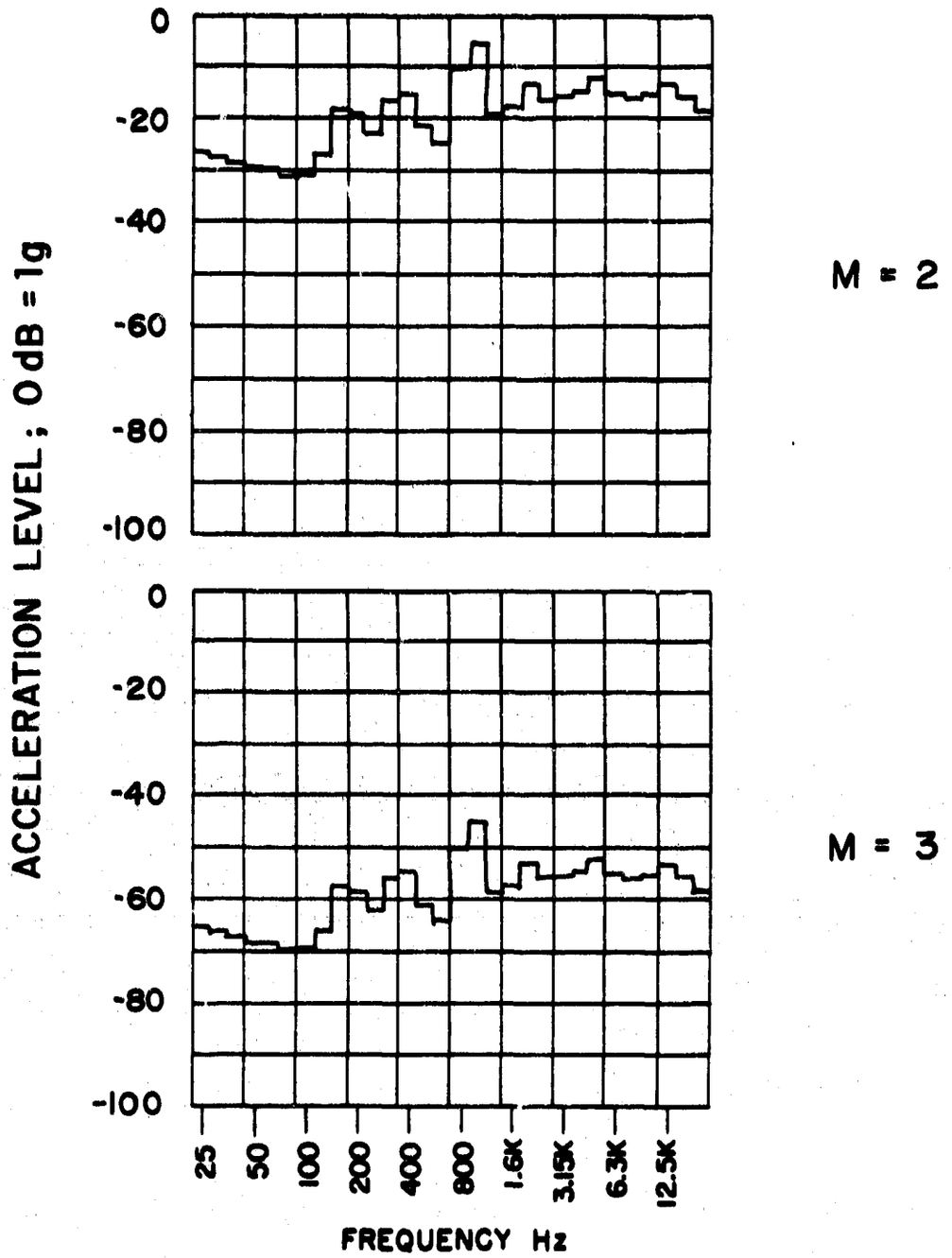

FIGURE 61b. ACCELERATION SPECTRUM AT CENTER LOCATION OF CAVITY FLOOR—CAVITY WITH ONE STORE; L/D = 4; P_0 = 10 psia.

REFERENCES

1. Dunham, W.H. "Flow-Induced Cavity Resonance in Viscous Compressible and Incompressible Fluids," 4th Symposium on Naval Hydrodynamics - Ship Propulsion and Hydrodynamics, Washington, D.C., ACR-73, p. 939, 1962.

2. Krishnamurty, K. "Acoustic Radiation from Two Dimensional Rectangular Cutouts in Aerodynamic Surfaces," NACA TN-3487, August 1955.

3. Gibson, J.E. "An Analysis of Supersonic Cavity Flow," MIT Aerophysics Lab., Tech. Rept. 299, Oct. 1958.

4. Covert, E.E. "An Analytical Investigation of Cavity Oscillations - Cavities with Unobstructed Openings and Discontinuous Velocity Profile," MIT Aerophysics Lab., Tech. Rept. 38, October 1962.

5. Rossiter, J.E.; Kurn, A.G., "Wind Tunnel Measurements of the Unsteady Pressures in and behind a Bomb Bay," Royal Aircraft Establishment-Farnborough, Rept. No. Aero 2677, August 1963. (SECRET)

6. "Environmental Criteria Report for the XAIM-54A Guided Missile System (Phoenix) PMS 5-7/2175, "Hughes Aircraft Company Report ASD 5908R, September 1965.

7. Blokhintsev, D.I. "Excitation of Resonance by Air Flow," SLA Translation Pool No. 270 (ONR) from *ZhTF*, 15, pp 63-70, 1945.

8. Plumblee, H.E.; Gibson, J.S.; Lassiter, L.W. "A Theoretical and Experimental Investigation of the Acoustic Response of Cavities in an Aerodynamic Flow," Flight Dynamics Lab. Aeronautical Systems Division-Air Force Systems Command, Wright-Patterson Air Force Base, Ohio, WADD-TR-61-75, March 1962.

9. East, L.F. "Aerodynamically Induced Resonance in Rectangular Cavities," *J. Sound Vib.*, 3 (3), pp 277-287, 1966.

10. Rossiter, J.E. "A Review of the Current Work in the Aerodynamics Department on Bomb Bay Buffet," RAE unpublished ARC 23, 412, November 1961.

11. Rossiter, J.E., "The Effect of Cavities on the Buffeting of Aircraft," Paper presented to Structures and Materials Panel of AGARD, July 1962.

12. Rossiter, J.E., "Wind Tunnel Experiments on the Flow over Rectangular Cavities at Subsonic and Transonic Speeds," ARC R&M 3438, 1966.

13. Covert, E.E., "An Approximate Calculation of the Onset Velocity of Cavity Oscillations," submitted to *AIAA Journal*, August 1969.

14. Baker, R.W., "Sound Production in Aerodynamic Cavities (Resonator)," MIT Master's Thesis, 1960.

15. Leupold, M.J.; Baker, R.W., "A Report on Research Directed Toward the Design, Development, Construction and Testing of 'Aerodynamic Cavities'," MIT Aerophysics Lab., Tech. Rept. 417, November 1959.

16. Morse and Feshback, *Methods of Theoretical Physics*, Chapter 9.

17. Ffowcs-Williams, *Proc. Royal Society*, May 1969.

18. Morozov, M.G., "Interaction Between a Supersonic Stream and a Rectangular Depression on a Flat Plate," *Soviet Technical Physics*, 3 (1), January 1958.

19. Morozov, M.G., "Acoustic Emission of Cavities in Supersonic Airflow," News of the Academy of Sciences of the USSR Mechanics and Machine Building, (2), pp 40-46, 1960.

20. White, R.A.; McGregor, O.W., "Dynamics of Resonant Two-Dimensional Cavities in Aerodynamic Surfaces at Transonic and Supersonic Mach Numbers," Technical Information Service, *AIAA*, (later than 1967).

21. Unsteady-pressure data obtained in a BBN supersonic wind tunnel study of the RVTO I-A vehicle were scaled to a real flight situation. Later flight tests confirmed the validity of the scaling procedure.

BIBLIOGRAPHY

Baker, R. "Sound Production in Aerodynamic Cavities (Resonators)," M.S. Thesis, Dept. Aeronautics and Astronautics, MIT, 1960.

Bowey, G.S. "An Investigation into the Vibration Environment in Bomb Bays of the Victor and Vulcan Aircraft," RAE Rept. TN WE 72, August 1964.

Burggraf, O.R. "A Model of Steady Separated Flow in Rectangular Cavities at High Reynolds Number," 1965 *Heat Transfer and Fluid Mechanics Institute Proceedings*, (13), pp 190-229, 1965.

Charwat, A.F.; Roos, J.N.; Dewey, F.C.; Hitz, J.A. "An Investigation of Separated Flows - Part I: The Pressure Field," *J. Aerosp. Sci.* 28 (6) pp 457-470, June 1961.

Charwat, A.F.; Dewey, C.F.; Roos, J.N.; Hitz, J.A. "An Investigation of Separated Flows - Part II: Flow in the Cavity and Heat Transfer,: *J. Aerosp. Sci.* 28 (7) pp 513-527, July 1961.

Curle, N. "The Mechanics of Edge-Tones," *Proc. Roy. Soc.* 216A, pp 412-424, 1953.

Deitchman, S.J. "A Study of Bomb-Airplane Separation Problems," Cornell Aeronautical Lab., Inc., Project No. GC-910-C, Project MX-939, February 1956.

Dyer, I. "Sound Scattering by a Cylindrical Vortex," MIT PhD Thesis, 1954.

Fail, R.; Owen, T.D.; Ewre, R.C. "Low Speed Tunnel Tests on the Flow in Bomb Bays and its Effect on Drag and Vibration," RAE Rept. May 1954.

Fox, J. "Surface Pressure and Turbulent Airflow in Transverse Rectangular Notches," NASA TN D-2501, November 1964.

Fox, J. "Heat Transfer and Airflow in a Transverse Rectangular Notch," *Int. J. Heat-Mass Trans.* 8, pp 269-279, February 1965.

Hahn, M. "Experimental Investigation of Separated Flow over a Cavity at Hypersonic Speed," *AIAA Journal* 7 (6) pp 1092-1098, August 1969.

Harrington, M.C. "Excitation of Cavity Resonance by Air Flow," *J. Acoust. Soc. Amer.* 29 p 187, 1957.

Harrington, M.C.; Dunham, W.H. "Studies of the Mechanism for Flow Induced Cavity Resonance," *J. Acoust. Soc. Amer.* 32 p 921, July 1960.

Hoffman, S.; Wolff, A. "Effect on Drag of Longitudinal Positioning of Half-Submerged and Pylon-Mounted Douglas Aircraft Stones on a Fuselage with and without Cavities between Mach Numbers 0.9 and 1.8," NACA RM L54E26, July 1954.

Illingworth, J.K.B. "Flight Measurements of Bomb Bay Drag on a Canberra," RAE TN 2273, November 1953.

Ingard, U.; Dean, L. "Excitation of Acoustic Resonators by Flow," 2nd Symposium on Naval Hydrodynamics – Ship Propulsion and Hydrodynamics.

Ingard, U.; Ising, H. "Acoustic Nonlinearity of an Orifice," *J. Acoust. Soc. Amer.* 42 (1) 1967.

Kiwior, T.M.; Mandish, R.P. "Phoenix (XAIM-54A) T-20/F-111B Weapons Bay Environmental Measurements," Hughes Aircraft Company Rept. 2342.30(385), November 1967.

Knight, A.R. "Simultaneous Vibration and Bomb Bay Fluctuating Pressure Measurements in a Canberra B2 Aircraft," RAE TN STRUCT 1954.

McDearmon, R.W. "Investigations of the Flow in a Rectangular Cavity in a Flat Plate at a Mach Number of 3.55," NASA TN D-523, 1960.

Maull, D.J.; East, L.F. "Three Dimensional Flow in Cavities," *J. Fluid Mech.* 16 (4) pp 320-332, 1963.

Mehto, U.B., Lavan, Z. "Flow in a Two-Dimensional Channel with a Rectangular Cavity," NASA CR-1245, 1969.

Miles, J. "On the Reflection of Sound at an Interface of Relative Motion," *J. Acoust. Soc. Amer.* 29 (2) 1957.

Norton, D. "Investigation of B-47 Bomb Bay Buffeting," Boeing Airplane Company Doc. No. D-12675, February 1952.

Nyborg, W.; Burkhard, M.; Schilling, H. "Acoustical Characteristics of Jet-Edge and Jet-Edge Resonator Systems," *J. Acoust. Soc. Amer.* 24 (3) 1952.

Nyborg, W. "Self-Maintained Oscillations of the Jet-Edge System," *J. Acoust. Soc. Amer.* 26 (2) 1954.

Peterson, H.C.; Ezra, A.A. "Analysis of Similitude Requirements and Scaling Laws for Transonic Buffeting," RTD/AIA Symposium on Aeroelasticity and Dynamic Modelling Technology, Dayton, Ohio, RTD-TAR-63-4197 Pt.1, March 1964.

Quinn, B. "Flow in the Orifice of a Resonant Cavity," *AIAA Student Journal* 1 (1) pp 1-5, 1963.

Rainey, R.W. "Investigation of the Effects of Bomb Bay Configuration upon the Aerodynamic Characteristics of a Body with Circular Cross Section at Supersonic Speeds," NACA RM L55E27, August 1955.

Rainey, R.W. "Investigation at Supersonic Speeds of the Effects of Bomb Bay Configuration upon the Aerodynamic Characteristics of Fuselages with Noncircular Cross-Sections," NACA RM L56H20, November 1956.

Rhodes, C.W. "Bomb Bay Buffeting and Weapon Vibration in Open Bomb Bays," RAE TN ARM 709, December 1961.

Roshko, A. "Some Measurements of Flow in a Rectangular Cutout," NACA TN 3488, August 1955.

Seban, R.A.; Fox, J. "Heat Transfer to the Air Flow in a Surface Cavity," International Developments in Heat Transfer, *ASME*, pp 426-431, 1963.

Serbin, H. "Flow Induced by a Cavity in a Supersonic Stream," *J. Aerosp. Sci.* 28 (3) pp 247-8, March 1961.

Spee, B.M. "Wind Tunnel Experiments on Unsteady Cavity Flow at High Subsonic Speeds," AGARD Conference Proceedings No. 4, Separated Flows, Pt. 2, 1966.

Toni, I.; Iuchi, M.; Komoda, H. "Experimental Investigation of Flow Separation Associated with a Step or Groove," University of Tokyo Aeronautical Research Institute Rept. 364, 1961.

Tillman, W. "Additional Measurements of the Drag of Surface Irregularities in Turbulent Boundary Layers," NACA Translation TM 1299, January 1951.

Tucholski, L. "Bomb Carriage, Release and Separation Studies, Fuselage and Bomb Bay Flow Field Characteristics. Part I, Transonic Studies and Part II, Supersonic Studies," Cornell Aeronautical Lab. Rept. No. GC-910-C-17, March and April 1957.

Wagner, R.J.; Bilanger, J.R. "AGM-69A/FB-111 Weapons Bay Buffet-Wind Tunnel Test-Report and Analysis," The Boeing Company, March 1968 (SECRET).

Weiss, R.; Florsheim, B. "Flow in a Cavity at Low Reynolds Number," *Physics of Fluids* 8 (9) pp 1631-1635, Sept. 1965.

"Missile Response Report PMS 38-49/2222," Hughes Aircraft Company, July 1965.

"Flight Test Plans, Reports and Data, AF49-1901," Boeing Airplane Company Report B-10653, Restricted.

"T.S.R.2 Bomb Bay Buffeting Exercise," Vickens Armstrong (Aircraft) Ltd., VTO/D/571/38, September 1961.

UNCLASSIFIED
Security Classification

DOCUMENT CONTROL DATA - R & D

(Security classification of title, body of abstract and indexing annotation must be entered when the overall report is classified)

1. ORIGINATING ACTIVITY (Corporate author)	2a. REPORT SECURITY CLASSIFICATION
BOLT BERANEK AND NEWMAN, INC. 50 Moulton Street Cambridge, Massachusetts 02138	UNCLASSIFIED 2b. GROUP

3. REPORT TITLE

FLOW-INDUCED PRESSURE OSCILLATIONS IN SHALLOW CAVITIES

4. DESCRIPTIVE NOTES (Type of report and, inclusive dates)

Final-Report 1 March 1969 to 1 July 1970

5. AUTHOR(S) (First name, middle initial, last name)

Heller, Hanno H.
Holmes, Graham D.
Covert, Eugene E.

6. REPORT DATE	7a. TOTAL NO. OF PAGES	7b. NO. OF REFS
December 1970	147	22

8a. CONTRACT OR GRANT NO.	9a. ORIGINATOR'S REPORT NUMBER(S)
F33615-69-C-1428	
b. PROJECT NO. 1471	BBN Report No. 1972
c. Task No. 147102	9b. OTHER REPORT NO(S) (Any other numbers that may be assigned this report) AFFDL-TR-70-104
d.	

10. DISTRIBUTION STATEMENT This document is subject to special export controls and each transmittal to foreign government or foreign nationals may be made only with prior approval of the Air Force Flight Dynamics Laboratory/FYA (AFSC), Wright-Patterson Air Force Base, Ohio 45433

11. SUPPLEMENTARY NOTES	12. SPONSORING MILITARY ACTIVITY
	Air Force Flight Dynamics Laboratory Wright-Patterson AFB, Ohio 45433

13. ABSTRACT

This report presents the results of an experimental wind-tunnel study of flow-induced pressure oscillations in shallow cavities (length-to-depth ratio from 4 to 7). A variable-depth rectangular cavity was exposed to tangential flow over the open surface in the Mach-number range from 0.8 to 3, with flow stagnation pressures varying from 2 to 15 psia. The cavity was tested in an empty stage and with one or two stores. Third-octave band and narrowband fluctuating-pressure spectra were obtained at various locations within the cavity and under the approaching boundary layer; these spectra yielded information on broadband and resonant-response characteristics. Information on the longitudinal and lateral energy distribution, on recirculating-flow velocities, and on temperatures within the cavity was also obtained. This information was used to develop a scheme for predicting resonant frequencies and associated pressure-mode shapes, as well as discrete-frequency and broadband pressure amplitudes.